

Chromatic Dispersion Compensation in 40 Gbaud Optical Fiber WDM Phase-Shift-Keyed Communication Systems

Zur Erlangung des akademischen Grades

DOKTOR-INGENIEUR

am Institut für
Elektrotechnik und Informationstechnik
der Fakultät für Elektrotechnik, Informatik und Mathematik
der Universität Paderborn
genehmigte Dissertation

von

M.Sc. Ahmad Fauzi Abas
aus Malaysia

Referent: Prof. Dr.-Ing. R. Noé

Korreferent: Prof. Dr.-Ing. K. Meerkötter

Tag der mündlichen Prüfung: 23. Juni 2006

Paderborn 2006

D14-222

Acknowledgements

In the name of God, the Compassionate, the Merciful.

First, I thank my supervisor Professor Dr.-Ing Reinhold Noé, for inviting me to work in his group, and accepting me to pursue my studies under his supervision. During my early days in the laboratory, his close guidance, useful advices and funny jokes had helped me progressing well and faster than I have expected.

Secondly, I would like to acknowledge Malaysian Ministry of Science, Technology and Innovation for their three years financial support.

To my beloved parents, thank you very much for teaching me on how to manage this tricky world. I love both of you so much.

Special thanks go to all my colleagues in the Optical Communications group, especially to some of them with whom I explored the ideas, discussed the problems, digesting the lecture notes, struggled to catch the conference deadlines, wrote the technical papers and not forgotten, had coffee together. Working with them gave me wonderful experiences, which made me more matured to face the challenging world. Not forgotten also Herrn Gerhard Wiessler, Herrn Dipl.-Ing. Bernhard Stute, Herrn Dipl.-Ing. Bernd Bartsch and Herrn Michael Franke for their tireless support as technical assistants and also for informally training me to speak German.

I would also like to thank the committee members of my doctoral examination, Professors Dr. Sybille Hellebrand, Dr.-Ing. Klaus Meerkötter, Dr.-Ing. Rolf Schuhmann for reviewing my dissertation and providing constructive comments.

To my beautiful wife, Sariaah, my cute daughter, Sarah, and my handsome little son, Adam, I thank them for their loves, understanding, patience and continuous moral supports. Without them, my studies might not be as smooth as it was. Not forgotten also my brothers and sisters in Malaysia, I thank them for their moral support and sharing my ambitions.

Finally, I would like to thank all my friends in Malaysia, United Kingdoms and United States for their direct and indirect supports, especially Dr. Khazani, a person who introduced me to my first Optical Communications text book. Trust me, whether they realized it or not, all of them must have contributed something to this Dr.-Ing. dissertation. Million thanks to everybody.

Erklärung

- Die gültige Promotionsordnung vom 25.01.1991 ist mir bekannt.
- Die Dissertation wurde im Fachgebiet für Elektrotechnik und Informationstechnik der Universität Paderborn unter der Betreuung von Prof. Dr.-Ing. Reinhold Noé angefertigt.
- Die Dissertation wurde selbständig verfasst. Alle benutzten Hilfsmittel sind vollständig angegeben.
- Die Dissertation wurde nicht in dieser oder ähnlicher Form an anderer Stelle im Rahmen eines Promotions- oder Prüfungsverfahrens vorgelegt.
- Frühere Promotionsversuche haben nicht stattgefunden.

Declarations

- I understand the valid rules of Dr.-Ing. promotion that is used since 25.01.1991.
- This thesis has been made in the Department of Electrical Engineering and Information Technology of the University of Paderborn under the supervision of Prof. Dr.-Ing. Reinhold Noé
- This thesis has been written independently. All references are listed completely.
- This thesis has not been delivered in this or a similar form within the scope of a Dr.-Ing dissertation or an examination.
- Earlier attempts of Dr.-Ing examination have not taken place.

Zusammenfassung

Chromatisches Dispersionsmanagement ist ein wichtiger Aspekt heutiger faseroptischer Systeme. In Zukunft, wenn hohe Transmissionskapazität benötigt wird, kann im Gegensatz zur Amplitude die Phase des optischen Trägers herangezogen werden, um die Anforderungen an Bandbreite zu erfüllen. Übertragungsformate wie differentielle Phasenumtastung (DPSK) und differentielle Quadraturphasenumtastung (DQPSK) sind vielversprechende Alternativen für zukünftige faseroptische Netzwerke. Daher wurde in dieser Dissertation eingegangen auf Wellenlängenmultiplex (WDM) kombiniert mit Phasenumtastungssystemen. Bei Verwendung fortschrittlicher Modulationsformate wie DPSK, DQPSK und Polarisationsmultiplex (PolDM) müssen zahlreiche faseroptische Beeinträchtigungen beim Dispersionsmanagement berücksichtigt werden. Neben der chromatischen Dispersion selbst spielen Effekte innerhalb eines Kanals, nichtlineares Phasenrauschen, Kreuzphasenmodulation (XPM) und Vierwellenmischung (FWM) eine wichtige Rolle. Die Transmissionsexperimente im System mit 160 Gbit/s, entwickelt aus einem 40 Gbaud DQPSK mit PolDM in einer WDM-Umgebung wurden erfolgreich durchgeführt mit einem Netzwerk mit konventioneller dispersionskompensierender Faser (DCF). Durch die Verwendung eines kostengünstigen DCF-basierten chromatischen Dispersionskompensator zum Abgleich der Restdispersion wurde eine Funktion besser als das Limit für Vorwärtsfehlerkorrektur (FEC) erzielt für Übertragungslängen bis zu 100 km, eine totale Transmissionskapazität von etwa 5 Tbit/s. In 40 Gbaud-Experimenten mit dynamischer Dispersionskompensation wurde die Transmissionsstrecke aus Standard-Einmodenfaser (SSMF) erfolgreich kompensiert unter Verwendung eines auf gechirptem Faser-Bragg-Gitter basierten abstimmbaren Mehrkanal-Dispersionskompensators (MTDC). Unter allen verwendeten Modulationsformaten zeigte DPSK die besten Ergebnisse, wobei ein Dispersionskompensationswert bis hin zu -1520 ps/nm implementiert wurde. Dieser Kompensationswert kompensierte eine chromatische Dispersion von 94,2 km SSMF. Ein erfolgreicher Test bei 80 Gbit/s WDM DQPSK brachte das Potential des 10 Gbit/s MTDC an sein Limit. Es ist daraus zu schließen, dass sich der MTDC für Netzwerke mit kurzer Übertragungslänge eignet. Für längere Strecken ist eine Bandbreite von mindestens 60 GHz nötig, um Einbußen wegen zu geringer Bandbreite zu vermeiden. Wir schlagen vor, dass eine Kombination aus MTDC und dispersionsverschobene Faser mit Restdispersion (NZDSF) die beste Lösung darstellt für zukünftige faseroptische Hochleistungsnetzwerke. Durch Kombination von MTDC mit Ankunftszeitdetektion wurde eine automatische Dispersionskompensation für alle 40 Gbaud-Formate (OOK, DPSK, DQPSK) gezeigt. Diese Dissertation wertet sowohl die Möglichkeit aus, konventionelles Dispersionsmanagement zu verwenden, um Systeme zu Dispersion coefficientnterstützen, welche fortschrittliche Modulationsformate verwenden als auch die Notwendigkeit und Machbarkeit von fortschrittlichem Dispersionsmanagement, um die Leistung solcher Systeme noch zu verbessern.

Abstract

Chromatic dispersion management is an important part of today's fiber optic networks. In the future, when high transmission capacity is necessary, other than amplitude, the phase of optical carrier can be explored to support bandwidth requirement. Transmission systems such as Differential-Phase-Shift-Keyed (DPSK) and Differential-Quadrature-Phase-Shift-keyed (DQPSK) will become promising alternatives for future fiber optic networks. Therefore, the implementation of chromatic dispersion compensation in advanced Wavelength Division Multiplexed (WDM) phase-shift-keyed transmission systems is addressed in this dissertation. By using advanced modulation formats, namely DPSK, DQPSK and polarization division multiplex (PoIDM), numerous fiber impairments need to be considered in chromatic dispersion management. Besides the chromatic dispersion itself, intrachannel effects, nonlinear phase noise, and the resonance generated from Cross Phase Modulation (XPM) and Four Wave Mixing (FWM) are also important. The transmission experiments in 160 Gbit/s system, developed from 40 Gbaud DQPSK with PoIDM, in a WDM environment were successfully conducted in a conventional Dispersion Compensating Fiber (DCF) supported network. By using a low cost DCF-based chromatic dispersion compensator for residual dispersion compensation, performance above the Forward Error Correction (FEC) limit was achieved over span lengths of up to 100 km, and transmission capacity of around 5 Tbit/s. In 40 Gbaud WDM dynamic dispersion compensation experiments, the transmission line (SSMF) dispersion was successfully compensated by using a 10 Gbit/s Chirped-Fiber Bragg grating-based multichannel tunable dispersion compensator (MTDC). Among all modulation formats used, the best performance was shown in DPSK, where compensation value of up to -1520 ps/nm was implemented. This compensation value has successfully compensated chromatic dispersion of 94.2 km SSMF. Successful test on 80 Gbits/s WDM DQPSK system pushed the potential of this 10 Gbits/s MTDC to the limit. It is concluded that at 33 GHz bandwidth, MTDC is suitable for short span networks. For long-haul systems a bandwidth of at least 60 GHz is required to avoid a bandwidth limitation penalty. We suggest that the combination of MTDC and Non-zero Dispersion Shifted Fiber (NZDSF) is the best solution to produce a high performance future fiber optic network. Combining MTDC with arrival time detection, automatic chromatic dispersion compensation was demonstrated in all 40 Gbaud formats (OOK, DPSK and DQPSK). This dissertation validates the possibility of using conventional dispersion management to support the systems that implement advanced modulation formats, and the need and feasibility of implementing advanced dispersion management to further improve the performance of these systems.

List of Abbreviations

ADN	Add Drop Node
ASK	Amplitude Shift Keying
BER	Bit Error Rate
CD	Chromatic Dispersion
CDM	Chromatic Dispersion Map
CDR	Clock and Data Recovery
CFBG	Chirped Fiber Bragg Grating
CSRZ	Carrier Suppressed Return to Zero
CW	Continuous Wave
DCF	Dispersion Compensating Fiber
DCM	Dispersion Compensating Fiber Module
DEMUX	Demultiplexer
DM	Dispersion Map
DMF	Dispersion Managed Fiber
DPSK	Differential Phase Shift Keying
DQPSK	Differential Quadrature Phase Shift Keying
DSF	Dispersion Shifted Fiber
EDFA	Erbium Doped Fiber Amplifier
EOP	Eye Opening Penalty
ETDM	Electrical Time Domain Multiplexing
FBG	Fiber Bragg Grating
FEC	Forward Error Correction
FR	Frequency Range
FTTH	Fiber To The Home
FTTP	Fiber To The Premises
IFWM	Intrachannel Four Wave Mixing
IMDD	Intensity Modulation Direct Detection
IXPM	Intrachannel Cross Phase Modulation
LEAF	Large Effective Area Fiber

MTDC	Multi-channel Tunable Dispersion Compensator
MUX	Multiplexer
MZM	Mach Zehnder Modulator
NLPN	Non-Linear Phase Noise
NLS	Non-Linear Schrödinger
NRZ	Non-Return-to-Zero
NZDSF	Non-Zero Dispersion Shifted Fiber
OADM	Optical Add Drop Multiplexer
OOK	On Off Keying
OXC	Optical Cross Connect
PBC	Polarization Beam Combiner
PBS	Polarization Beam Splitter
PLL	Phase Locked Loop
PM	Phase Modulation
PMD	Polarization Mode Dispersion
PolDM	Polarization Division Multiplexing
PSK	Phase-Shift-Keying
QAM	Quadrature-Amplitude-Modulation
CDC	Configurable Dispersion Compensator
SE	Spectral Efficiency
SPM	Self Phase Modulation
SSMF	Standard Single Mode Fiber
TEC	Thermo-Electric Cooler
TWRS	True Wave RS
VIPA	Virtual Image Phase Arrays
WDM	Wavelength Division Multiplexing

List of Symbols

γ	Nonlinear coefficient
a	Signal amplitude
π	Pi
β	Propagation constant
β_1	Inverse of group velocity delay
β_2	Group velocity dispersion
V_g	Group velocity
τ	Group delay
l	Propagation distance
D	Dispersion coefficient
S	Dispersion slope coefficient
c	Light velocity
λ	Wavelength
$\delta\lambda$	Spectralwidth
$\Delta\lambda$	WDM wavelength range
ΔU	Small nonlinear induced pertubation
ϕ	Signal phase
α	Attenuation constant
A_{eff}	Fiber effective area
t	time
L_{DCF}	DCF length
n	Length factor
r	Radius
W	Total number of fiber turns
n_w	Number of turns for specified length
Γ	Total optical noise
N	Number of fiber span

List of Figures

2.1	Phasor diagram of (a) OOK and (b) DPSK (MZM)	6
2.2	Phasor diagram of DQPSK	7
2.3	Eye diagrams of the signal affected by intrachannel effects: (a) IXPM, (b) IFWM [37]	9
2.4	Various dispersion maps	13
2.5	Transmission link with Dispersion Managed Fiber (DMF)	15
3.1	Experimental setup	18
3.2	Slope compensation curves, \circ : measured, \times :simulated	19
3.3	CDC design layout	20
3.4	Several empty reels prepared for fiber winding	21
3.5	CDC arrangement with two external DCM-20s	25
3.6	Schematic representation of the testbed used for transmission experiment	26
3.7	Four spans transmission line.	27
3.8	Dispersion map of four spans 16 channels WDM transmission.	27
3.9	The residual dispersion for the outermost wavelengths after transmission, and dispersion compensation (curve 1,2 and 3 are the dispersion slope after the CD compensation of λ_1 , middle-band λ and λ_2).	29
3.10	BER after 273 km fiber and dispersion compensation.	29
3.11	Eye diagrams for I channel in both orthogonal polarizations: (a) Back-to-back (first polarization), (b) Back-to-back (second polarization), (c) After 273 km (first polarization), (d) After 273 km (second polarization)	30
3.12	Three spans transmission line.	30
3.13	Dispersion map of three spans 16 channels WDM transmission.	31
3.14	The residual dispersion for the outermost wavelengths after transmission, and after compensation (Curve 1,2 and 3 are the dispersion slope after the CD compensation of λ_1 , middle-band λ and λ_2).	32
3.15	BER after 292 km fiber and dispersion compensation	32
3.16	Eye diagrams for both I and Q channels in one polarization: (a) Back-to-back (I), (b) Back-to-back (Q), (c) After 292 km (I), (d) After 292 km (Q)	33
3.17	Transmission line arrangement for 32 channels WDM transmission	34
3.18	Dispersion map of four-span 32 channels WDM system	35
3.19	The residual dispersion for the outermost wavelengths after transmission, and dispersion compensation (1,2 and 3 are the dispersion slope after CD compensation of λ_1 , middle-band λ and λ_2).	35
3.20	BER after 323 km fiber and dispersion compensation	36

3.21	Eye diagrams for I channel in both polarizations: (a) Back-to-back (x), (b) Back-to-back (y), (c) After 323 km (x), (d) After 323 km (y)	36
4.1	Teraxion Multi-channel Tunable Dispersion Compensator	39
4.2	Principle of operation of MTDC	41
4.3	Temperature setting of the TECs for specified dispersion values.	42
4.4	Group delay vs wavelength for three different dispersion setting	43
4.5	The chirping of sampling period [21]	43
4.6	MTDC reflectivity and group delay for 51 WDM channels [22]	44
4.7	Dispersion values at highest, middle and lowest dispersion tuning[22]	45
4.8	Tuning characteristics of MTDC's channel 1 and 51[21]	45
4.9	Dispersion and dispersion slope of MTDC[23]	46
4.10	The resulting passband characteristic of MTDC	47
4.11	Experimental setup for OOK, DPSK and DQPSK	49
4.12	OOK: Q factors after transmission and compensation.	50
4.13	OOK: Q-factors against transmission distances.	50
4.14	OOK: Eye diagrams at two outermost optical carriers for several transmission distances	51
4.15	DPSK: Q-factors vs frequencies after several ranges of transmission distance.	52
4.16	DPSK: Q-factors vs distance for the best, middle and worst WDM channels	53
4.17	DPSK: Eye diagrams for various range of transmission distance	54
4.18	DQPSK: Q-factors vs optical frequencies for several transmission distances. Markers Δ represent I-quadrature, and \circ represent Q-quadratures.	56
4.19	DQPSK: Receiver sensitivity at various compensation settings.	57
4.20	DQPSK: Eye diagrams of the first (192.1 THz), middle (194 THz) and last (196 THz) optical frequencies for back-to-back and various transmission distances	58
4.21	Automatic chromatic dispersion compensation setup	58
4.22	BER vs dispersion value for different transmission distances.	59
C.1	40 Gbaud CSRZ DPSK:(a) Without filter, (b) With 65 GHz filter, (c) With 45 GHz filter	70
C.2	40 Gbaud NRZ DQPSK	71
C.3	40 Gbaud CSRZ DQPSK	71
D.1	Optical filtering effect in a CS-RZ DPSK eye diagram : (a) Without filter, (b) With 65 GHz filter, (c) With 45 GHz filter	74
D.2	Optical filtering effect in a NRZ DQPSK eye diagram : (a) Without filter, (b) With 65 GHz filter, (c) With 45 GHz filter	75
D.3	Optical filtering effect in CS-RZ DQPSK eye diagram before MZDI: (a) Without filter, (b) With 65 GHz filter, (c) With 45 GHz filter	76
D.4	Optical filtering effect in CS-RZ DQPSK eye diagram after MZDI: (a) Without filter, (b) With 45 GHz filter	77
E.1	First stage EDFA characteristics: (a) EDFA-L ,(b)EDFA-H	80
E.2	Second stage EDFA characteristic: (a) EDFA-L ,(b) EDFA-H	81

E.3	Gain characteristic at -22 dBm/ch input power: (a) EDFA-L: 980 nm EDFA output is -5 dBm/ch and +11 dBm total ,(b) EDFA-H: 980 nm EDFA output is 0dBm/ch and +16 dBm total	81
E.4	Gain characteristic at -15 dBm/ch input power: (a) EDFA-L: 980 nm EDFA output is -5 dBm/ch in average, and +11 dBm total ,(b) EDFA-H: 980 nm EDFA output is 0dBm/ch in average, and +16 dBm total	82
E.5	Gain characteristic at -6 dBm/ch input power: (a) EDFA-L: 980 nm EDFA output is -5 dBm/ch in average, and +11 dBm total ,(b) EDFA-H: 980 nm EDFA output is 0dBm/ch in average, and +16 dBm total	83
F.1	Experiment setup	85
F.2	Raman gain at different input power	86
F.3	Combination of Raman and EDFA gain	86
H.1	The comparison of CD tolerance between 40 Gbaud DPSK, 20 Gbaud DQPSK and 40 Gbaud DQPSK	90
J.1	The setup of WDM transmitter for OOK, DPSK and DQPSK formats with PolDM	93
K.1	WDM receiver setup	96
L.1	Schematic of the dual-grating MTDC [23]	97

List of Tables

3.1	Insertion loss for all CDC Parts measured at 1550 nm wavelength	24
4.1	MTDC Specifications	41
A.1	The specifications of several types of optical fiber	65
B.1	Number of turns for specified compensation lengths	67
I.1	List of WDM lasers linewidth	92

Contents

1	Introduction	1
2	Phase-Shift-Keyed Systems and Chromatic Dispersion	5
2.1	Phase-Shift-Keying	5
2.1.1	Differential-Phase-Shift-Keying (DPSK)	5
2.1.2	Differential-Quadrature-Phase-Shift-Keying (DQPSK)	6
2.2	Chromatic Dispersion (CD)	7
2.2.1	Impact of pulse overlapping in 40 Gbit/s system	8
2.3	Chromatic Dispersion Management (CDM)	10
2.3.1	Dispersion Compensating Fiber (DCF)	11
2.3.2	Tunable Dispersion Compensator (TDC)	11
2.3.3	Dispersion map	12
2.4	Conclusion	15
3	DCF-based Dispersion Compensator	17
3.1	Introduction	17
3.2	Development and Characterization	18
3.2.1	Device Development	18
3.2.1.1	Material characterizations	18
3.2.1.2	Material Preparation	19
3.2.1.3	Device Assembly	23
3.2.2	Insertion Loss Characterization	24
3.3	Transmission Experiments	25
3.3.1	Testbed	25
3.3.2	16 channels WDM transmission	25
3.3.3	32 channels WDM Transmission	31
3.4	Conclusion	34
4	Chirped-Fiber Bragg Gratings-based Dispersion Compensator	39
4.1	Motivation	39
4.2	CFBG Multi-channel Tunable Dispersion Compensator	40
4.2.1	Principle of operations	40
4.2.2	Performance assessment	43
4.2.2.1	Dispersion and dispersion slope tunability	44
4.2.2.2	Operating optical bandwidth	46
4.2.2.3	Insertion loss and PMD	47
4.3	System experiments	48

4.3.1	Introduction	48
4.3.2	On-Off-Keying (OOK)	48
4.3.2.1	Experimental setup	48
4.3.2.2	Results and Discussions	49
4.3.3	Differential-Phase-Shift-Keying (DPSK)	51
4.3.3.1	Experimental setup	52
4.3.3.2	Results and Discussion	52
4.3.4	Differential-Quadrature-Phase-Shift-Keying (DQPSK)	54
4.3.4.1	Experimental Setup	54
4.3.4.2	Results and discussions	55
4.3.5	Automatic CD detection and compensation	57
4.3.5.1	Experimental setup	57
4.3.5.2	Results and discussions	59
4.4	Conclusion	60
5	Conclusions and Future Work	63
A	Optical Fiber Parameters	65
B	CDC: Number of turns for specified compensation lengths	67
C	Optical Spectrum with filtering effect	69
D	Eye diagrams of filtered 40 Gbaud DPSK and DQPSK signal	73
D.1	CS-RZ DPSK	73
D.2	NRZ DQPSK	73
D.3	CS-RZ DQPSK	73
D.3.1	Before Inteferometric demodulation	76
D.3.2	After Interferometric demodulation	76
E	Double-stage Erbium-doped fiber amplifier	79
E.1	First Stage (980 nm)	79
E.2	Second Stage (1480 nm)	80
E.3	Cascaded configuration (980 nm + 1480 nm)	80
E.3.1	Pin = -22 dBm	80
E.3.2	Pin= -15 dBm	82
E.3.3	Pin= -6 dBm	82
F	Raman Amplifier	85
G	Phase variance in quasi-linear system	87
H	Chromatic Dispersion Tolerance	89
I	WDM Laser Linewidth	91
J	Detailed description of WDM Transmitter	93

K Detailed description of WDM Receiver	95
L MTDC: Dual-grating arrangement	97

Chapter 1

Introduction

The advances in data communication and information technology allow tremendous amounts of data to be transferred through the networks. This is supported by high bandwidth optical fiber and also the emergence of fast computer processors, whose speed increases every-day. As a result, all business activities which require high data bandwidth such as Video on Demand, video conferencing, digital photography and others can be conveniently realized. From one year to another, the required network capacity increases exponentially, which shows that Tbit/s capacity is not far from reality. Future technologies such as Fiber-To-The-Premise (FTTP) and Fiber-To-The-Home (FTTH) which deploy the fiber up to the consumer premises are being considered seriously as an alternative to satisfy bandwidth demand [1].

Wavelength Division Multiplexing (WDM) technology has recently shown its potential to support high bandwidth data transfer [2, 3, 4]. It allows multiple wavelength to be simultaneously transmitted in a single fiber, therefore increasing the fiber capacity. For example, about forty WDM channels can be accommodated in the C-band at 100 GHz channel spacing. This shows that with the existence of S and L-bands [5], and by considering channel spacing of as close as 12.5 GHz [6], more WDM channels could be transmitted in a single fiber. This technology can be realized by using existing transmitter and receiver without severe quality degradation. As an example, the capacity of 6 Tbit/s was demonstrated by using 10 Gbit/s system [2]. Besides increasing the transmission bandwidth, WDM technology also introduces network management flexibility. This is achieved by implementing Optical Add Drop Multiplexer (OADM) and Optical Cross Connect (OXC) in the system, which allows WDM channels to be added or dropped at any location in the network, and switch their transmission paths [3].

Apart from WDM, another means of increasing the transmission capacity is by increasing the symbol rate. In today's optical network backbone, 10 Gbaud systems have already been implemented. From the laboratory experimental results, it could also be expected that commercial 40 Gbaud system will be ready for implementation when it is required. Recently, 85.4 Gbaud ETDM transmission was demonstrated [7], followed by the introduction of a 107 Gbaud ETDM transmitter [8].

In term of transmission system, On-Off-Keying (OOK) [10] is the simplest architecture available. By changing the intensity of the carrier by means of a very fast switch, which turns the laser's intensity ON and OFF referring to input data stream, the data is modulated. Today, all fiber optic networks implement this system due to its technology maturity and simple

architecture. OOK is one of several amplitude-based systems in Amplitude-Shift-Keyed (ASK) technology. Among other amplitude-based systems are binary and quaternary-On-Off-Keying (4-OOK) and Quadrature-amplitude-Modulation (QAM), which are referred as multilevel ASK format.

Beside OOK system, Differential-Phase-Shift-Keyed (DPSK) [9, 10], a system where the data is encoded onto optical phase, has emerged as a system of interest since the last few years. This is partly due to its 3 dB less required Optical Signal to Noise Ratio (OSNR) at the receiver in comparison to conventional OOK system. For the same average optical power, the DPSK symbol distance (expressed in electrical field) is greater than for OOK by a factor of $\sqrt{2}$. Therefore, at the same symbol distance, only half the average power should be needed, which is advantageous to reduce the fiber nonlinearity effect. As the data is modulated in the optical carrier's phase, the amplitude of the carrier is relatively constant between different WDM channels regardless of transmitted bit patterns. By using this modulation format, transoceanic transmission distance and Tbit/s capacity was demonstrated [2].

Differential-Quadrature-Phase-Shift-Keyed (DQPSK) system [11, 12, 14] is introduced as a system which is highly tolerant to Chromatic Dispersion (CD) and Polarization Mode Dispersion (PMD) at the same bitrate as OOK or DPSK. This is because it allows two data bits to be transmitted in one symbol duration (one bit per quadrature). In order to achieve the same bitrate, the required symbol rate is only half in comparison to OOK or DPSK. On the other hand, if the same symbol rate is used, the data rate is doubled [13] and in WDM system, this will double the Spectral Efficiency (SE). By using this format a transmission capacity of 5.12 Tbits/s was reported with SE of 1.6 bits/Hz/s [15].

Beside DQPSK, Polarization Division Multiplex (PoIDM) system [16, 32] also doubles transmission capacity. In this system, two data channels are modulated (amplitude or phase) onto two optical carriers that have the same optical frequency, but orthogonally different polarization states. This allows the two signals to be multiplexed in a Polarization Beam Combiner (PBC), thus producing a PoIDM signal. For polarization demultiplexing, polarization controller and Polarization Beam Splitter (PBS) are required. This doubling of capacity is a multiplexing technique, contrary to DQPSK, which is a modulation format. Implementing this multiplexing technique to DQPSK format allows the operator to either transmit a certain bitrate per WDM channel at four times reduced symbol rate (40 Gbit/s transmission at 10 Gbaud symbol rate), or quadruple the WDM channel capacity by transmitting the data at the same symbol rate as the conventional systems (OOK or DPSK). By combining DQPSK and PoIDM, 160 Gbit/s transmission at 40 Gbaud symbol rate was demonstrated with better system tolerance to fiber impairments in comparison to 160 Gbit/s ETDM system [17].

Chromatic dispersion compensation, either optically [19, 20, 21, 24] or electrically [33, 34] is very important in fiber optic transmission system. In low bitrate networks, a transmission over several hundreds kilometer is still possible without dispersion compensation. At high bitrate such as in a 40 Gbit/s system, only a distance of less than 5 km can be reached without dispersion compensation. Advances in Erbium-doped Fiber Amplifier (EDFA) and Raman amplifier technologies allow the realization of ultra long-haul data transmission. In future networks, where data is transmitted over several thousand kilometers without regeneration, any system will require CD compensation. To date, several technologies are used for CD compensation such as Dispersion Compensating Fiber (DCF)

[52, 53, 54], Fiber Bragg Gratings (FBG) [20, 21, 24], virtual-image phase-arrays (VIPA) [25, 26], and Gires-Tournois etalons [27, 28, 29]. The operations of these compensators are complemented by several CD detection techniques [19, 35, 36, 73]. The combination of both technologies produces automatic CD compensation which is necessary for fiber optic transmission at 40 Gbit/s and beyond. In addition to that, the dispersion map management is also important to ensure network reliability [38, 59, 60].

PMD is another factor which contributes to the system performance degradation [30, 31, 32]. It is seriously experienced in a high bitrate system which is installed in an old network. Several solutions for this problem are suggested including the introduction of new types of fibers, besides inventing several types of compensator. Until now no commercially reliable compensator is available. This is due to the PMD random nature, which required very close monitoring and adaptive compensation. However, after many laboratory experiments it was noticed that PMD compensation is only required in the long-haul system with symbol rate of 40 Gbaud and beyond, that utilizes old fiber. In the laboratory, several experiments at 40 Gbit/s with a variety of modulation formats showed that long-haul transmission is possible without PMD compensation. As 40 Gbits/s system has not yet become a commercial system, it is expected that by the time it becomes commercial, new fiber will be partly available in the networks. Hence, we can conclude that PMD is a relatively small deteriorating factor in comparison to CD.

Optical pulses that are affected by CD broaden, which results in pulse overlapping. When adjacent pulses overlap with each other, phase modulation (PM) is induced due to the Kerr effect. This PM introduces two impairments namely Intrachannel Four Wave Mixing (IFWM) and Intrachannel Cross Phase Modulation (IXPM) [37, 38]. In OOK systems, IFWM introduced ghost pulses which causes amplitude jitter while IXPM produced timing jitter. In PSK systems, IXPM additionally produced phase modulation to adjacent pulses apart from timing jitter while IFWM shows a similar contribution as that in OOK. However both factors were shown to contribute less degradation to PSK compared to OOK systems [45].

Generally in this dissertation, the implementation of two types of CD compensator in the system with advanced modulation formats are studied. The first compensator is constructed from the conventional Dispersion Compensating Fiber (DCF) and tested in a 160 Gbit/s WDM system which is based on 40 Gbaud DQPSK with PolDM. The second compensator, which is a Chirped-Fiber Bragg Grating-based multichannel tunable dispersion compensator (MTDC) that was initially designed for 10 Gbits/s operation was tested in a 40 Gbaud OOK, DPSK and DQPSK transmission systems. Automatic CD detection and compensation was also studied by combining arrival time detection and the MTDC.

Specifically, this dissertation is arranged as follows. The first chapter is the general introduction on the development of a high speed optical network and its limitation factors. The second chapter discusses in more detail about DPSK and DQPSK systems together with CD issues in 40 Gbit/s systems. Chapter 3 explains in detail the development of a DCF-based CD compensator and the transmission tests in WDM DQPSK with a PolDM system. In Chapter 4, the operation of 10 Gbit/s WDM CFBG-based CD compensator is demonstrated. The compensator was tested in a 100 GHz spaced forty channels WDM 40 Gbaud OOK, DPSK and DQPSK system. Finally Chapter 5 concludes the dissertation.

Chapter 2

Phase-Shift-Keyed Systems and Chromatic Dispersion

2.1 Phase-Shift-Keying

Phase-Shift-Keyed (PSK) fiber optic systems is a topic of interest since around 1980. Early experiments focused on its potential to increase receiver sensitivity. However when Erbium-doped Fiber Amplifier (EDFA) was introduced and became the technology of choice, On-Off-Keying (OOK) seemed to be sufficient for long-haul transmission. Nevertheless, the tolerance of OOK to fiber nonlinearity is not satisfactory. The introduction of DPSK systems that have a constant average power independent of transmitted bits, and 3 dB less required Optical Signal-to-Noise Ratio (OSNR) at the receiver to achieve the same sensitivity as OOK, partly solved the problem and allowed extended transmission distance. Since then, the advantages of PSK systems were further explored. Beside the increase of receiver sensitivity, this format offers better solutions to increase spectral efficiency. In this section only asynchronous PSK systems, namely DPSK [9, 10] and DQPSK [9, 11, 13] are discussed. Both systems are used as the main testbeds in the experiments presented in this dissertation.

2.1.1 Differential-Phase-Shift-Keying (DPSK)

Differential Phase Shift Keying (DPSK) is generated either by using a phase modulator or a Mach-Zehnder modulator (MZM). Fig. 2.1 shows the phasor diagram for DPSK, compared to OOK. Each data pulse is represented by a single point (or a vector connecting the origin to that point) in the phasor diagram, in which the radial direction represents the E-field amplitude and the angular direction is the E-field phase. In contrast to conventional OOK in Fig. 2.1 (a), where the data are represented by either 0 or 1, binary DPSK essentially encodes the data as 1 or -1 (0 or π phase shift). When using a phase modulator (phasor diagram is not shown) the bitstreams are encoded onto the optical carrier in such a way that the optical carrier's phase is continuously changed from its original phase to a relative π phase shift, which produces a constant output power independent of transmitted bits. While performing the modulation, chirp is introduced which reduces the system tolerance to chromatic dispersion (CD). Another alternative is by the use of MZM (Fig. 2.1(b)). When

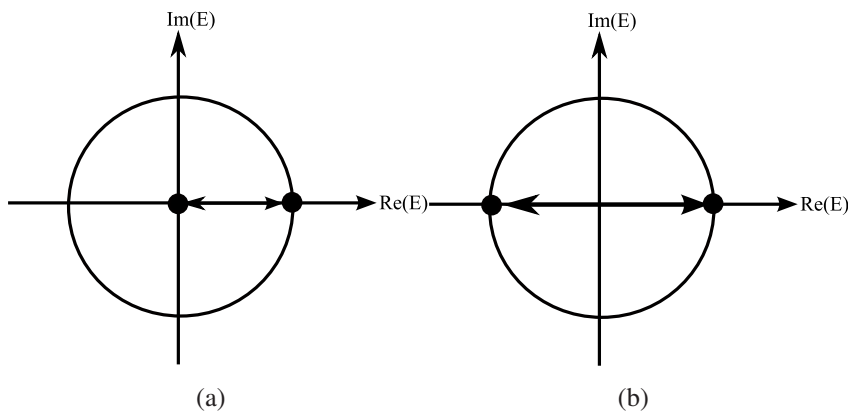


Figure 2.1: Phasor diagram of (a) OOK and (b) DPSK (MZM)

using this modulator the π phase shift is obtained without passing through the imaginary part of the E-field and thus, no chirp is produced. In contrast to the uniform amplitude produced by first method, an instantaneous amplitude dip occurs between two adjacent bit slots when there is a phase transition. As a result the average power becomes minorly dependent to the bit pattern. However, this problem can be solved by using RZ format, which slices-out the instantaneous dip in the RZ modulator, and produces constant average power independent to transmitted bits. At the same average power, both methods produce a symbol separation of $\sqrt{2}$ times larger than OOK. Therefore, for the same symbol separation, only half the average optical power is needed. This is referred to as the 3 dB lower OSNR advantage of DPSK. Since the latter method does not introduce any chirp, it becomes the method of choice in our chromatic dispersion compensation experiment. At the receiver, a one-bit delay Mach-Zehnder Delay Interferometer (MZDI) is needed to perform phase-to-amplitude conversion, which enables a simple balanced direct detection to be implemented. Balanced detection produces electrical eye diagrams 3 dB higher in amplitude compared against single detection, which means that it allows the advantage of 3 dB lower transmitted OSNR of DPSK to be benefited from. The lower OSNR requirement of DPSK is useful to reduce the system optical power requirement or to extend the transmission distance.

2.1.2 Differential-Quadrature-Phase-Shift-Keying (DQPSK)

The next PSK system is Differential-Quadrature-Phase-Shift-Keying (DQPSK) [4, 11, 13]. The advantage of DQPSK is more towards increasing the spectral efficiency rather than the transmission distance. In this system two optical quadratures are used to carry the data, which allows transmission of two bits of data in every symbol duration. Thus, with the same number of WDM channels and symbol rate, transmission capacity and spectral efficiency are doubled. On the other hand, this system could also be used to relax the system tolerance towards fiber impairments. This could be achieved if a specified bitrate is transmitted at a reduced symbol rate by a factor of two. For example, 40 Gbit/s data can be transmitted at 20 Gbaud symbol rate, which has better tolerance to CD and PMD. The typical way to produce DQPSK format in the laboratory is by using a phase modulator together with Mach-Zehnder modulator (MZM). The output of MZM is fed into the phase modulator which introduced another $\pm \frac{\pi}{4}$ phase shift. This process produces 4 constellation points in the phasor diagram.

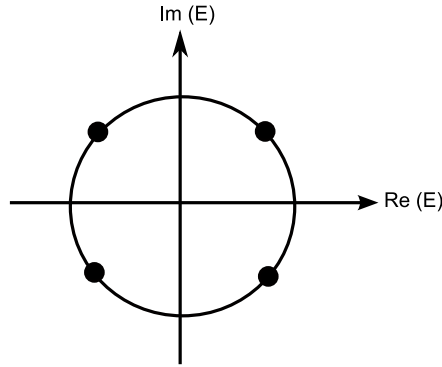


Figure 2.2: Phasor diagram of DQPSK

In real-world system, two independent MZMs are needed, where each of them modulates one data stream that is independent of each other. The phase of the output of one modulator is shifted by $\frac{\pi}{2}$ and coupled with the output of another modulator. The phasor diagram of DQPSK is depicted in Fig. 2.2. At the receiver, two MZDI are needed to demodulate the I and Q data separately. However, in laboratory experiment, one MZDI is sufficient. The phase difference between the two MZDI's arms is tuned to either $+\frac{\pi}{4}$ or $-\frac{\pi}{4}$ in order to recover both quadratures. The OSNR advantage of this system is only 1 to 2 dB in comparison to OOK, which is less than for DPSK.

2.2 Chromatic Dispersion (CD)

Chromatic dispersion (CD) is a pulse broadening phenomenon, which is caused by the interaction between the light pulse and the material used to manufacture the optical fiber. For every kilometer of fiber, the travelling pulses are affected by a specified amount of CD, resulting in pulse broadening. After some distance, the pulses become broad and overlap with adjacent pulses, which increases the zero level in the transmitted bits stream. As a result, the data can not be recovered by the receiver, and thus proper correction is required.

Let assume that a signal propagates along a transmission distance l with propagation constant β . The Taylor expansion of propagation constant, β about center frequency ω_0 can be written as

$$\beta(\omega) = \beta_0 + \beta_1(\omega - \omega_0) + \frac{1}{2}\beta_2(\omega - \omega_0)^2 + \dots \quad (2.1)$$

where β_1 is the inverse of Group Velocity, V_g , which is written as

$$\beta_1 = \frac{1}{V_g} \quad (2.2)$$

which unit is in $\frac{\text{second}}{\text{meter}}$. The signal Group Delay, τ can be calculated by multiplying Eq. 2.2 with transmission distance l as follows.

$$\tau = \beta_1 \cdot l = \frac{l}{V_g} \quad (2.3)$$

β_2 is the Group Velocity Dispersion coefficient, which is expressed as

$$\beta_2 = -\frac{\lambda^2}{2\pi c}D \quad (2.4)$$

where D is the fiber dispersion coefficient, λ is the optical carrier's wavelength, and c is the speed of light in vacuum. Eq. 2.4 can be rearranged to produce the CD coefficient D as

$$D = -\frac{2\pi c}{\lambda^2}\beta_2 \quad (2.5)$$

which is the signal group delay per unit spectral width, $\delta\lambda$ per unit distance l and expressed in $ps/nm/km$.

After transmission, the accumulated CD can be calculated by multiplying Eq. 2.5 by the transmission distance l . Accumulated CD is expressed as group delay, τ (ps) per unit carrier spectral width, $\delta\lambda$ (nm).

$$CD_{accumulated} = D.l = \frac{\tau}{\delta\lambda}(ps/nm) \quad (2.6)$$

Based on Eq. 2.6, we can see that the signal's spectral width determines the system's transmission limit. With the same amount of $CD_{accumulated}$, the signal with larger spectral width, $\delta\lambda$ experiences larger group delay, τ in comparison to the signal with narrow spectral width.

In WDM system, every optical carrier travels at different speeds. This is due to the wavelength dependence of the fiber refractive index. This phenomenon is represented by the fiber dispersion slope coefficient, S .

$$S = \frac{D}{\Delta\lambda} \quad (2.7)$$

where $\Delta\lambda$ is the WDM wavelength range. The unit of S is in $ps/nm^2/km$. The resulting total dispersion slope at the end of the transmission line is obtained by multiplying Eq. 2.7 with fiber length, l . The total dispersion slope value is different for different fiber types.

CD-induced pulse broadening results in overlapping between neighbouring pulses. Besides Inter Symbol Interference (ISI), in quasilinear systems, pulse overlapping also produces two intrachannel effects which are called Intrachannel Cross Phase Modulation (IXPM) and Intrachannel Four Wave Mixing (IFWM). These effects are discussed in the following Section.

2.2.1 Impact of pulse overlapping in 40 Gbit/s system

Chromatic dispersion (CD) lets neighbouring pulses overlap. As a result, in quasilinear systems, two effects are introduced which are called Intra-channel Four Wave Mixing (IFWM) and Intra-channel Cross Phase Modulation (IXPM). These two effects were demonstrated for the first time by Essiambre et. al. [37] where they were suggested as the limiting factors in high speed OOK Time Division Multiplexed (TDM) system. The eye diagrams illustrating both effects are depicted in Fig. 2.3. In Pizzinat et. al. [38] the nonlinear Schrödinger (NLS) equation was solved. By considering that the dispersion length is much shorter than nonlinear length, the nonlinearity was considered as a small perturbation in comparison to

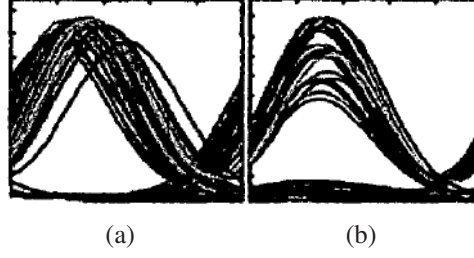


Figure 2.3: Eye diagrams of the signal affected by intrachannel effects: (a) IXPM, (b) IFWM [37]

linear distortion by CD. Assuming a solution in a form of $U_0 + \Delta U$, and replacing U_0 with $U_1 + U_2$, the equation for ΔU is obtained as shown in Eq. 2.8.

$$\begin{aligned}
 \frac{\partial \Delta U}{\partial z} + i \frac{\beta_2}{2} \frac{\partial^2 \Delta U}{\partial t^2} + \frac{\alpha \Delta U}{2} &= i\gamma |U_1 + U_2|^2 (U_1 + U_2) \\
 &= i\gamma [|U_1|^2 U_1 + |U_2|^2 U_2] + \\
 &\quad i\gamma [2 |U_2|^2 U_1 + 2 |U_1|^2 U_2] + \\
 &\quad i\gamma [U_1 U_2^* U_1 + U_2 U_1^* U_2] \quad (2.8)
 \end{aligned}$$

where U_1 and U_2 are the two adjacent Gaussian pulses, and ΔU is the small nonlinear induced perturbation. The right hand side of this equation is divided into three parts where the first, second and third part represent Self Phase Modulation (SPM), IXPM and IFWM respectively. Generally higher perturbation is experienced when the fiber nonlinear coefficient, γ is large.

SPM is defined as the phase modulation caused by the Kerr effect refractive index changes. This effect is induced by the interaction between the optical signal and Amplified Spontaneous Emission (ASE) noise, which contributes phase variations in transmitted pulses and causes pulse distortion. This is also an intrachannel effect and could be referred as ISPM. In PSK system, this factor influences the system performance and is known as a major contributor of Nonlinear Phase Noise (NLPN) [41, 42]. However, this effect is partly suppressed in a highly dispersed transmission system [54].

IXPM is an inter-pulses effect. It is a phase perturbation that occurs to a specified pulse, resulting from the phase of neighbouring pulses, in the same WDM channel. In OOK systems, phase modulation changes the frequency of the pulse which results in timing jitter. This timing jitter happens randomly and yields timing jitter variation. In PSK systems, apart from timing jitter it also introduces phase modulation which perturbs the phase of neighbouring pulses, resulting in phase variation. Since the data encoding of PSK system is based on the phase difference between subsequent bits, therefore, phase variation could possibly distort the signal. Regarding the timing jitter, it happens uniformly to all pulses due to uniform pulse intensity. Therefore, in contrast to the effect in OOK, no timing jitter variation is experienced in PSK systems. The beating of a pulse with the amplifier noise located at the center of the neighbouring pulses, which is also referred to as IXPM, induces similar effects as ISPM. Hence, both effects can be considered as the combined effect that contributes to NLPN [42].

Overlapping between adjacent pulses also introduces ghost pulses, which is known as IFWM [42, 44]. IFWM ghost pulses interfere with neighbouring pulses, cause the level of zero bits to increase and the amplitude of one bits to fluctuate. In quasilinear systems, IFWM-induced ghost pulses introduce extra eye closure to the signal, which is only caused by fiber attenuation, α and intersymbol interference (ISI) in linear systems. In multispans transmission, the IFWM effect is added coherently from one span to another. In Dispersion Shifted Fiber (DSF), when 1550 nm wavelength is considered, there is no performance degradation due to IFWM. This can be easily understood because no pulse overlapping is experienced. In NZDSF, ($D=4 \text{ ps/nm/km}$) IFWM effect is noticeable when the accumulated dispersion increases, but after one point, its increment rate reduces, and after a long distance of transmission, no more increment can be noticed. However, the system perturbation caused by IFWM is very minimum. In comparison to the combined effect of IXPM and ISPM induced NLPN, IFWM effect is considered insignificant [42].

The experimental investigation of these intrachannel effects on DPSK system was conducted by Gnauck et. al. [45]. The results were compared with those obtained in an OOK system. It was found that DPSK, especially when the RZ format was used, was more robust to IFWM and IXPM in comparison to OOK, even when using a single-ended detection. The performance was further improved when a balanced receiver was used. The performance improvement is due to reduced pulse energy in DPSK and correlation between the nonlinear phase shifts of two adjacent pulses [44]. Therefore, IXPM and IFWM effects, which contribute significant penalties to OOK systems, are not so pronounced in DPSK systems.

2.3 Chromatic Dispersion Management (CDM)

Chromatic Dispersion Management (CDM) is very important in high speed WDM transmission. After some transmission distance, the accumulated CD causes pulse distortion. However, the information carried is not lost and can be recovered if the distorted pulses are restored [22]. This is the role of CDM. In early days, Dispersion Shifted Fiber (DSF) was introduced to solve problems associated with CD. This fiber has zero dispersion at 1550 nm wavelength and works well in a single channel transmission. However when WDM is introduced, another problem surfaces, which is called Four Wave Mixing (FWM), an effect that generates two new frequency components around the original optical carriers, and create crosstalk to them. This effect is introduced when two or more optical frequencies stay in-phase for a significant distance [39]. In contrast to SSMF, which ensures that the phase of all WDM channels are decorrelated and thus suppresses FWM, DSF is unable to suppress FWM [40]. Therefore, this solution is not suitable in today's fiber optics network. Dispersion Compensating Fiber (DCF) is a popular solution to compensate the dispersion after every span. However in reconfigurable optical networks, where the wavelength changes its path, the accumulated dispersion always changes. These changes can not be managed by DCF because of its fixed dispersion and length. It means that another solution which allows dispersion tunability is necessary. In the last few years, tunable dispersion compensators (TDC) were introduced based on various technologies. This device complements the DCF solution beside introducing network design flexibility. In WDM systems, the dispersion map is shown to have a noticeable influence on the system performance [54, 50]. Earlier works suggested that symmetric dispersion map is the best solution for optimum perfor-

mance. However, recent works proposed more alternative solutions with better performance [59, 60].

2.3.1 Dispersion Compensating Fiber (DCF)

Dispersion Compensating Fiber (DCF) is a low cost conventional solution for CD compensation [51, 52, 53, 54], which is suitable for WDM systems. It has very good dispersion characteristics that follow the transmission fiber, which enable to reverse CD impairment. DCF is designed specifically for different transmission fiber types. The insertion loss of DCF is around 0.5 dB/km. This is relatively high, hence this fiber can not be included in the transmission fiber span. DCF has higher CD coefficient than transmission fiber, and with opposite sign, in the order of -80 ps/nm/km to -100 ps/nm/km. This fiber is normally prepared according to the dispersion value of the standard transmission fiber length. Therefore, the DCF length required is around 4 (SSMF) to 20 (NZDSF) times shorter than the transmission fiber, subsequently reduces the space required for installation. DCF is normally installed in the middle of double-stage EDFA. In contrast to SSMF, DCF core diameter is smaller. Therefore, it tolerates less input power before the effect of nonlinearity is suffered by the system. Thus, extra efforts are needed to monitor the DCF input power after the first stage of the double-stage EDFA in order maintain a good transmission quality. Normally complete dispersion and dispersion slope compensation in the network is nearly impossible because of the the length mismatch between transmission fiber and DCF. In term of slope compensation, modern DCF provides full band compensation, even though old versions can only provide around 60% to 70% slope compensation [18]. Beside implementing DCF as in-line and post-dispersion compensator, it may also be installed at the beginning of the transmission line as a pre-compensator. Dispersion pre-compensation is important to pre-shape the pulses before transmission, in order to increase the tolerance to non-linear impairments [56].

2.3.2 Tunable Dispersion Compensator (TDC)

Advances in Tunable Dispersion Compensator (TDC) technology have realized a number of commercial optical solutions for dispersion compensation. Popular technologies are virtual-image phase-arrays (VIPA) [25, 26], Gires-Tournois etalons [27, 29] and fiber Bragg gratings (FBG) [20, 21, 22, 23, 24]. Each technology has its own advantages and disadvantages which depend on the system requirements.

VIPAs utilize a combination of mirrors and lenses to control the propagation distance of the signal. By mechanically adjusting the optical path length, dispersion tuning is obtained. This technology is able to produce both positive and negative dispersion. It has medium tuning speed with fine tuning resolution. One main disadvantage is its narrow passband characteristic which is not suitable for broad spectrum signals in 40 Gbit/s systems.

Gires-Tournois etalon technology produces a TDC with active dispersion tuning, which is realized by varying the separation of etalon mirrors. Both positive and negative dispersion tuning can be achieved. By using multistages architecture, multi-channel flat top response can be realized. It has broader pass-bandwidth than VIPA, which made this TDC become a better solution for high bitrate system. Furthermore its tuning speed is also fast. However the insertion loss of the device is high. The tuning resolution is coarse due to

the inability to perform accurate fine separation of etalon mirrors. At the same time, the performance of this compensator is also highly temperature dependent.

The last technology discussed here is the fiber Bragg gratings (FBG) technology. This technology is a mature technology and has been used in many telecommunications applications. FBGs are reflection-based devices, created by modulating the refractive index of the fiber core by using ultraviolet light. Positive or negative chirp is introduced to the sampling period to produce a dispersion value which is opposite to the transmission line CD. FBGs introduce minimum insertion loss due to their all-fiber characteristic. The dispersion tuning is produced either by thermal control on linearly chirped grating [23] or mechanical stretching on non-linearly chirped grating. Today, all commercial TDCs based on this technology implement the former method which produces fine tuning resolution but slow response time. Similarly to previous technologies, this device is able to compensate both positive and negative dispersion. This feature is further discussed in Appendix L. One obvious advantage of FBG compared to the previously mentioned technologies is its high pass-bandwidth which is one of the important requirements for today's high bitrate fiber optics network. Another advantage of this TDC is its ability to provide high negative dispersion with minimum degradation from nonlinearity effect, which is not the case of DCF.

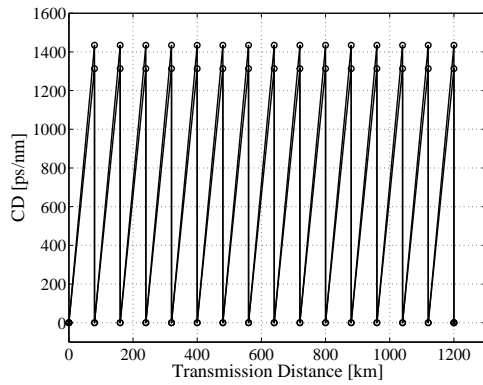
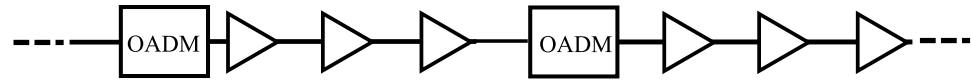
2.3.3 Dispersion map

In high bitrate WDM optical communication systems, designing a good dispersion map (DM) is important. Initially, the objective of DM design is simply to eliminate the accumulated CD in all WDM channels. To achieve this objective, DCFs with dispersion slope compensation are installed between the transmission spans. The transmission span's CD and dispersion slope are therefore compensated. However in quasi-linear transmission systems, the conventional DM is vulnerable to the resonance of XPM and FWM [50, 59], reduces the Phase Noise suppression by CD [54], and does not suppress nonlinear intrachannel effects [56]. Thus, better DM designs, which should consider the mentioned limiting factors, are required.

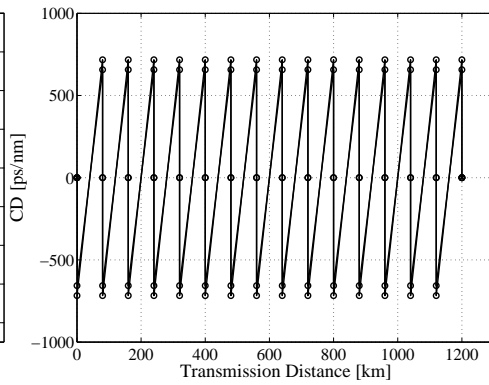
In this section several proposed dispersion maps are discussed, starting from the simplest symmetric DM to double period DM. The discussion is focused on the implementations of these maps in a reconfigurable fiber optics network. For all DMs, we assumed that the system implements fourty 100 GHz spaced WDM channels. The transmission spans consists of 80 km SSF. The value of inline- and pre-compensation are varied according to DM. Between two Add Drop Nodes (ADNs), five EDFA spans are located, producing 400 km ADN distance. The DMs discussed are presented in Fig. 2.4.

The simplest DM which is shown by Fig 2.4(a) implemented the DCF with exact compensation after every transmission fiber. This DM produces zero accumulated dispersion along the optical network, which simplifies the add-drop process. In a single channel long distance EDFA-supported transmission, this DM can reduce the distortion caused by Kerr nonlinearity effect [48]. However it was later on proven that this symmetric arrangement is vulnerable to the effect of modulational instability (MI) [49]. In WDM system, this DM is influenced by the resonance effect of XPM and FWM [50].

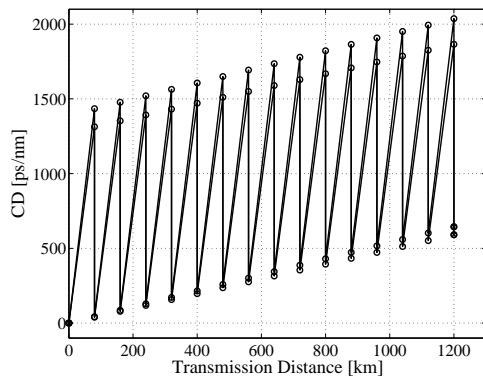
Dispersion pre-compensation is an important factor which needs to be considered in designing DM. This is because pre-compensation reduces the averaged pulse width over the



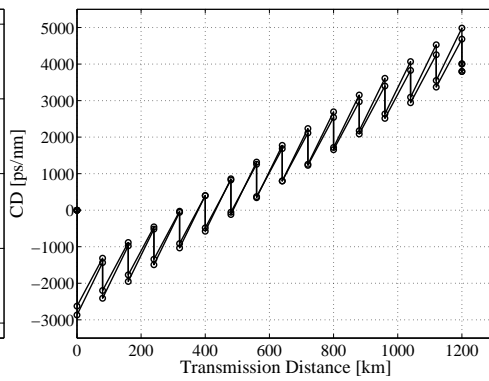
(a) Symmetric dispersion map (SDM)



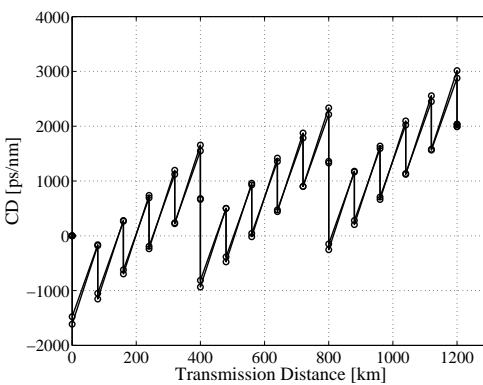
(b) SDM with dispersion pre-compensation



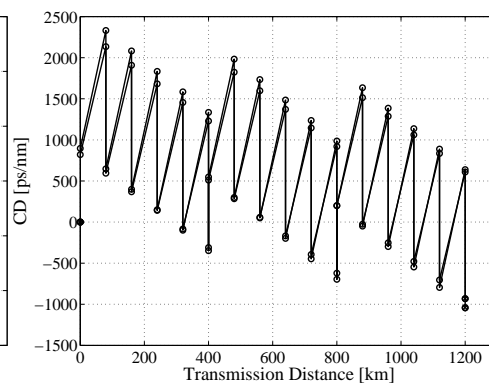
(c) 97 percent compensated spans



(d) 75 percent compensated spans



(e) Negative pre-compensation and reset



(f) Positive pre-compensation and reset

Figure 2.4: Various dispersion maps

span distance, and consequently delays the pulse overlapping occurrence, so that it happens at the low power fiber section. It was shown that pre-compensation can effectively reduce the effect of IFWM ghost pulses in Killey et. al. [56]. A pre-compensation value of around 25% of the transmission span's CD was shown to optimally reduce IFWM. 40% of pre-compensation was shown to contribute to bad system performance, which was also reported in Weinert et. al. [57], due to the creation of large IFWM ghost pulses. At the same time, by implementing pre-compensation, a periodic DM as shown in Fig. 2.4(b) might be produced. This map was shown to inverse the effect of IXPM at the output of every span [58]. However, concatenating several similar spans together between two ADNs results in a similar DM to Fig. 2.4(a). Therefore this DM is also exposed to the resonance effect of XPM and FWM.

In a highly dispersive systems, it was demonstrated that the effect of NLPN is reduced. However, the suppression of NLPN by CD is significantly reduced when the dispersion is fully compensated in every span. However, Green et. al. [54] showed that lump-dispersion compensation at the receiver produced better performance in term of NLPN suppression, but is not practically feasible when DCF nonlinearity is considered. A more practical DM was suggested by implementing only 97% of CD compensation in every span, which is depicted in Fig. 2.4(c). This DM performs better than 100% compensation case, which is due to the existence of residual CD at the amplification points. It is also less resonant than the previously discussed DMs. The formula explaining the relationship between phase variance and CD is included in Appendix G.

Based on the DM in Fig. 2.4(c), a DM with only 75% of CD compensation per span was analyzed by Vasilyev et. al. [50], which is shown in Fig. 2.4(d). In this DM, shorter DCFs are used for in-line CD compensation, which reduces the effect of fiber nonlinearity. At the same time, higher residual dispersion per span reduces the phase variance at every repeater side. This DM showed better performance than the DM with 97% of CD compensation. However, the slope of this DM is steeper than the previous DM. Therefore, higher post-compensation range are needed at every Add-Drop-Node (ADN), which is undesirable.

The four previously discussed DMs are referred as single period DM in Antona et. al. [59]. From all of them the DM similar to Fig. 2.4(d) is considered as the best single period DM. In the same reference, double period DMs were also discussed which are illustrated in Fig. 2.4(e) and (f). This strategy resets the CD of the last span in every ADN range so that the residual dispersion is minimum at every ADN. The DM in Fig. 2.4(e) is the improvement from Fig. 2.4(d) where reset at every ADN was implemented. This DM produces less residual CD at every ADN so that low tuning range TDC could be utilized for post-compensation. However, for inline dispersion compensation, it requires long DCF to be placed between every ADN spans which is a disadvantage in term of nonlinearity. As a solution, DM in Fig. 2.4(f) was introduced. This DM utilizes positive dispersion precompensation at the beginning of every span. In this DM, the accumulated residual dispersion is lower than the previous double period DM. In practical system the combination of positive and negative dispersion, which occurs at every ADN in this DM, could be replaced by a short DCF. This DM is totally non-resonant and provide 1 dB higher power margin compared to the best single period DM [59].

A more advanced way to manage CD in the network is by implementing Dispersion Managed Fiber (DMF) [53, 61]. DMF is a fiber which is design with either positive or negative CD and installed in a symmetric arrangement. In contrast to DCF, DMF with negative

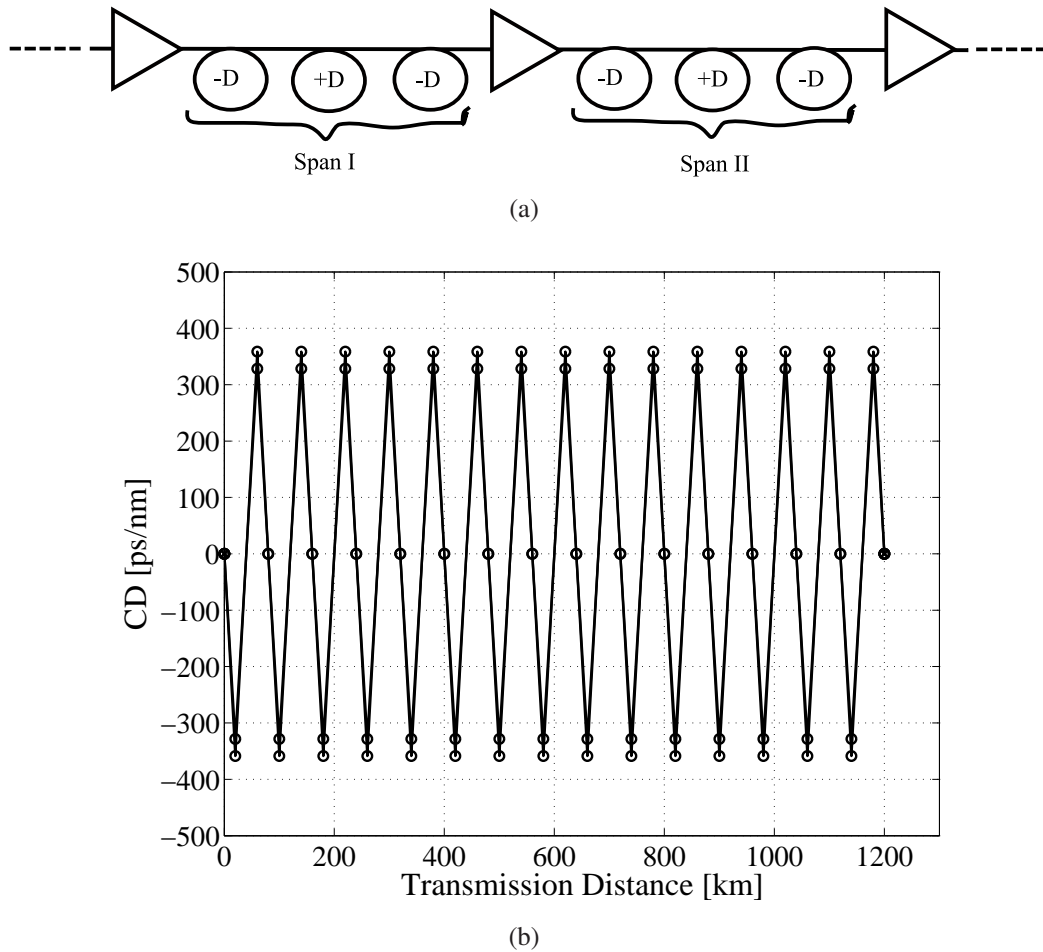


Figure 2.5: Transmission link with Dispersion Managed Fiber (DMF)

dispersion has lower attenuation and nonlinear coefficient (larger effective area). Hence, launching high input power into negative DMF will not produce high nonlinearity effect as in the case of DCF. Based on this characteristic, negative DMF can be included as transmission fiber. As a result, all the EDFAs needed to compensate DCF loss can be excluded, and this leads to the reduction of NLPN in long-haul transmission system. In Add-Drop networks, the channel could be added or dropped in the middle of the two negative DMF because of two benefits. Firstly, the dropped channel will have zero dispersion. Secondly, the added channel will experience sufficient dispersion precompensation. The example of DMF network and its DM is shown in Fig. 2.5. Successful experiment over 4000 km transmission distance that consisted of 200 km span DMF was demonstrated in Hagiwara et al. [62]. Detailed specifications of DMF are included in Appendix A.

2.4 Conclusion

This Chapter has discussed several important issues in dispersion management. Firstly, two asynchronous PSK systems were introduced, namely DPSK and DQPSK systems. The main

advantage of DPSK is its larger symbol distance compared to OOK, which can be exploited by balanced detection. For DQPSK, its advantage is mainly a high spectral efficiency, which is useful either to double the data rate of OOK or DPSK, or to increase the system tolerance to fiber impairments when transporting equal bitrate as OOK and DPSK. It is found that the latter advantage is more popular in the published literatures. The CD definition has been presented and the parameters which determine the system performance were highlighted. CD causes adjacent pulses to overlap. In quasi-linear systems, intrachannel effects namely IXPM and IFWM are introduced due to pulse overlapping. These two effects were shown by the literature to limit the OOK system performance. However, DPSK systems have higher tolerance to both intrachannel effects, especially IFWM. IXPM is considered as part of NLPN. Several dispersion management techniques were also introduced, which include the implementation of DCF, TDC and several conventional and advanced dispersion maps (DM). Apart from dispersion compensation, some of these DM are useful to reduce inter-channel and intrachannel nonlinear effects. It was also highlighted that the implementation of advanced dispersion maps may become a necessity in the future high speed and advanced WDM networks.

Chapter 3

DCF-based Dispersion Compensator

3.1 Introduction

Dispersion compensating fibers (DCFs) are important elements in today's optical fiber transmission systems, especially in long haul 10 Gbit/s [51, 53] and in any 40 Gbit/s systems [2, 4, 17]. They are used to compensate fiber dispersion which is no longer tolerable by the system after some transmission length. In Wavelength Division Multiplexed (WDM) transmission, different optical carriers experience different amounts of dispersion, depending on the transmission fiber's dispersion slope [21, 22]. In order to have a good transmission quality, only an acceptable amount of dispersion is allowed at the receiver side for all optical carriers. This amount depends on the system and modulation format used. Forward Error Correction (FEC) supported systems [63] can tolerate larger uncompensated dispersion compared to conventional systems. Symmetric dispersion maps [58], which result in equal dispersion for all optical frequencies at every repeater, were introduced to facilitate the dispersion compensation at the receiver side. However, the requirement of this system is very tight and not yet practical in today's installed optical fiber networks, where fibers with different lengths and types exist. Furthermore, as discussed in Chapter 2, this technique produces a Dispersion Map (DM) which is vulnerable to the resonance effect of Cross Phase Modulation (XPM) and Four Waves Mixing (FWM). In a reconfigurable optical network it is possible that in one transmission path, a signal passes through several types of fiber with different lengths. Depending on the network configuration, this path might change, and hence produces variation in accumulated residual dispersion. Tunable dispersion compensator (TDC) [20, 22] is therefore preferred to handle this variation.

The cheapest and easiest means of realizing a TDC is by using DCF. By arranging several short pieces of DCF in a reconfigurable way, several values of negative dispersion can be obtained, which is sufficient to compensate CD in a network with positive residual dispersion. In Section 3.2, the development and realization of a DCF-based TDC is explained. Optical switches are used to configure different dispersion compensation values, hence the term configurable is used instead of tunable. From this point onwards, the compensator is referred as Configurable Dispersion Compensator (CDC).

System tests conducted are reported in Section 3.3. All tests are conducted in a WDM DQPSK system with polarization division multiplexing [17]. This system is more sensitive to CD variations than conventional OOK or DPSK [13]. Thus, a proper CD compensation is

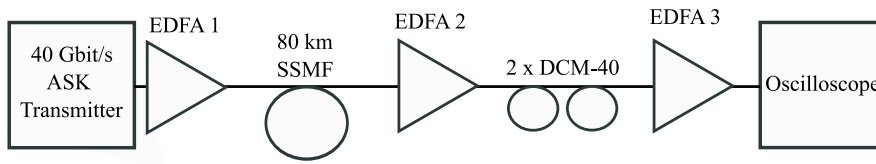


Figure 3.1: Experimental setup

important to produce good transmission quality. For an initial test, sixteen 100 GHz-spaced WDM channels were used to assess the compensator's tuning range and operation band. The experiment was conducted with several transmission span lengths in the range of 60 km to 100 km. The success of the first part of the experiment paves the way to increase the WDM channel count to 32 channels.

3.2 Development and Characterization

This Section discusses in detail the material characterization, device assembly, and also insertion loss and PMD characterization. The characterization stage of this study is important towards producing a reliable product. A comprehensive characterization record will assist the troubleshooting and calibration.

3.2.1 Device Development

The development process of this product is divided into three steps. Firstly, the raw material (DCF) was characterized to obtain its actual specifications. Based on these information, several short pieces of DCF were prepared, with lengths reflecting the required compensation values. Therefore, a reliable way of measuring DCF length is important. Finally, all the materials were assembled to produce a complete device.

3.2.1.1 Material characterizations

The raw material used is DCF that is designed for SSMF. The total dispersion value and the SSMF length which is represented by the DCF are specified. However, there is no information about the slope compensation ratio, the actual DCF length and the dispersion coefficient. These missing information is important for preparing several short pieces of DCF with different dispersion values. The DCF module (DCM) used was a DCM-20 (compensates 20 km of SSMF), with total dispersion value at 1545 nm wavelength of -343 ps/nm.

In order to know the DCF's dispersion slope, the dispersion values experienced by several different optical carriers are determined. The full experimental setup is depicted in Fig. 3.1. In this experiment, a 40 Gbit/s NRZ OOK transmission system with PRBS $2^7 - 1$ was used as a testbed with a tunable DFB laser source as the carrier. For the transmission line, 80 km SSMF was connected to two DCM-40s. The output signal was monitored on the oscilloscope. The first optical carrier acted as the reference, and the position of the received bits was marked as t_0 . Then, the tunable laser source was tuned to another optical frequency.

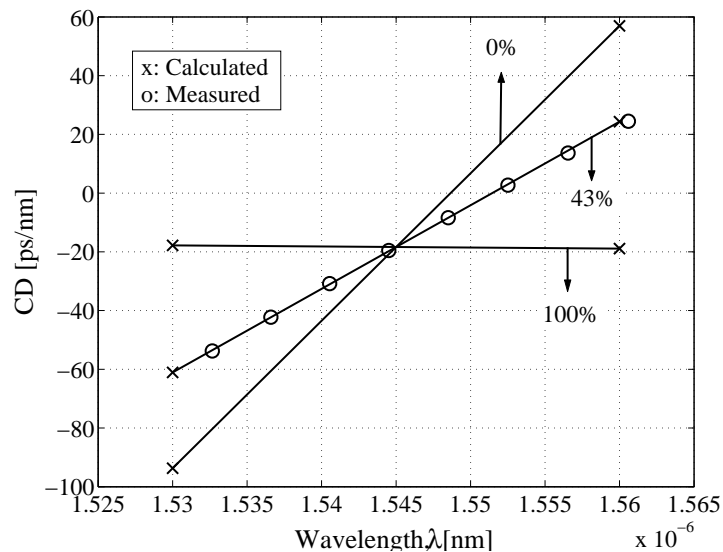


Figure 3.2: Slope compensation curves, \circ : measured, \times : simulated

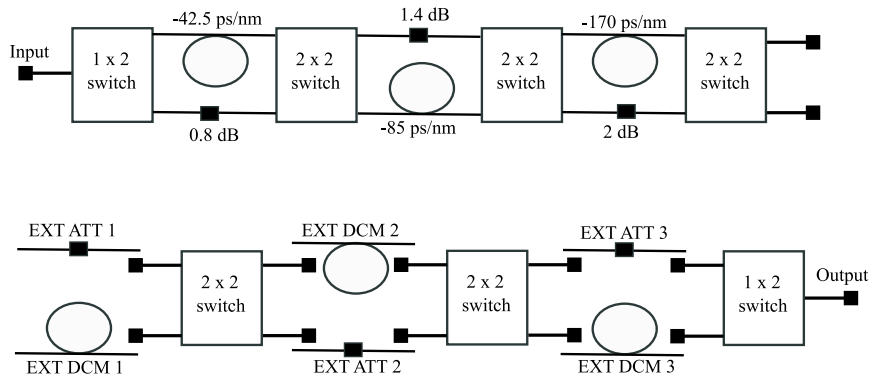
As the bit slot is only 25 ps, large tuning steps will cause the bit position to differ more than 127 bits (1 stream of bits), producing measurement errors. Therefore, the optical frequency changes should be very small to ensure that the bits-shift is always within the 127-bit window. For the second optical frequency, the bits stream arrives at the receiver at a different time, and marked as t_1 . Several more arrival times were measured in order to get sufficient data points. From these data, the dispersion slope for the whole transmission line is plotted in Fig. 3.2. The DCM slope compensation percentage is calculated by using the available SSMF dispersion slope. Apart from the measured data, the curves obtained from calculation, for 0%, 43% and 100% slope compensation are also presented in the same Figure. The curve of the measured data fit nicely with the calculated 43% slope compensation curve.

The loss of DCM-20s at 1550 nm wavelength ranges from 2.7 dB to 3 dB, and 4 dB loss for the DCM-40. The parameter which is left to be measured is the DCF length, so that the DCF dispersion coefficient can be calculated. This parameter will be measured after the DCF is coiled out from its original spool, which will be discussed in the next section.

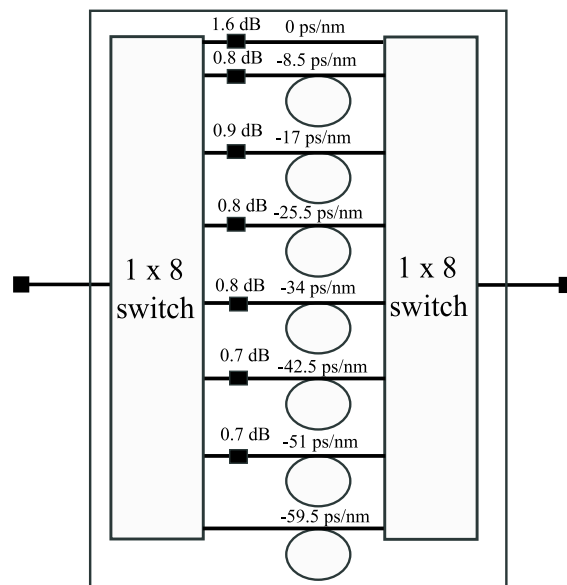
3.2.1.2 Material Preparation

The objective of this section is to prepare several short pieces of DCF reflecting the desired dispersion compensation values. Firstly, we need to refer the design and identify the requirements of CDC.

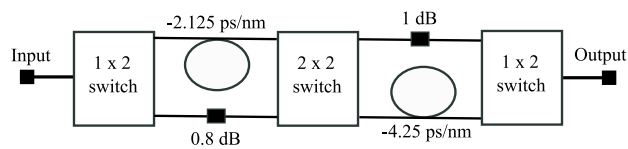
As depicted in Fig. 3.3, the developed CDC consists of three parts. The first part is designed for coarse residual dispersion compensation. The second part, offers smaller resolution, which is mainly prepared to fine-tune the dispersion in -8.5 ps/nm increment. In principle, this resolution is sufficient to support 40 Gbit/s system [67]. However, to be on the safe side, the third part was also designed, offering as small as -2.125 ps/nm resolution. Based on this information, the shortest and longest DCF needed are 125 m and 10 km respectively. The design of CDC architecture as shown in Fig. 3.3 was chosen due to the availability of optical switches.



(a) Part I



(b) Part II



(c) Part III

Figure 3.3: CDC design layout

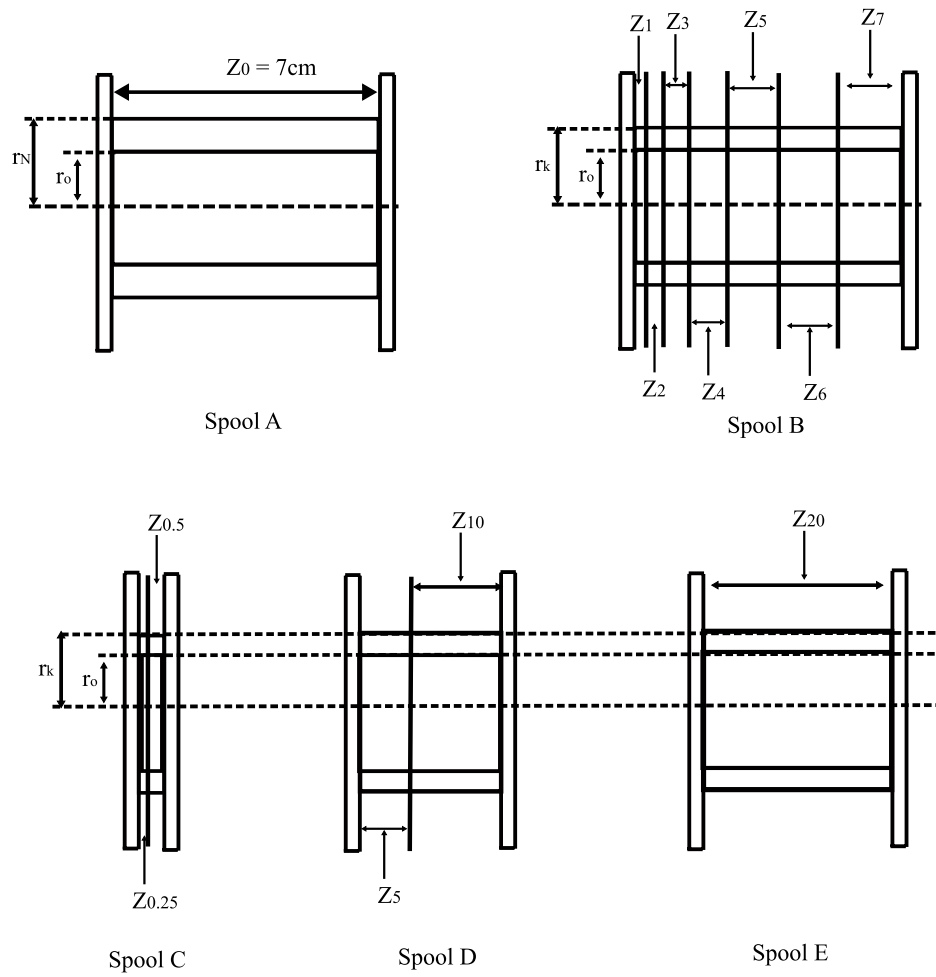


Figure 3.4: Several empty reels prepared for fiber winding

The next process is to measure the total DCF length in a DCM-20. As depicted in Fig. 3.4, several empty reels were prepared to produce a number of new fiber spools. The first reel is used to develop Spool A which consisted of all the fiber found in DCM-20. The DCF from DCM-20 was spooled out and rewound on this reel. By using a winding machine that is equipped with a turn-counter, the DCF was successfully coiled onto the new reel and the total turns were counted. The total number of turns, W is 10025. The radius of the innermost turns, r_o and the outermost turns, r_N are 55.3 mm and 71.5 mm respectively. This are important information which needed to calculate the total DCF length.

The exact DCF length is difficult to calculate, therefore, only the best approximation is used. Fig. 3.4 provides the assistance to understand the approximation made. Let say the total DCF length is L , which could generally be represented as

$$L = \sum_{n_w=1}^W L_{n_w} \quad (3.1)$$

with L_{n_w} is the DCF length for every turns. From Fig. 3.4, it is obvious that the turn radius increases with turn counts. For simplicity, we assume that for every turn, the radius r increases by $\frac{n_w}{W}(r_N - r_o)$, where n_w is the number of turns corresponding to a specified

length, and W is the total number of turns. The radius of the innermost turn, r_o differs from the outermost turn, r_N . The radius difference, Δr depends on the reel length, Z . When two reels with different Z are compared, the same fiber length produces smaller Δr in the reel with larger Z .

DCF length for every turn is

$$L_{n_w} = 2\pi r_o + \frac{2\pi n_w}{W}(r_N - r_o) \quad (3.2)$$

Eq. 3.2 is inserted into Eq. 3.1, and $\pi(r_N - r_o)$ is assumed to be very small in comparison to L , the total length is approximately

$$L = \pi W(r_N + r_o) \quad (3.3)$$

From Eq. 3.3, a total DCF length of 3.995 km is obtained. With the total dispersion value of -343 ps/nm, the resulting dispersion coefficient is -86 ps/nm/km. This value is within the standard DCF specification (-80 ps/nm/km to -100 ps/nm/km), and validates the approximation derived.

The next step is to coil the DCF onto the actual reels to produce several DCF spools with different fiber lengths. For this purpose several empty reels were prepared as shown in Fig. 3.4. Every reel has different value of Z to accommodate different fiber lengths.

Firstly, we discuss the preparation of Spool B. From the design, we know that the dispersion of this part must be configurable from -8.5 ps/nm (0.5 km SSMF) to -59.5 ps/nm (3.5 km SSMF) with -8.5 ps/nm increments. Therefore, the shortest fiber which needs to be coiled onto the reel correspond to 0.5 km of SSMF and is around 0.099 km of DCF. This SSMF length was used as a reference, and all other required fiber lengths were divided by this value to produce the length factor, n . A reel with Z_0 long (7 cm) was prepared, and divided into 7 parts, which are referred as divisions, D_n as shown in Fig. 3.4. The value of Z_n for every D_n is

$$Z_n = n \left(\frac{Z_0}{28} \right) \quad (3.4)$$

By calculating Z this way, we have produced all D_n with the same outermost radius. We named the part with the smallest Z as D_1 with the length of Z_1 , and used it as the reference. DCF was then coiled onto the second reel, knowing that only around 70% of DCF found in Spool A is needed to produce Spool B. Since Spool B has the same total Z as Spool A but different L , the value of the outermost turn radius differs from Spool A, as shown in Eq.3.2. This outermost radius is referred as r_k , where $r_o < r_k < r_N$.

Now the method to estimate the fiber length, L will be discussed. Here L is estimated by counting the number of turns made when coiling the fiber onto the reel. For a fiber spool with r_N we can write the fiber length as a function of total fiber turns, w as follows.

$$L(w) = \pi(r_N + r_o)w \quad (3.5)$$

For Spool B, the radius of the outermost turn is r_k . Therefore Eq. 3.5 can be rewritten as

$$L'(w) = \pi(r_k + r_o)w \quad (3.6)$$

with $L'(w)$ representing the actual DCF length for a given dispersion value.

At this point, radius r_k is still an unknown value. Let say the total fiber's volume in Spool A, V_A is

$$V_A = \pi(r_N^2 - r_o^2)z \quad (3.7)$$

We know that this spool represents 40 D_1 . Out of that, 28 D_1 were taken out and coiled onto Spool B with radius r_k . V_B can be written as

$$V_B = \pi(r_k^2 - r_o^2)z \quad (3.8)$$

And we know $V_B = \frac{28}{40}V_A$. Eq.3.7 and Eq.3.8 are manipulated to produce

$$r_k = \sqrt{\frac{7r_N^2 + 3r_o^2}{10}} \quad (3.9)$$

In our case the value of r_k is around 67.0 mm. This value was inserted into Eq. 3.6 and the result is rearranged by including D_{SSMF} (17 ps/nm/km), D_{DCF} (-86 ps/nm/km) and L_{SSMF} to produce the number of turns, W required for the the given distance of SSMF as

$$W(L_{SSMF}) = \left(\frac{-D_{SSMF}}{D_{DCF}(r_k + r_o)\pi} \right) L_{SSMF} \quad (3.10)$$

By using Eq.3.10, Spool B was prepared. For this part of the compensator the smallest CD value was fixed at -8.5 ps/nm (0.5 km SSMF or 0.099 km DCF), which was placed in D_1 . For D_2 the CD was fixed at -17 ps/nm. With -8.5 ps/nm increment, the last part consists of -59.5 ps/nm CD (3.5 km SSMF or 0.699 km DCF). In total, 2.796 km of DCF was utilized to build this part of the compensator, which is able to compensate 0.5 km to 3.5 km SSMF.

The preparation of the next two parts follows the same steps stated above. From the remaining DCF, Spool C was prepared. This spool consists of two parts. The dispersion values are equivalent to the negative dispersion of 0.25 km (-4.25 ps/nm) and 0.125 km (-2.125 ps/nm) SSMF. The third part was divided into two spools, namely Spool D and Spool E. For these Spools, another DCM-20 was utilized. Spool D consisted of two parts to accomodate the DCF which compensates 2.5 km and 5 km of SSMF. Finally, Spool E was developed with the dispersion value of -170 ps/nm (10 km of SSMF). The number of turns for all spools together with the fiber length and corresponding dispersion are shown in Appendix B. The remaining DCF are 0.879 km (4.395 km SSMF) on the first DCM-20 and 0.5 km (2.5 km SSMF) on the second DCM-20.

3.2.1.3 Device Assembly

This section discusses the device assembly. From the CDC design presented in sect. 3.2.1.2, it is concluded that three types of optical switches are required, which are 1x2 and 2x2 switches (for Part I and Part III), and 1x8 switches (for Part II).

Table 3.1: Insertion loss for all CDC Parts measured at 1550 nm wavelength

CDC Part	Insertion Loss, IL (dB)
I	6.5
II	4.0
III	3.0

ETEK optical switches were used. The response time of this switch is less than 10 ms. For 1x2 and 2x2 switches, the insertion loss is around 0.3 dB. For 1x8 switch, around 1 dB loss was measured. Two 1x8 optical switches were placed in a single housing. The fact that they work together to select one of the seven DCF sections from Spool B, therefore, this arrangement is very convenient. Spool B was also placed inside the same housing. The single fiber port of both 1x8 switches were assigned as input and output port. For the other CDC's parts, the 2x2 switches were used so that the DCF can be selected in binary manner.

Referring to Fig. 3.3 the DCF pieces were spliced. For Part I and III, attenuation splices (a splicing method which produces lossy connection [66]) were performed in the branches without the DCF. The splice loss was equalized to the loss of the DCF in the parallel branches. For Part II the attenuation splice was used to connect the DCF to the switches, and the loss of all paths were equalized. This loss equalization ensures that the insertion loss of the compensator will stay the same and independent of dispersion values.

3.2.2 Insertion Loss Characterization

Before all CDC parts are assembled, their insertion loss (IL) were measured and presented in Table 3.1. As shown, the IL of all parts are quite large. If all parts are connected together, the resulting IL is 13.5 dB, which is comparable to the loss of 80 km SSMF. Without including any additional external DCF in the CDC, all parts can be directly connected together. However in order to increase the compensation range, external DCFs are necessary. Initially, two DCM-20s were installed with each DCM contributing around 2.8 dB loss. These additional DCMs increased the IL of Part I to around 12 dB. By assuming the DCF launched power of -5 dBm/channel, which is necessary to reduce the effect of fiber nonlinearity, the resulting output power of Part I is -17 dBm/channel. This power level is considered low in 40 Gbaud system and therefore amplification is necessary before the signal is passed through the next CDC stages. By including only two external DCM-20s, the CDC parts were arranged in a way depicted in Fig. 3.5. The amplified signal was attenuated to -5 dBm/channel before entering Part II and Part III. However when another external DCM is installed in Part I, for example DCM-20, the IL increases by another 2.8 dB, which reduces the input to the subsequent EDFA to around -20 dBm/channel. This power is too low for amplification. The simplest way to solve this problem is to increase the input power of Part I as much as the IL introduced by the external DCM. This solution exposes the system to the effect of fiber nonlinearity, which is mainly the disadvantage of DCF-based dispersion compensator, beside its large IL and size.

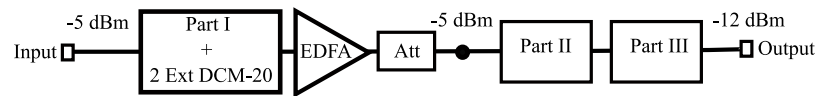


Figure 3.5: CDC arrangement with two external DCM-20s

3.3 Transmission Experiments

In this Section, the transmission experiments are presented, which are important to explore the potential and limitation of the CDC. The main objective of developing CDC is to enable channel-by-channel dispersion compensation by using a single device. Therefore, its capability in a multi-channel system need to be tested up to the limit, which should cover its performance at different optical frequencies and dispersion compensation values. A WDM comb is essential for this test. Basically, the main building block for this test are the WDM system (transmitter and receiver), the transmission line and the CDC. The testbed is explained further in the following section.

3.3.1 Testbed

The testbed used for accessing the CDC performance employs a system consisting of 100-GHz-spaced WDM channels with 160 Gbit/s DQPSK and Polarization Division Multiplex (PolDM). Detailed description of WDM transmitter and receiver are presented in Appendices J and K respectively. In this system, the symbol rate is 40 Gbaud. However, 2 bits (1 bit per quadrature) are transmitted in every symbol, which is carried by two orthogonal polarizations. Therefore, for every optical frequency, a total of 160 Gbit/s is transmitted. At the receiver, the polarizations are demultiplexed. This is followed by a DQPSK receiver, which recovers the two quadratures. The testbed is schematically depicted in Fig. 3.6. In this testbed, although only one modulator is used for data modulation, due to the MZDI used to produce DQPSK, all WDM channels have at least one neighbour with different polarity bit pattern [17], and hence the WDM interchannel effects can be tested. This made the system practical to represent a real system.

The experiments were performed in the C-band. First, the CDC was tested in a 16 channels 100-GHz-spaced WDM system (192.2 THz (1559.79 nm) to 193.7 THz (1547.72 nm)). Then its potential was fully tested to compensate the dispersion in the full C-band (192.2 THz (1559.79 nm) to 195.3 THz (1535.04 nm)). In all experiments, the performance parameters measured are the BER and the eye diagram. In today's advanced high capacity transmission, Forward Error Correction (FEC) [63, 64, 65] is normally implemented to improve the system performance. In this experiment a third generation FEC [4] is considered, which has the capability to improve the system with the BER of 3.9×10^{-3} or Q-factor of 8.5 dB to error free transmission with 7% overhead bits.

3.3.2 16 channels WDM transmission

In the first experiment, 16 WDM channels were used with optical frequencies ranged from 192.2 THz to 193.7 THz. At the receiver, an optical switch was placed after the Demul-

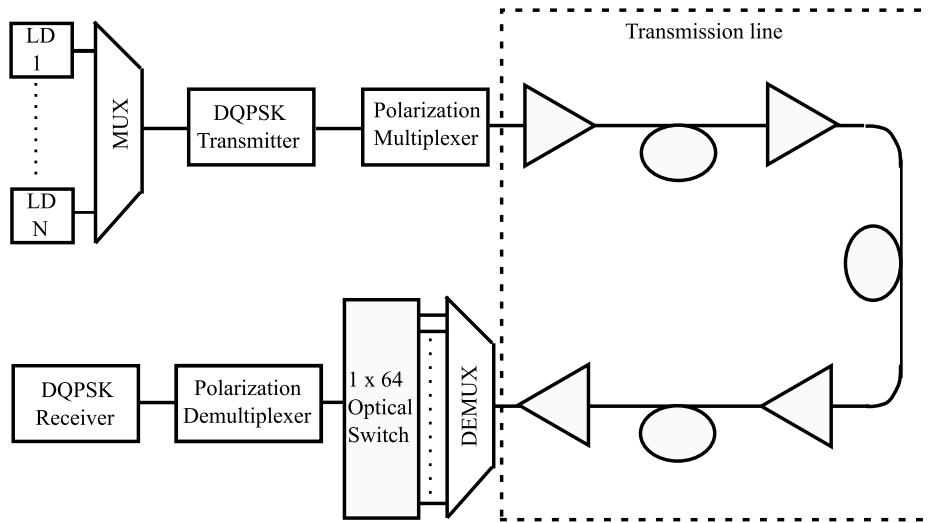


Figure 3.6: Schematic representation of the testbed used for transmission experiment

plexer. The single fiber output was connected to the CDC for dispersion compensation. At a time, only one channel was compensated as explained in Appendix K. The dispersion compensated signal was fed into the receiver block for quality assessment.

The transmission line was composed from SSMF and Non-zero Dispersion Shifted Fiber (NZDSF). In-line dispersion was compensated by Dispersion Compensating Module (DCM). The detailed parameters of the optical fibers are listed in Appendix A. In order to represent the real WDM optical network, fiber spans with different fiber types and lengths were employed. During this time, only a total of 273 km fiber was available. With a single fiber type for each span, four spans of around 60 km to 81 km were prepared. The span distances were within the range of standard transmission span in the field. The span's input power per-channel was limited to 0 dBm.

The fiber arrangement in the transmission line is depicted in Fig. 3.7. As can be seen, the transmission line consists of four spans with alternating SSMF and NZDSF. The first span was developed by 60 km NZDSF, followed by two pieces of DCMs (DCM-20 and DCM-45). At the end of this span, the dispersion for the outermost optical frequencies are negative. The second span consisted of 81 km of SSMF and two DCMs (DCM-20 and DCM-40). The third span was realized by using 60 km NZDSF followed by the same sequence of DCM as the second span. Finally, the last span was built from 72 km of SSMF. The dispersion map of this transmission link is shown in 3.8. It can be seen that there is residual dispersion of +100 ps/nm at 192.2 THz channel and -50 ps/nm at 193.7 THz. This means the positive residual dispersion does not exceed the CDC tuning range. Hence, in this experiment, external DCF is not necessary. For compensating the negative residual dispersion, short pieces of SSMF were used.

Fig. 3.9 shows the dispersion slope after 273 km fiber, and dispersion compensation of the middle-band and the two outermost WDM channels. This figure will explain on how CDC compensates the dispersion of all WDM channels. However, in Fig. 3.9, we only

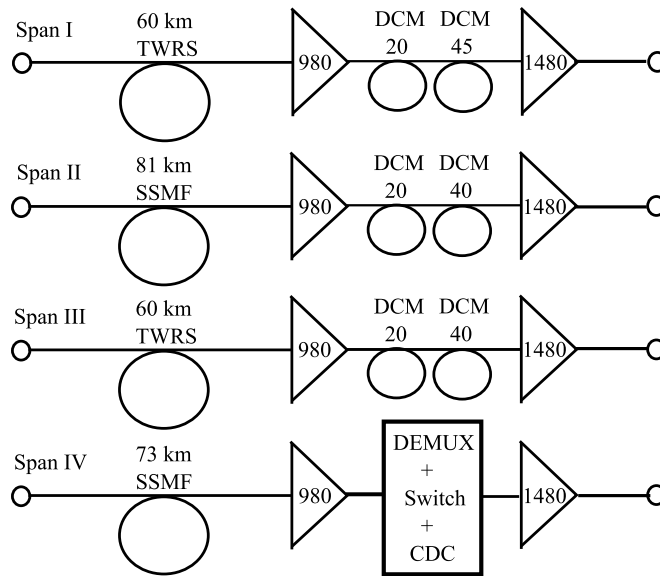


Figure 3.7: Four spans transmission line.

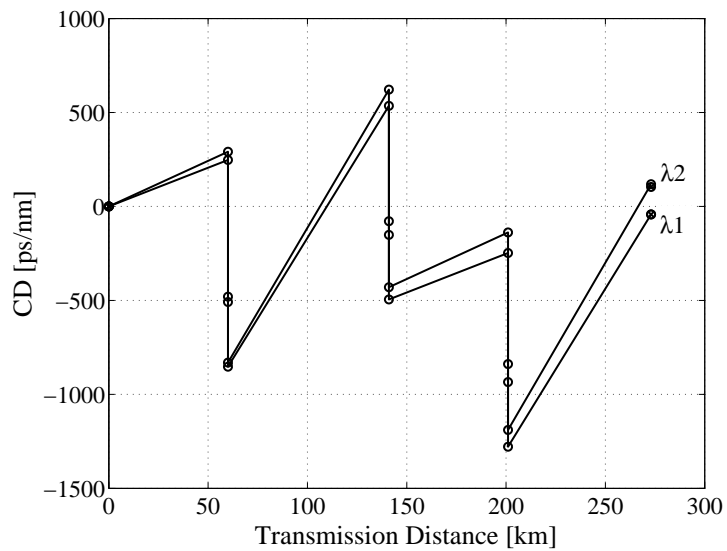


Figure 3.8: Dispersion map of four spans 16 channels WDM transmission.

show how CDC works on three WDM channels (two outermost channels, and middle-band channel). This information is sufficient to represent all other WDM channels. The most left points on every curve represents the reference wavelength of CDC (1545 nm). When setting the compensation values, we always refer the dispersion of this reference wavelength. By analysing the curve obtained after 273 km fiber, we can see that the residual dispersion in λ_2 and the middle-band λ are positive. The dispersion compensation within the range of -100 ps/nm to -30 ps/nm were applied to compensated the dispersion of WDM channels located between these two wavelengths. These are not the exact dispersion values at each λ . Instead, it is the dispersion value of the 1545 nm channel. The exact values are -104 ps/nm and -30.5 ps/nm respectively. The dispersion slope of both compensated channel are illustrated by curves 2 (the middle λ) and 3 (λ_2) in Fig. 3.9. To compensate the residual dispersion in λ_1 channel, 3 km SSMF was placed after the last EDFA and before the CDC. As a result, the dispersion slope is shifted up (top curve in Fig 3.9). Then the dispersion of this channel was compensated by setting the CDC to -10 ps/nm, corresponding to the actual value of -11 ps/nm at λ_1 . The dispersion slope when λ_1 is compensated is represented by curve 1 in Fig. 3.9. In that curve, the dispersion of λ_1 is zero. From the same figure we can also learn that the CDC can only compensate the dispersion of one specified wavelength, but not the dispersion slope. Regarding the extra SSMF, it was added after the last EDFA, thus, it can not be included as transmission distance. After transmission and CD compensation, the BER of the received data for all WDM channels were recorded channel-by-channel and the result is shown in Fig. 3.10. We can see that the best and the worst BER are 1×10^{-5} and 8×10^{-4} respectively. These values are better than the FEC threshold. Therefore, with the raw transmitted capacity of 2.56 Tbit/s, we have achieved the net transmission capacity of 2.38 Tbit/s over a transmission distance of 273 km. The net capacity is calculated by deviding the raw capacity by 1.07 (42.7/40).

The eye diagrams of the received signal of one of the quadrature channels in both polarizations are shown in Fig. 3.11. These are the eye diagrams after 273 km fiber and dispersion compensation. The eye openings are clearly visible, which indicate that the dispersion compensation is satisfactory. However, in our experiment, other possible deteriorating factors such as interchannel crosstalk and phase noise were not compensated, which could be the reason of non-error-free transmission. The results of this experiment proved to us that the low-cost CDC is capable to compensate the residual dispersion of the standard transmission span in advanced modulation format WDM systems.

The experiment on 16 channels WDM transmission was continued by using 100 km span length [55]. In this experiment the span launched powers were increased to compensate for the extra loss introduced by additional fiber length. The span input power ranged from +3 dBm to +7 dBm. As shown in Fig. 3.12, every span is around 100 km long. The first span consists of 41.5 km SSMF and 60 km TWRS (NZDSF) resulting in a 101.5 km transmission distance with around +900 ps/nm of accumulated CD. This span is followed by two DCM-40 with around -1368 ps/nm comepasating dispersion. The second span was built from 97.7 km SSMF with accumulated dispersion of +1660 ps/nm, and followed by two DCM-20s and one DCM-45 (total CD of -1440 ps/nm). The last span was developed from 32.2 km SSMF and 60 km TWRS, producing 92.2 km transmission distance with accumulated CD of around +730 ps/nm. As a result, three spans were developed with total distance of 292 km. The complete dispersion map is shown in Fig. 3.13.

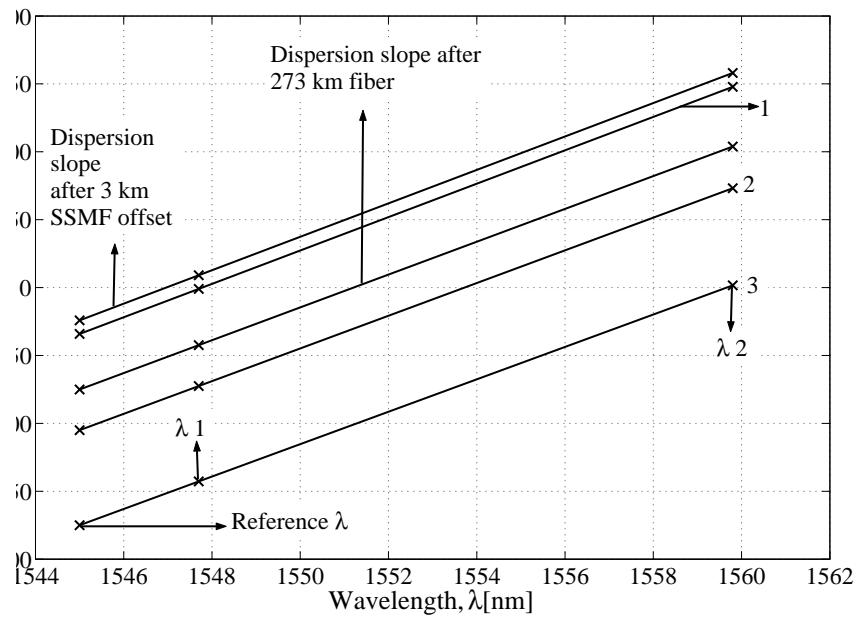


Figure 3.9: The residual dispersion for the outermost wavelengths after transmission, and dispersion compensation (curve 1,2 and 3 are the dispersion slope after the CD compensation of λ_1 , middle-band λ and λ_2).

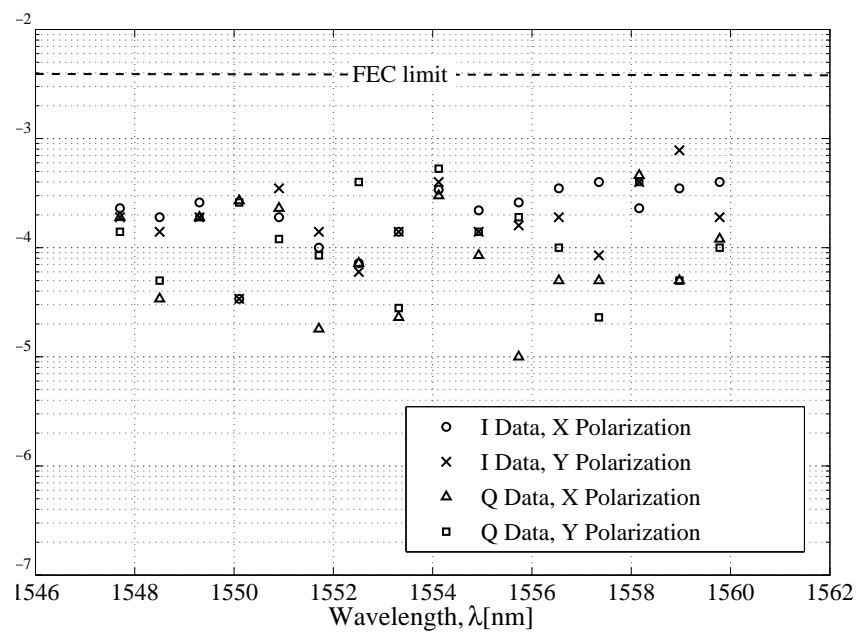


Figure 3.10: BER after 273 km fiber and dispersion compensation.

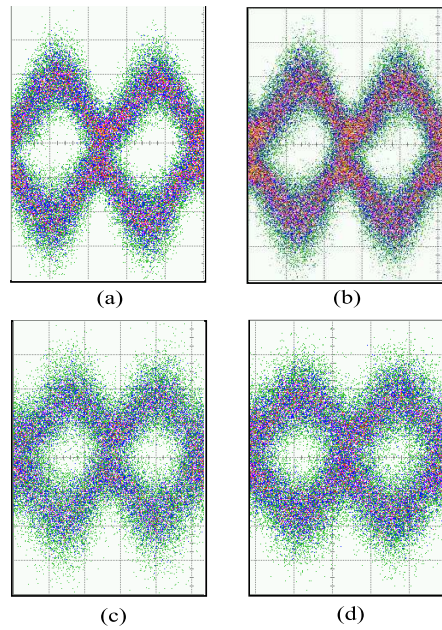


Figure 3.11: Eye diagrams for I channel in both orthogonal polarizations: (a) Back-to-back (first polarization), (b) Back-to-back (second polarization), (c) After 273 km (first polarization), (d) After 273 km (second polarization)

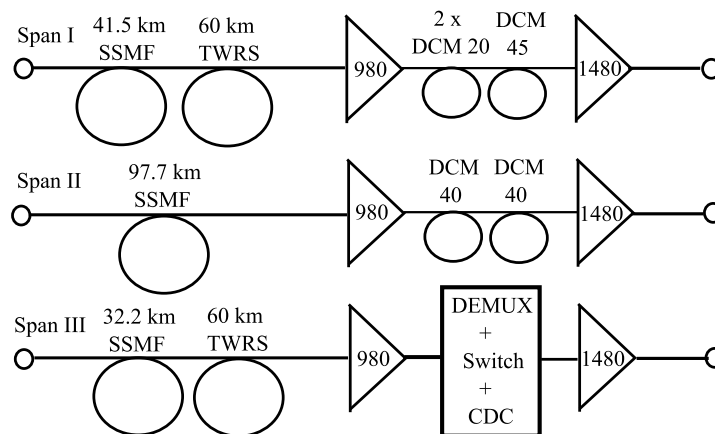


Figure 3.12: Three spans transmission line.

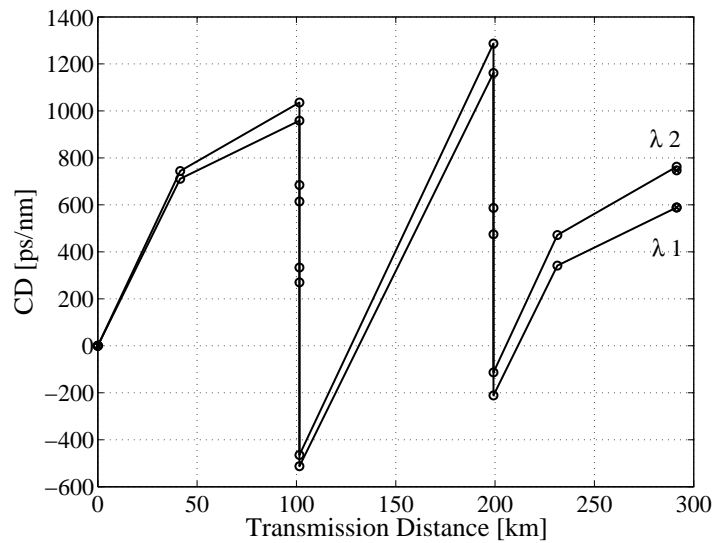


Figure 3.13: Dispersion map of three spans 16 channels WDM transmission.

From Fig. 3.14, it can be seen that the residual dispersion after transmission are +588 ps/nm at λ_1 and +747 ps/nm at λ_2 . In comparison to the first experiment, the transmission line in Fig. 3.12 has produced higher accumulated dispersion in both outermost carriers. This is because from the setup in the previous experiment, around 18.4 km of SSMF were added that carried around +313 ps/nm CD, while one DCM-20 was taken out. The DCM-20 was taken out to partly reduce the nonlinearity effect in this high power transmission setup. As mentioned before, referring to 1545 nm wavelength, the total negative dispersion in CDC is only -363.375 ps/nm. Therefore, two external DCM-20s were inserted to ensure that +730 ps/nm (at 1545 nm) CD can be compensated.

Fig. 3.15 and Fig. 3.16 depict the performance of the transmission. The BER degrades compared to the first experiment. The average BER is around 1×10^{-3} with the worst BER of 2.4×10^{-3} . This performance resulted from firstly, lower OSNR of the amplified and received signal. At the same time, higher nonlinearity was introduced by high negative dispersion found after each long span, and also high transmitted power per channel. The eye opening is sufficient to produce error-free performance after FEC operation. Therefore, we have successfully achieved a capacity x distance of $16 \frac{Tb}{s} \cdot km$ per span in a 292 km transmission system.

3.3.3 32 channels WDM Transmission

In the previous section, the CDC was tested by using only approximately half of the C-band's channel capacity. In this section, another 16 WDM channels are added, therefore nearly full C-band optical frequency can be tested. The optical frequencies ranged from 192.2 THz to 195.3 THz. The last channel (195.3 THz) was very near to the ASE peak (ranges from 195.4 THz (1534.29 nm) to 196 THz), which is the noisy band. In the setup, the EDFA installed after CDC was designed without the ASE filter. As a result, the amplified signals within this band will be affected by higher EDFA noise. After amplification, the OSNR value of these signals are lower than the signals outside this noisy band. Considering

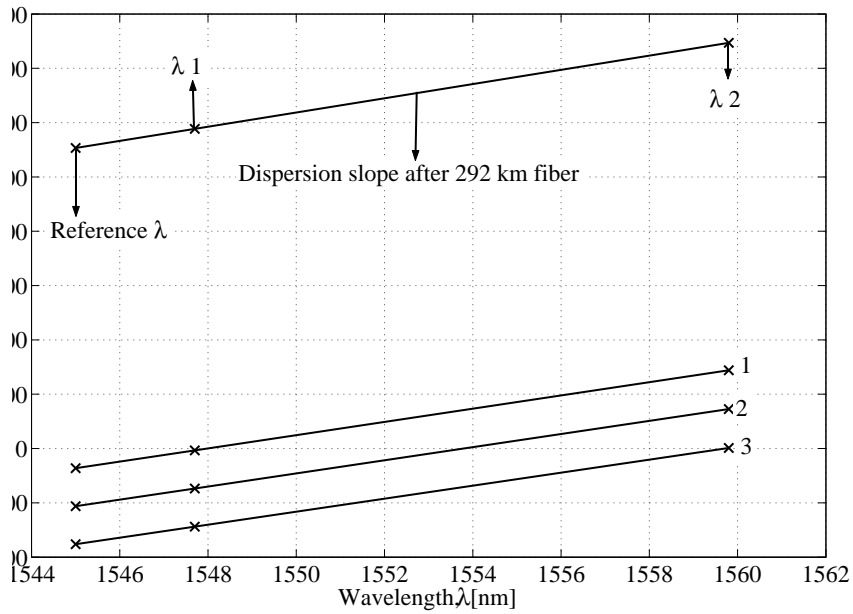


Figure 3.14: The residual dispersion for the outermost wavelengths after transmission, and after compensation (Curve 1,2 and 3 are the dispersion slope after the CD compensation of λ_1 , middle-band λ and λ_2).

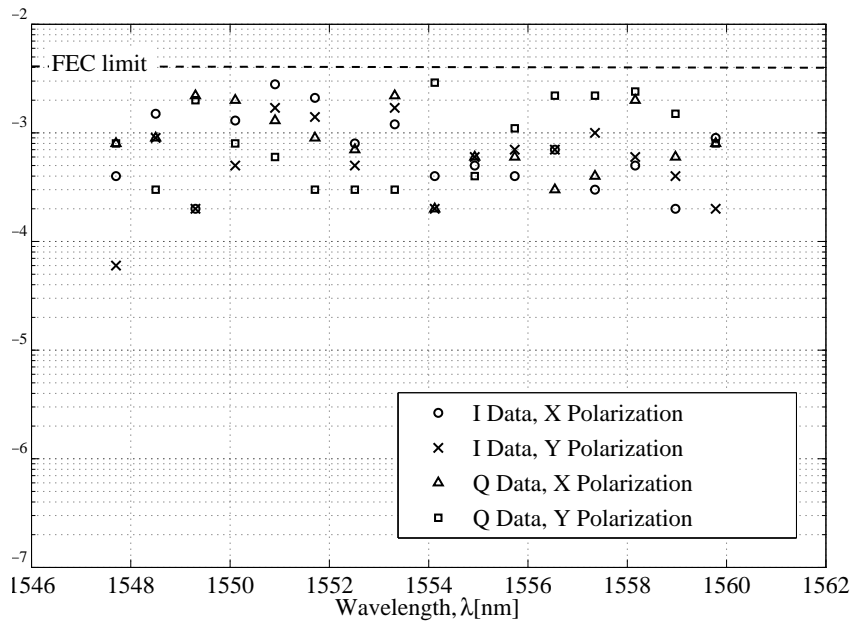


Figure 3.15: BER after 292 km fiber and dispersion compensation

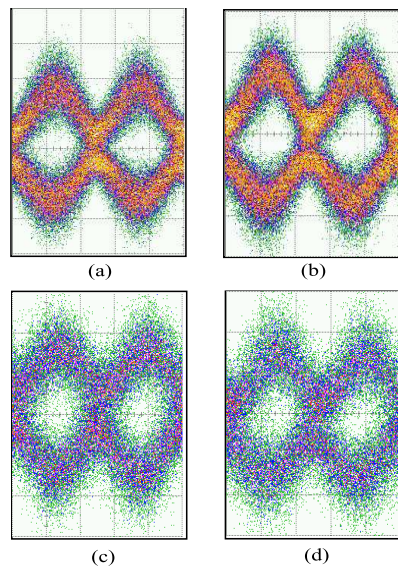


Figure 3.16: Eye diagrams for both I and Q channels in one polarization: (a) Back-to-back (I), (b) Back-to-back (Q), (c) After 292 km (I), (d) After 292 km (Q)

this factor, we decided that the performance of the channels inside this noisy band can not provide fair comparison against the other WDM channels. Due to this reason, in our setup, the WDM channels inside this noisy region were not used.

Fig. 3.17 illustrates the transmission line with 32 optical carriers. The transmission fibers are 81 km SSMF for the first span, 80 km NZDSF (20 km LEAF + 60 km TWRS) for the second span, the combination of 41.5 km SSMF and 40 km TWRS for the third span, and 20 km SSMF plus 60 km TWRS for the last span. In term of transmission distance, this setup provided nearly uniform spans distance of around 80 km with total distance of 323 km. Dispersion pre-compensation was used in this experiment. A DCM-40 was installed before the booster, which resulted in -684 ps/nm of dispersion pre-compensation.

The dispersion map is shown in Fig. 3.18. Compared to Fig. 3.8 and Fig. 3.13, it is observed that the dispersion difference between the two outermost λ is two times larger than in both 16 channels experiments, around $+400$ ps/nm. Due to additional fiber length, the residual dispersion increased. However, because of the large pre-compensation before the transmission, only as large as -550 ps/nm (at 1545 nm) of post-compensation was needed. This compensation value can be offered by the CDC setup that was used in the last section. In contrast to the uniform loss in every span, the dispersion map produced by this setup is not symmetric. This resulted in nonuniformity in dispersion pre-compensation at the beginning of every span. It can be noticed that there exists as little as -50 ps/nm at one point compared to as much as -500 ps/nm at another point. As shown in Killey et. al. [56] this is not an optimized dispersion map, which efficiently suppresses the IXPM effect.

As shown in Fig. 3.19, after 323 km transmission distance, the dispersion slope is around $+16.28$ ps/nm². This is considered as a high residual dispersion slope in the future WDM networks. However this value represents the dispersion slope of currently installed networks. By using the CDC, the dispersion of λ_1 , mid-band λ , and λ_2 were compensated by setting the dispersion at 1545 nm to -159 ps/nm, -359 ps/nm and -555 ps/nm respectively.

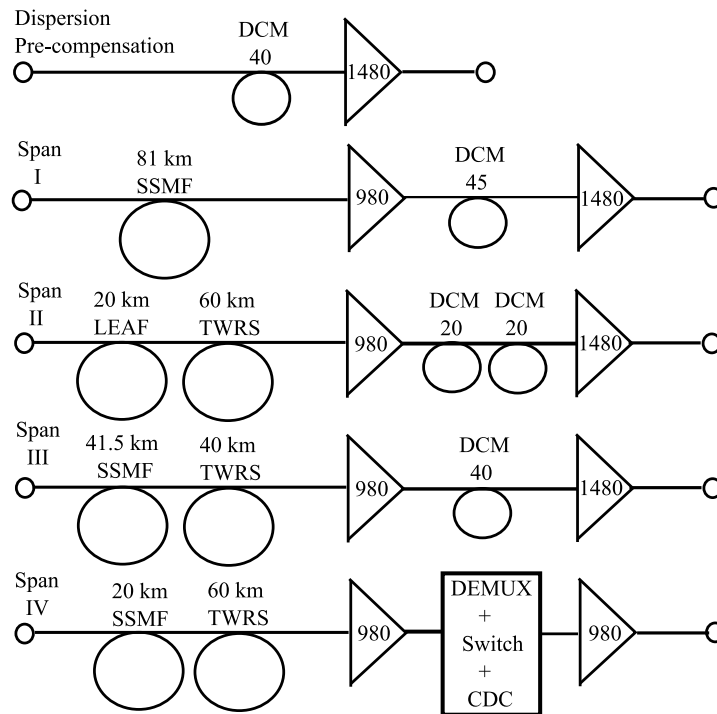


Figure 3.17: Transmission line arrangement for 32 channels WDM transmission

From the compensation values of these three wavelengths, compensation values for another WDM channels can be obtained.

The system performance after transmission and dispersion compensation is shown in Fig. 3.20 and Fig. 3.21. In terms of BER, the average performance is above FEC limit. The eye opening is also visible which corresponds to the BER obtained. In this experiment, 5.12 Tbit/s of data was transmitted with the net error-free transmission capacity (after excluding the FEC overhead bits) of 4.76 Tbit/s.

3.4 Conclusion

The development of a low cost DCF-based dispersion compensator and its applications were presented. The compensator was developed for a single channel CD compensation with colour-less characteristics, which means that the same compensator is able to operate at any WDM optical frequency. From the characterization process, the DCF specifications were obtained. The DCF insertion loss, dispersion coefficient and dispersion slope compensation ratio are 0.68 dB/km, -86 ps/nm/km, and 43% (SSMF) respectively. Without any external DCF, the dispersion compensator (CDC) has a tuning capability from 0 ps/nm to -363.375 ps/nm with -2.125 ps/nm resolution. This resolution is fine enough and better than that of a commercial device on the market [67]. In the system dispersion compensation experiments, a 160 Gbit/s WDM DQPSK PoIDM system was used as the testbed. The CDC successfully operated over several different transmission line distances and arrangements, and WDM channel counts. The highest compensated transmission line residual dispersion is +747 ps/nm (1545 nm). It was also shown that the CDC works for all WDM channels inside the

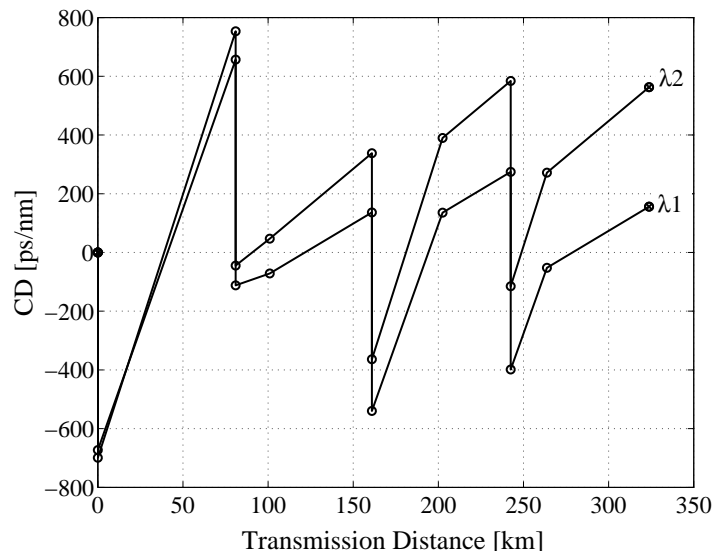


Figure 3.18: Dispersion map of four-span 32 channels WDM system

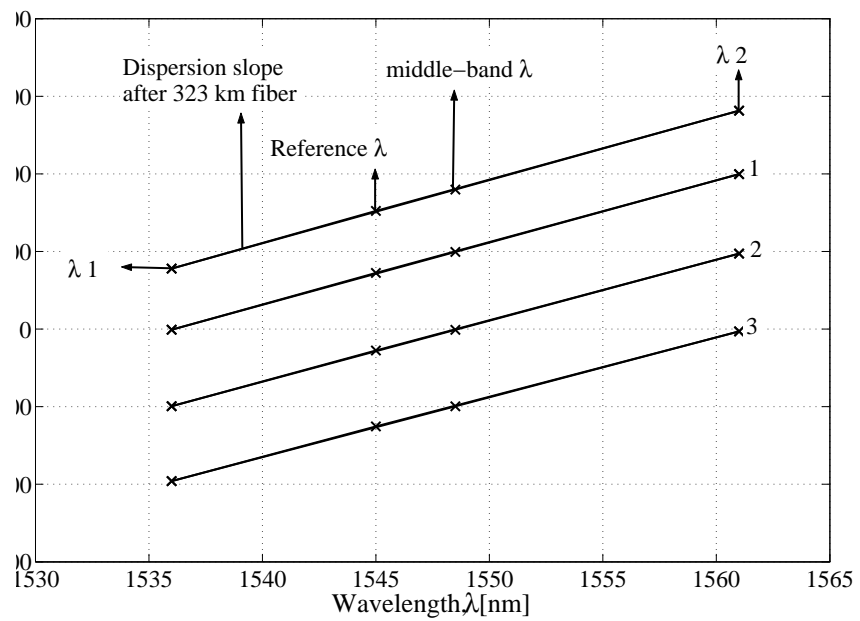


Figure 3.19: The residual dispersion for the outermost wavelengths after transmission, and dispersion compensation (1,2 and 3 are the dispersion slope after CD compensation of λ_1 , middle-band λ and λ_2).

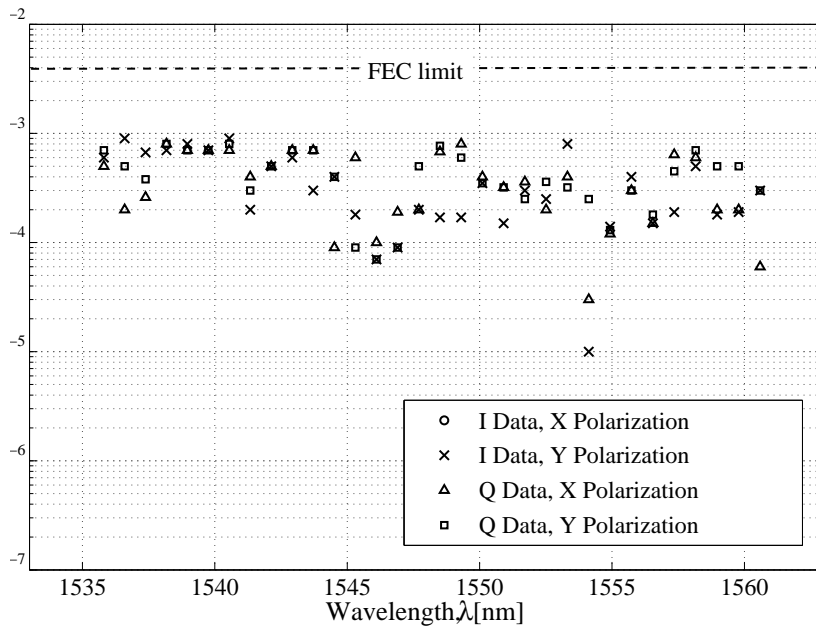


Figure 3.20: BER after 323 km fiber and dispersion compensation

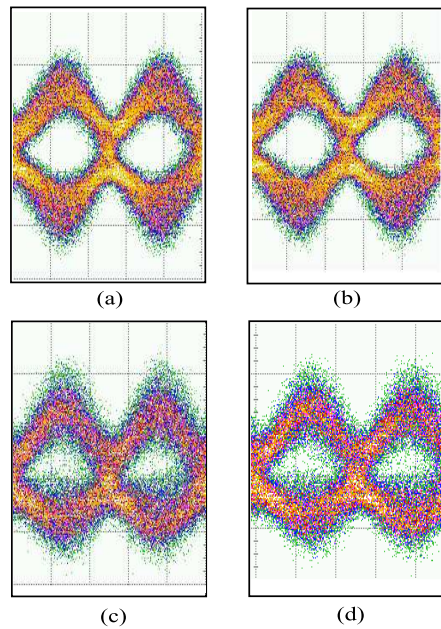


Figure 3.21: Eye diagrams for I channel in both polarizations: (a) Back-to-back (x), (b) Back-to-back (y), (c) After 323 km (x), (d) After 323 km (y)

C-band, and is able to support dispersion compensation for advanced modulation formats. For all channels, we have achieved performance of above the FEC limit.

In our setup, we were unable to include FEC overhead bits. Therefore the total bit rate was divided by 1.07 ($42.7/40$) in order to obtain the net transmission capacity. In FEC supported system, 42.7 Gbit/s of data rate is used in order to accommodate these overhead bits [15]. Therefore, the pulse duration is reduced to 23.4 ps instead of 25 ps, which is 1.07 times smaller. This pulse duration reduction reduces the system tolerance to CD by a factor of 1.14. This value is considered insignificant in comparison to the FEC coding gain. Therefore, we expect that the result of the experiments conducted in 42.7 Gbit/s system will not significantly differ from our results, which were obtained in a conventional 40 Gbit/s system with 25 ps pulsewidth.

The CDC has several advantages as well as disadvantages. Among the advantages are its smooth dispersion characteristics, huge compensation range, fast response time and low development cost. On the other hand, the CDC has a large size, high insertion loss, is vulnerable to fiber nonlinearity effect and is unable to provide positive dispersion compensation values. In terms of performance, we have demonstrated that this low-cost dispersion compensator is suitable and sufficient to support high speed transmission with advanced modulation formats. Supported by this compensator, a transmission experiment with a capacity around 5 Tbit/s was successful.

Chapter 4

Chirped-Fiber Bragg Gratings-based Dispersion Compensator

4.1 Motivation

In presently installed fiber optic networks, dispersion compensating fiber (DCF) is a popular solution to solve problems associated with chromatic dispersion (CD). DCF is preferred because it is a passive device, offering low installation and maintenance cost. Moreover, it provides broadband operation with smooth dispersion properties and good optical characteristics. However, the dispersion value of DCF is fixed. Therefore, tailoring the DCF length to compensate some specified dispersion values of transmission fiber is necessary. However, such procedure does not guarantee accurate compensation values. There must be some resulting positive or negative residual dispersion after each compensated fiber span. In term of dispersion slope compensation, an earlier generation of DCF provides only around 60% to 70% slope compensation [18]. In contrast, today's new generation DCF offers 100% dispersion slope compensation.

With 40 Gbit/s systems emerging as the future transmission system backbone in place of 10 Gbit/s systems, more stringent requirements for dispersion management exist. Due to four times reduced of signal pulsewidth, the tolerance to chromatic dispersion increases sixteen fold. Hence, current tolerable residual dispersion at 10 Gbit/s is no more acceptable

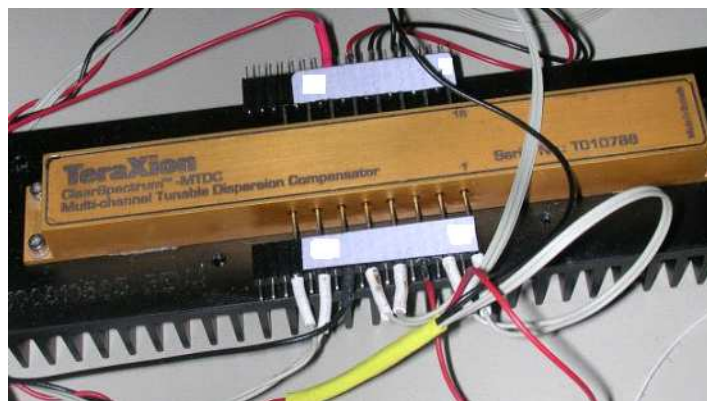


Figure 4.1: Teraxion Multi-channel Tunable Dispersion Compensator

and needs to be compensated. Since the environmental temperature contributes to CD variation, the implementation of Tunable Dispersion Compensator (TDC) is unavoidable in 40 Gbit/s systems. As normally practiced in 10 Gbit/s Metro systems, the in-line dispersion is compensated by the DCF. To compensate variable residual CD, a TDC (compensates both positive and negative dispersion as discussed in Appendix L) needs to be installed before every receiver. Typically, this kind of TDC has a smaller tuning range [23] than a TDC which can only compensate positive dispersion. However, in 40 Gbit/s ultra-long-haul transmission over of several hundreds of fiber spans with several thousand kilometers length, the resulting accumulated residual dispersion at the receiver could exceed the TDC tuning range and the system's CD tolerance. This means the existing CD management may not be suitable for the future 40 Gbit/s systems. At the same time, residual dispersion also changes with temperature [68, 69] and fiber configurations. In four-season countries, the soil temperature changes with season [68], changes the CD of the underground fibers. In reconfigurable optical networks, wavelength paths change, and hence changes the total dispersion. Apart from CD variation, it was also reported that the EDFAs used to compensate the large DCF's insertion loss in long-haul transmission partly introduce non-linear phase noise (NLPN) into the system [43, 34, 42]. Considering all mentioned issues, an alternative solution to improve the system performance is required. With the advances in fiber optic device technology, the implementation of tunable dispersion compensation (tunable CD value, low insertion loss and non-linear coefficient) after every span could become reality. In order to realize this idea, the TDC need to have high tunability corresponding to up to 70 km or 80 km of SSMF with proper dispersion slope. At 10 Gbit/s this concept has been experimented by using chirped-FBG (CFBG) MTDC [70], the success of which motivated us to investigate the same implementation on 40 Gbit/s system. This concept is also useful to enable dynamic dispersion map management that is also important for future fiber optic networks.

4.2 CFBG Multi-channel Tunable Dispersion Compensator

4.2.1 Principle of operations

The Multi-channel Tunable Dispersion Compensator (MTDC), loaned by Teraxion, which is used in this experiment is designed for C-band WDM systems operating at 10 Gbit/s. Such a system requires wideband dispersion adjustment together with dispersion slope compensation. The MTDC was developed based on phase sampled chirped-Fiber Bragg Gratings (CFBG) technology. This device is designed specifically for SSMF dispersion compensation. It can be implemented in DWDM metro and also long-haul systems. Detailed specifications of the MTDC are listed in Table 4.1.

The basic principle of MTDC operation is illustrated in Fig. 4.2. The fastest optical subcarrier (red) which arrives first is reflected at the last position in the gratings. The slowest optical subcarrier (blue) arrives later and is reflected at an earlier position in the grating. This results in a compressed pulse, where CD effect is compensated [22]. Dispersion tuning is achieved by controlling the thermal gradient. A section of optical fiber containing a superimposed CFBG is coupled to a thermally conductive element. A thermal gradient is created along this element and the grating by using two thermoelectric coolers (TEC) located at both grating ends. At the same time the temperature at the center of the grating

Table 4.1: MTDC Specifications

Parameters	Details
Transmission rate	10 Gbits/s
Operation band	C-band
Operation bandwidth	33 GHz
Channel spacing	100 GHz to 200 GHz
Dispersion tuning range at 1545 nm	-700 ps/nm to -1550 ps/nm
Group delay ripple (unsmoothed)	< 40 ps
Group delay ripple (smoothed)	< 27 ps
Insertion loss	< 3 dB
Polarization Dependent Loss (PDL)	< 0.3 dB
Polarization Mode Dispersion (PMD)	5 ps
Response time	< 10 s
Operating Temperature	0 to 65 °C
Power consumption	Typical: 2 W, Maximum: 6 W

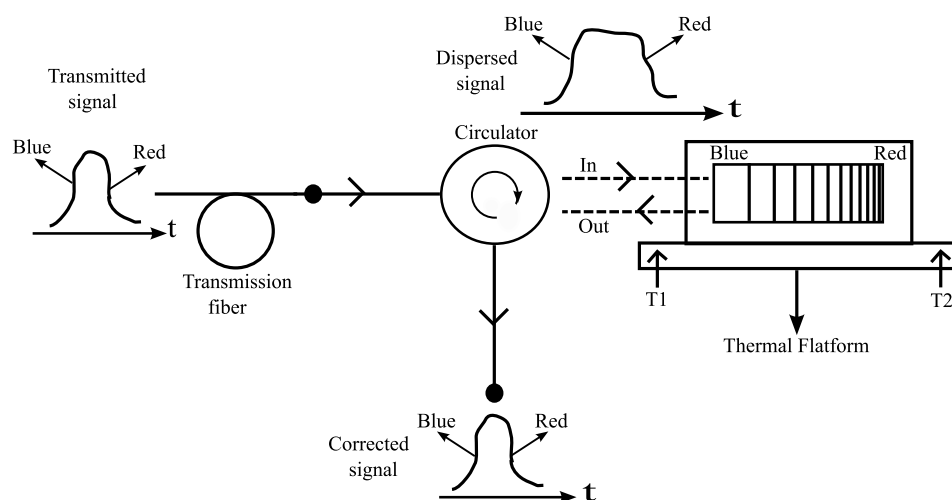


Figure 4.2: Principle of operation of MTDC

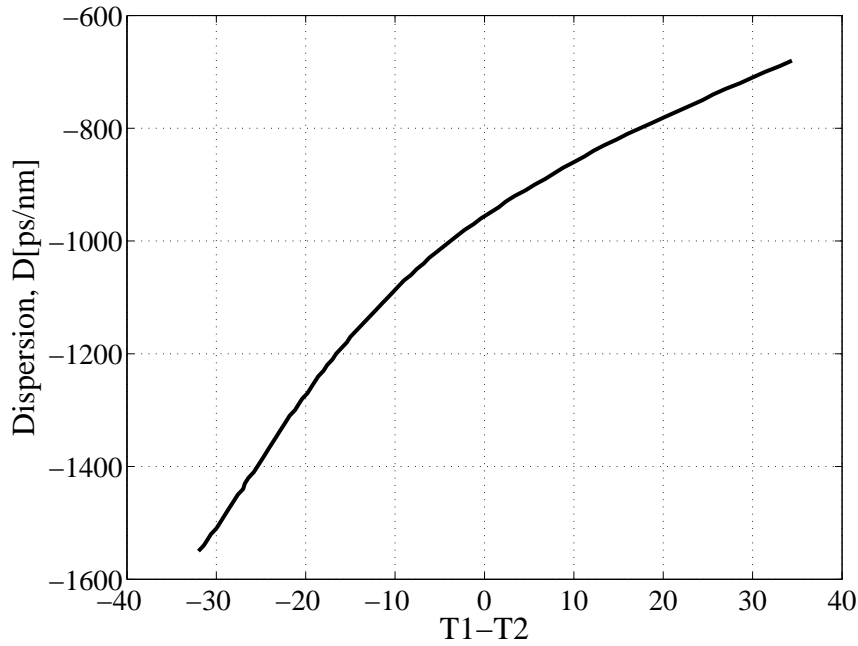


Figure 4.3: Temperature setting of the TECs for specified dispersion values.

is maintained constant. Depending on the gradient sign, which is set by the two TECs, the dispersion can be increased or decreased. By using the relation shown graphically in Fig. 4.3, the desired dispersion value can be obtained. The dispersion slope increases with dispersion value, which is the advantage of the device. This is achieved by chirping the grating sampling period. This feature emulates the actual fiber characteristic but in opposite direction.

First of all, we discuss the dispersion and dispersion slope tuning concept. Basically the dispersion is controlled by changing the thermal gradient of the grating. Fig. 4.4 shows three curves representing the minimum, middle and maximum dispersion tuning, resulted from three different temperature gradients. The slope of the curves represents the resulting dispersion. As can be seen, the three curves have different maximum and minimum group delays. By increasing the absolute value of the group delay, the slope becomes steeper, therefore the dispersion is increased.

The MTDC is designed for operation over 51 WDM channels. It is well known that due to the dispersion slope of transmission fiber, channel 1 and channel 51 have different accumulated dispersions. In order to compensate all WDM channels with a single dispersion setting, the sampling period is chirped as shown in Fig. 4.5. Without chirping the sampling period, all 51 channels would have the same group delay slope, therefore the same dispersion. Referring to the center frequency of every channel, the Frequency Range (FR) between one channel to another is identical because of the same sampling period. However, at GD_{Max} it can be seen that the FR+ is increased from one channel to another. This is because the chirping on the sampling period results in a reduction of sampling period from one channel to another. Contrary at GD_{Min} , FR- is decreased from one channel to another. As we can see in Fig. 4.5, this process increases the group delay slope from channel 1 to 51. Without increasing the group delay, the dispersion is increased from 1 to channel 51,

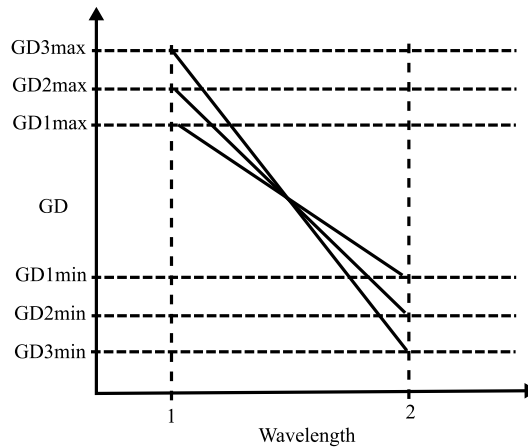


Figure 4.4: Group delay vs wavelength for three different dispersion setting

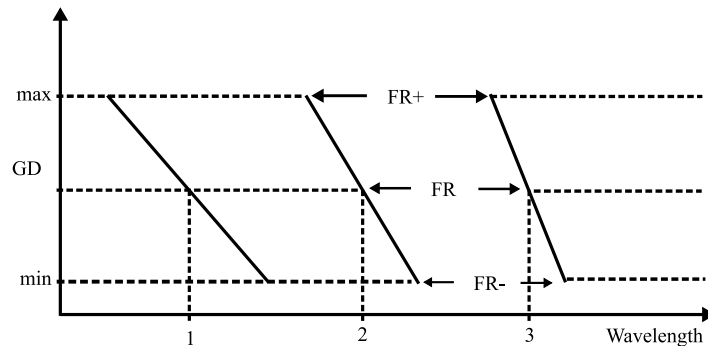


Figure 4.5: The chirping of sampling period [21]

and hence produces the dispersion slope. This sampling period chirping process (results in dispersion slope tuning) occurs together with dispersion tuning, which is the advantage of the device. The disadvantage is that the last channel (for longest wavelength) has a low passbandwidth.

4.2.2 Performance assessment

Before conducting the experiments, the performance parameters of the device were assessed. This procedure is important to decide whether the MTDC is suitable to be used in a 40 Gbit/s system. The performance of the MTDC was analyzed by using the data obtained from the manufacturer [23, 22, 20, 67]. For a tunable device, the dispersion tunability is the most important parameter that should be assessed. Then its operation bandwidth need to be known. This is because if the device has smaller bandwidth than the signal, a narrow passband characteristic will be introduced, deteriorating the 40 Gbit/s system performance [46]. Finally insertion loss and polarization mode dispersion (PMD) of the device need to be characterized. In general, this MTDC has fifty one 100-GHz-spaced channels [23, 22] with minimum bandwidth of 33 GHz at maximum compensation value. The compensation values are determined by the intrachannel group delay slope in every specific channel. These descriptions are illustrated in Fig. 4.6.

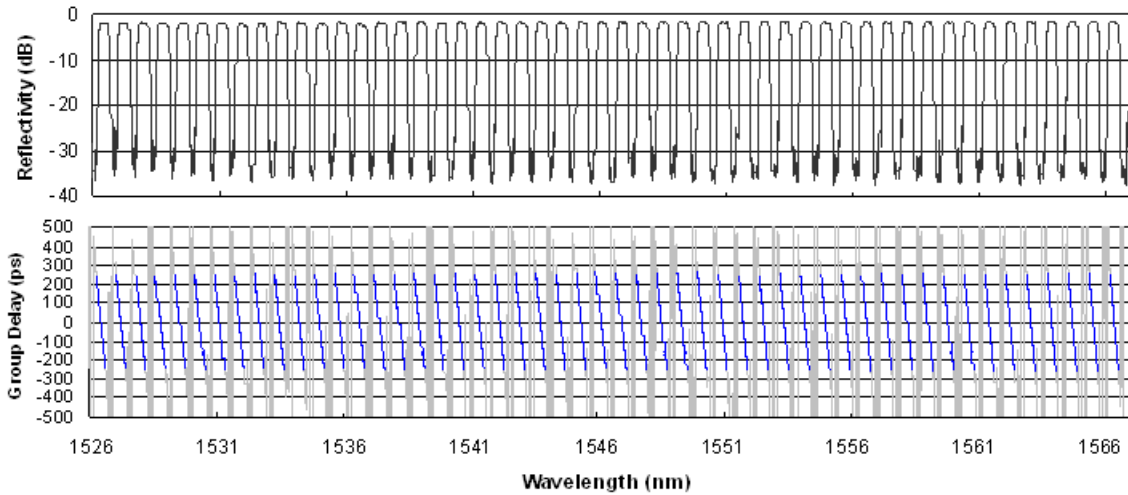


Figure 4.6: MTDC reflectivity and group delay for 51 WDM channels [22]

4.2.2.1 Dispersion and dispersion slope tunability

The fiber group delay changes proportional to the transmission distance and varies from one wavelength to another according to the dispersion slope. MTDC dispersion and dispersion slope tuning function is required to handle this effect. The dispersion tuning shown in Fig. 4.7 corresponds to the lowest, middle and highest value. As shown in the Figure, for highest dispersion tuning, the group delay slope is the steepest. By considering only the 33 GHz marked bandwidth, the group delay increment increases the dispersion. As shown in Fig. 4.8, for this compensator, there is around 6.25% group delay slope difference between the first and the last optical channel. This means that the last channel is compressed more than for the first channel for a specified compensation setting. The output spectral width of the last channel is smaller than the first channel because of the narrow passband characteristic caused by the steep group delay slope.

Fig. 4.9 shows dispersion and dispersion slope tuning characteristics. Referring to the center optical frequency of the band, the dispersion can be tuned from -700 ps/nm to -1550 ps/nm. Accordingly, the dispersion of the first and the last channel changes from -675 ps/nm to -1460 ps/nm and -730 ps/nm to -1715 ps/nm, respectively. These values correspond to SSMF transmission distances of 41 km and 93 km, respectively. By tuning the dispersion value, the dispersion slope will automatically be tuned. This feature simplifies the dispersion detection part. Instead of detecting the dispersion for all optical frequencies, only the dispersion of one optical frequency needs to be detected. From this information, the dispersion compensation for all WDM channels can be performed.

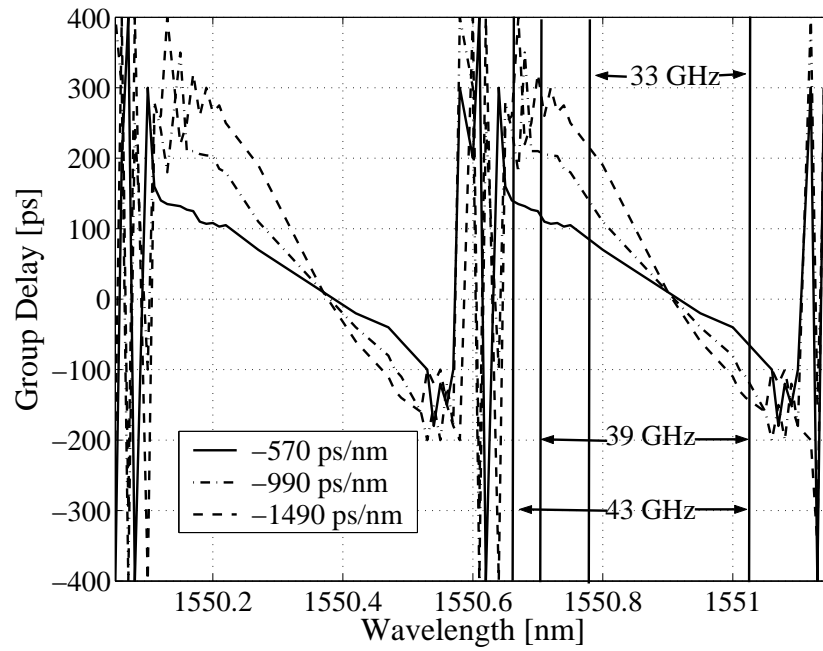


Figure 4.7: Dispersion values at highest, middle and lowest dispersion tuning[22]

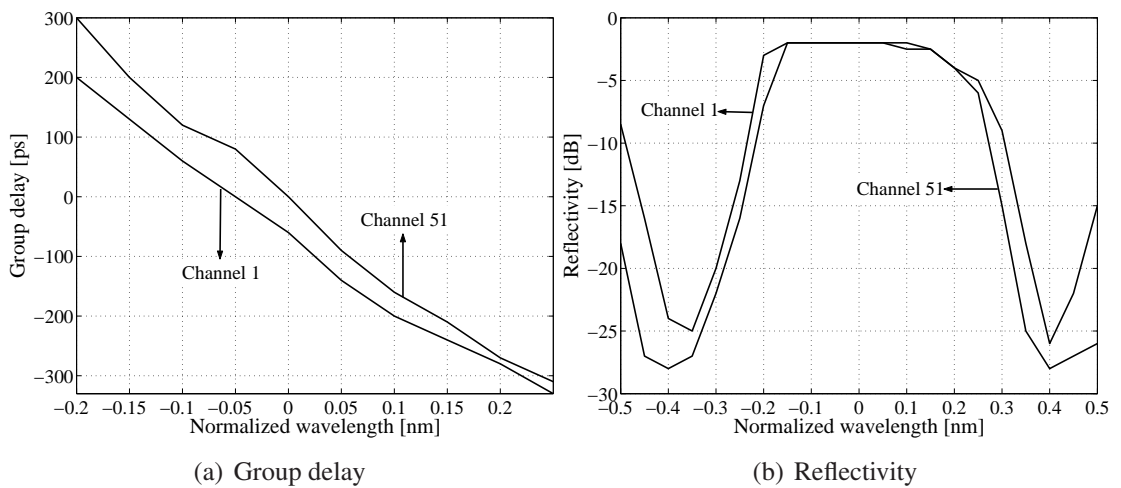


Figure 4.8: Tuning characteristics of MTDC's channel 1 and 51[21]

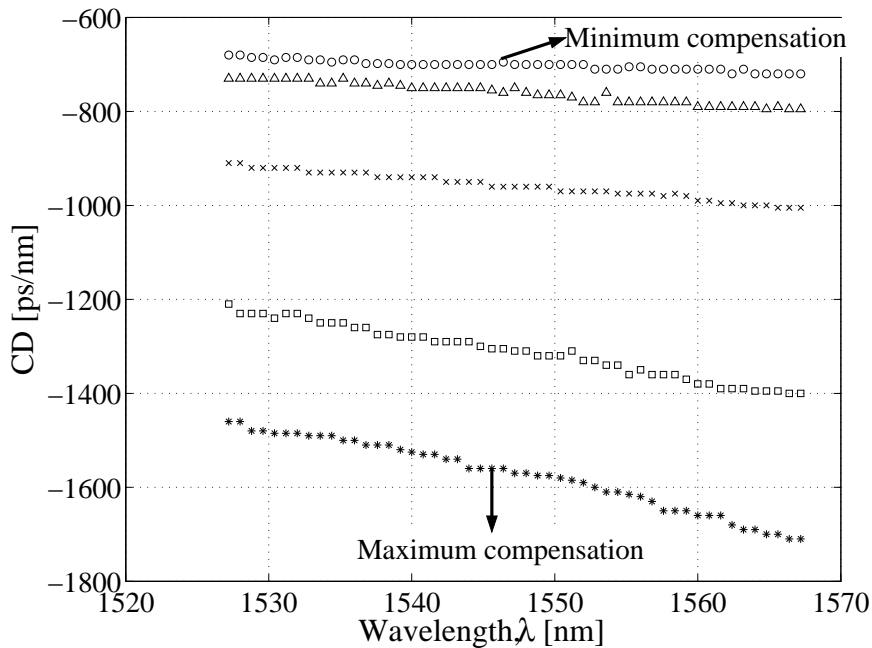


Figure 4.9: Dispersion and dispersion slope of MTDC[23]

4.2.2.2 Operating optical bandwidth

The MTDC has a specified minimum operating optical bandwidth. This is an important parameter which decides whether the MTDC is suitable for 40 Gbit/s systems. It is well known that a 40 Gbit/s signal has a higher optical bandwidth than a 10 Gbit/s signal. If the MTDC's operating bandwidth is so small and acts as a very narrowband filter, most of the signal spectrum will be filtered. As a result, the quality of MTDC output signal is degraded.

Fig. 4.7 (please refer to the previous section) shows the group delay for three dispersion settings. Apart from that, we could also use this figure to see the resulting bandwidth limitation for each setting. For the lowest dispersion setting, the compensator introduces insignificant bandwidth filtering. For the highest dispersion setting, we can notice that the resulting MTDC bandwidth is only 33 GHz. For 10 Gbit/s signals, 33 GHz is sufficient and no passband filtering characteristic will be experienced. However, at 40 Gbit/s, where the signal optical spectrum is around 100 GHz, this bandwidth is considerably small and affects the system performance [46]. Therefore we expect that some penalty will be introduced by this compensator when it is operated at 40 Gbit/s. To clarify this statement a simple early test was conducted to see the MTDC's effect on the bandwidth of a 40 Gbit/s signal, and the result is shown in Fig. 4.10. As we can see, the bandwidth of the MTDC's output signal reduces as a function of compensation value.

Regarding the pass-bandwidth, it is possible to produce large passband. By designing the MTDC for largely spaced WDM channel, e.g. 25 channels inside C-band with 200 GHz spacing, the device bandwidth can be made as large as 80 GHz[67]. Another alternative is to implement low compensation setting. In Lachance et. al. [20] the result for low dispersion setting (-500 ps/nm) was shown. It was observed that this compensation value produced around 60 GHz of group delay linear slope, which will introduce an insignificant bandwidth

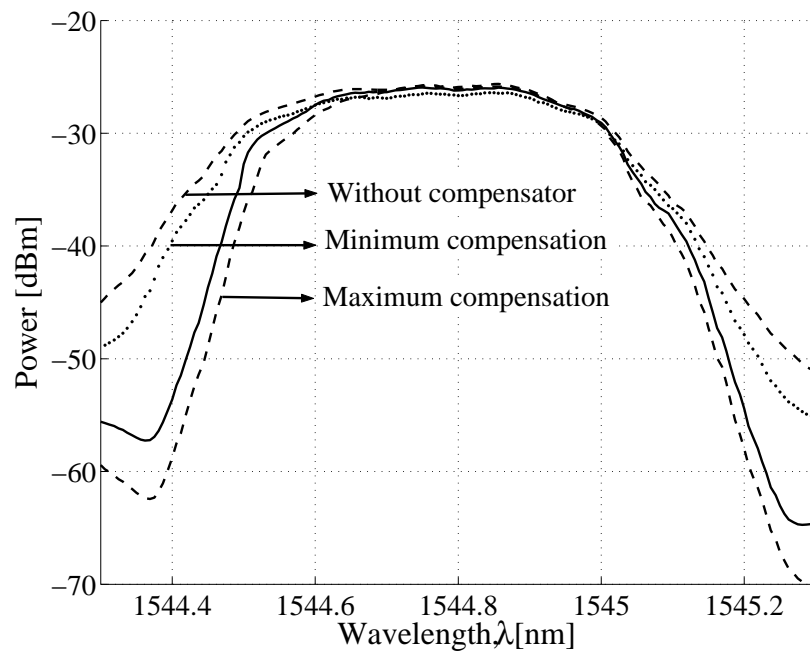


Figure 4.10: The resulting passband characteristic of MTDC

filtering penalty to a 40 Gbit/s system. Therefore, at 40 Gbit/s, in SSMF networks, MTDC can only be used in short spans networks or for residual dispersion compensation. However, when considering Non-Zero Dispersion Shifted Fiber (NZDSF) networks, 500 ps/nm correspond to around 125 km fiber length. Hence, we expect that the MTDC is suitable to support long NZDSF transmission spans, replacing the need for DCF.

4.2.2.3 Insertion loss and PMD

In comparison to DCF, the insertion loss, IL of the MTDC should be smaller. To verify this, the insertion loss was measured. The MTDC was connected to a circulator to form a three-port device as shown in Fig. 4.2. Together with a circulator, an IL of 5 dB was measured at 1550 nm wavelength. The total IL of the circulator itself is 2 dB by adding together the insertion loss from port 1 to 2 and from port 2 to 3. Therefore the IL of MTDC is only 3 dB. However, in order to operate, a circulator needs to be included, thus increasing the insertion loss. By considering the MTDC's ability to compensate as much as 80 km SSMF, this IL is still less than that of two cascaded DCM-40s (-1368 ps/nm) which is around 8 dB.

The PMD of this device was measured by using a PoIDM signal. After the polarizer, which is used to block one of the polarizations, the MTDC was connected. The output was monitored via an oscilloscope. From the eye diagram, the center position where the largest eye opening was observed, was recorded as an initial value. Then the second polarization was selected. By comparing the new eye position to the initial value, the polarization time shift or PMD was obtained, which is 5 ps. This value is 20% of the pulse width. In the system experiment, we can investigate whether the device PMD will become a significant deteriorating factor. In a standard device of the same model, the PMD value is only 1 ps.

4.3 System experiments

4.3.1 Introduction

From the MTDC characteristics discussed above, we understood that the MTDC is capable to compensate transmission line CD in a 10 Gbaud transmission system. However, its performance in 40 Gbaud system has never been assessed. In this section, MTDC is tested as a transmission line CD compensator in a 40 Gbaud system [19, 71]. Apart from bandwidth limitation, other characteristics such as dispersion tunability and slope compensation are expected to be sufficient for operation in a 40 Gbaud system. In the experiments, three transmission systems are used, namely OOK, DPSK and DQPSK, which allows us to investigate the MTDC's flexibility. As the three systems have different optical bandwidth, the bandwidth limitation can also be assessed. For OOK and DPSK, our goal is to provide economic transmission system with automatic dispersion compensation. For DQPSK, the main goal is to assess the MTDC's maximum capacity. The possibility of implementing automatic tunable dispersion compensation is also studied for DQPSK system. For CD detection, arrival time detection [16] is used.

4.3.2 On-Off-Keying (OOK)

On-Off-Keying (OOK) or sometime is referred as IMDD is a widely used system in today's optical communication networks. Normally systems use NRZ data format. The combination of OOK and NRZ is popular because of their simplicity. For example only one amplitude modulator is needed to generate this format and one photodiode is required for detection. The MTDC is also designed for today's optical communications system. By default it should reliably works in OOK system. It is also important to start the 40 Gbit/s MTDC test on an uncomplicated system where only few control parameters exist. In this experiment the CS-RZ format is used rather than NRZ. This is because, the NRZ OOK format was shown to produce poor results in a single channel TDC experiment [72].

4.3.2.1 Experimental setup

The experimental setup is depicted in Fig.4.11. Fourty Continuous Wave (CW) WDM lasers (192.1 THz (1560.61 nm) to 196 THz (1529.55 nm)) were fed into the multiplexer. The output signal of the multiplexer was passed through the first modulator (I), which is a dual-drive Mach-Zehnder modulator. In order to generate an OOK signal, only one out of its two driving ports was used. It was driven by 40 Gbits/s NRZ data with PRBS $2^7 - 1$. The output of the first modulator was fed into the RZ modulator (III) with 67% pulse carving to generate the CS-RZ OOK signal. The modulated signal with peak power of -15 dBm/channel was input to the booster. The input power to the line was around 0 dBm/channel. The transmission line consisted of SSMF. Its distance was varied from 47 km to 81.3 km. After the transmission line, the WDM signals were preamplified before being compensated by the MTDC. The MTDC compensation value was determined by referring to the dispersion experienced by the wavelength in the center of WDM band. Then the compensated signal was demultiplexed by a flat-top WDM DEMUX. Between the MTDC and DEMUX there was a 980 nm EDFA, which is used to compensate for MTDC loss. This EDFA is quite noisy in

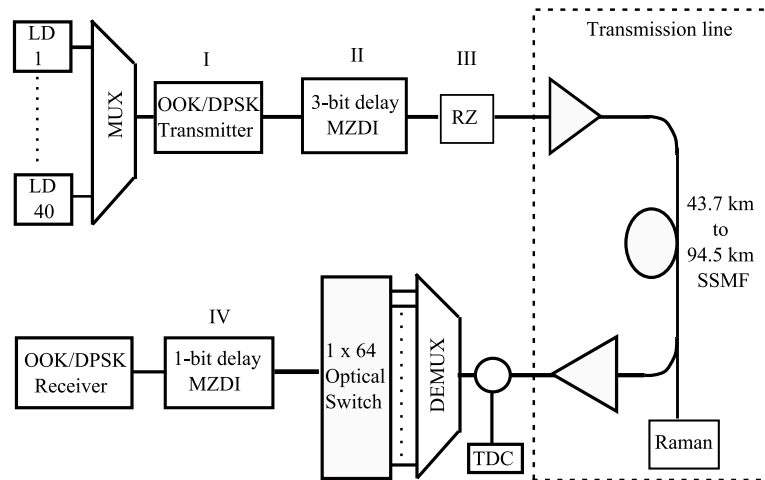


Figure 4.11: Experimental setup for OOK, DPSK and DQPSK

the shorter wavelength region, which affected the performance of the channels inside this band. The demultiplexed signal was detected by a photodiode and subsequently fed into the Clock and Data Recovery (CDR) for data regeneration. The BER was measured by a BER tester.

4.3.2.2 Results and Discussions

In this section, the results for CD compensation on OOK modulation format are presented and discussed. The important performance parameters that need to be analyzed are the Q-factors for all WDM frequencies, and the eye diagrams of the received signals.

In Fig. 4.12, the Q-factors for all WDM frequencies at various compensation values are presented. In this experiment, the fiber of 47 km, 62.9 km and 81.3 km were used. These distances correspond to -790 ps/nm, -1030 ps/nm and -1390 ps/nm of MTDC dispersion, respectively. From the Figure, several conclusions can be made. First, for all wavelengths and compensation values, quasi-error-free performance is obtained. This is indicated by the Q-factors which are above 15.6 dB. Secondly, the MTDC has performed a satisfactory dispersion slope compensation, which is shown by good Q-factors at every wavelength. Even after 81.3 km, it is shown that the worst Q-factor is 15.6 dB (195.6 THz (1532.65 nm)). Finally it can also be concluded that the Q-factors degrade with increasing dispersion compensation values. The average Q-factor after 81.3 km transmission and compensation is nearly 2 dB worse than the Q-factor after 47 km transmission and compensation.

In order to clearly see the Q-factor degradation against compensated transmission distances, Fig. 4.13 is plotted for the best, middle and the worst WDM channels. We can see that for all cases there is around 1.5 dB to 2.5 dB Q-factor degradation when the performance of the longest transmission line setup is compared to the shortest one. The degradation pattern is nearly linear, which enables the operator to predict system performance when a higher compensation value is implemented. Referring to earlier discussions, it is concluded that this Q-factor degradation is caused by bandwidth limitation introduced by the MTDC at high dispersion.

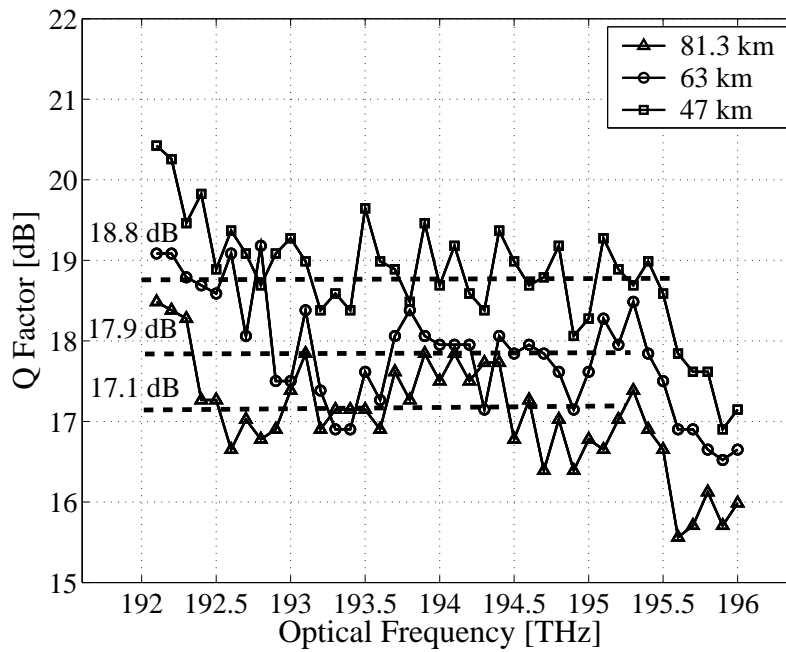


Figure 4.12: OOK: Q factors after transmission and compensation.

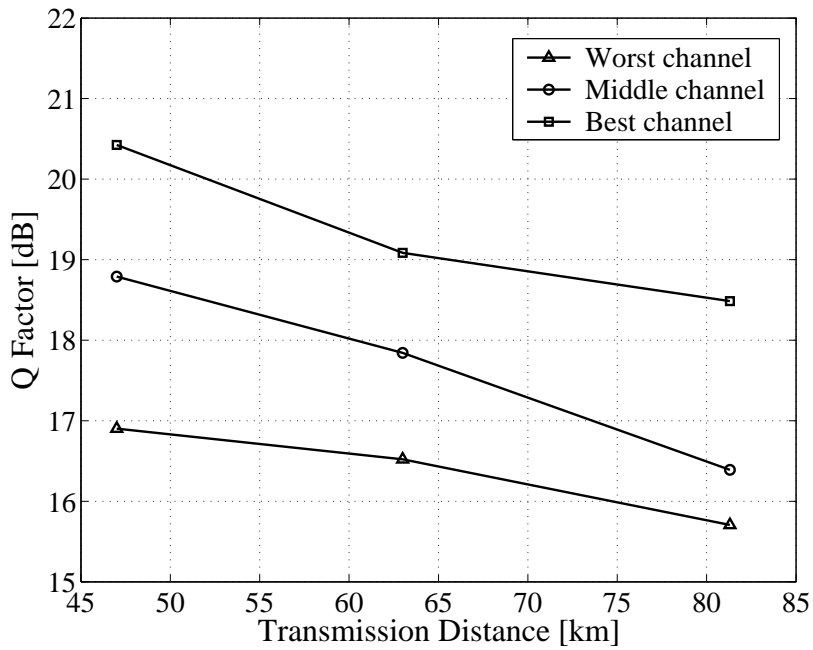


Figure 4.13: OOK: Q-factors against transmission distances.

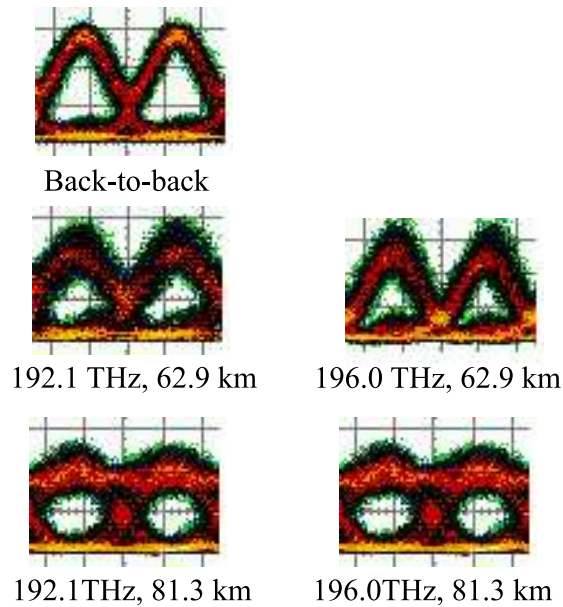


Figure 4.14: OOK: Eye diagrams at two outermost optical carriers for several transmission distances

In Fig. 4.14, an eye diagram comparison between the back-to-back and the received signal after 62.9 km and 81.3 km fiber with CD compensation is made. In order to represent the eye diagram quality for all WDM channels, the eye diagrams at the lowest and the highest optical frequencies were recorded for all transmission distances. We noticed that the back-to-back eye diagrams for both optical frequencies are similar. Therefore, only one of them is presented. From the eye diagrams, we can say that the dispersion and its slope are satisfactorily compensated. The signal OSNR after 62.9 km is similar to the back-to-back case. The horizontal eye opening penalty was around 3 dB, and is mainly caused by timing jitter. For the 81.3 km case, higher timing jitter can be observed, hence the horizontal eye opening penalty increases. Referring to a similar specified time slot, the OSNR penalty considerably increases compared to the previous eye diagrams. The vertical eye opening penalty is around 3 dB. However, the eye opening is still very clear, which indicates sufficient CD compensation.

4.3.3 Differential-Phase-Shift-Keying (DPSK)

In DPSK system the overall performance is expected to be better due to higher DPSK tolerance to nonlinearity and its superior sensitivity, 3 dB better than that of OOK. However a Mach-Zehnder delay interferometer (MZDI) is needed for demodulation, and two photodiodes are necessary for balanced detection [10]. These factors increase the cost, which is undesired by the system operators. We tried to reduce the cost by using the NRZ format. Its spectral width is smaller, which might be good for MTDC operation.

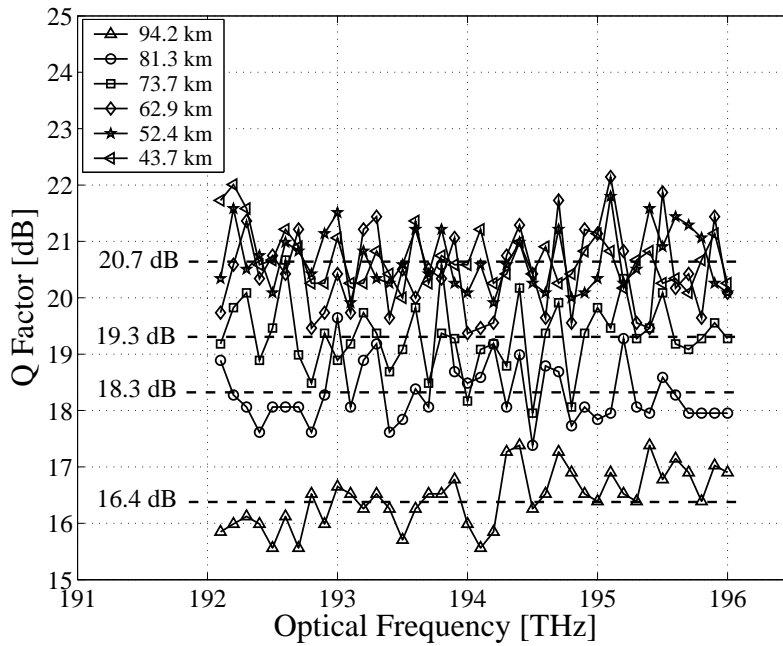


Figure 4.15: DPSK: Q-factors vs frequencies after several ranges of transmission distance.

4.3.3.1 Experimental setup

The setup was slightly modified from the previous OOK setup. Therefore, only the modifications are mentioned in this Section. To generate DPSK signal, the dual-drive Mach-Zehnder modulator (I) was driven at both arms by the data. The RZ modulator (III) was taken out. In this setup, the input power to the booster is higher compared to the setup in Sect. 4.3.2.1 (no RZ modulator loss) and thus the transmitted signal after the booster has higher OSNR. Another important modification is at the receiver, where MZDI (IV) was installed for DPSK demodulation and followed by two photodiodes for balanced detection.

4.3.3.2 Results and Discussion

Fig. 4.15 shows that all Q-factors in the 43.7 km, 52.4 km and 62.9 km setup are above the quasi-error-free limit. This result proves that MTDC is compatible to operate in DPSK systems. In comparison to OOK, DPSK has produced 3dB better Q-factors, and this can clearly be seen in 62.9 km setup. This is a good indication that longer span lengths than previously investigated with OOK can be studied. In a 73.7 km and 83.3 km system, the Q-factor degradation is 1.4 dB and 2.4 dB, respectively when they are compared against the previous transmission distances. When compared against OOK, in a 81.3 km system, DPSK shows better a Q-factor, around 1.2 dB. The worst average Q-factor was measured in 94.2 km system, around 16.4 dB. In the 73.7 km, 83.3 km and 94.2 km setup, the MTDC bandwidth penalty is noticeable.

Fig. 4.16 depicts the Q-factor degradation against transmission distance. Three wavelengths were sampled to represent the best, average and worst case. We can see that for each transmission distance, there is only a slight performance difference between the three wavelengths, suggesting a uniform performance for all WDM channels. The performance

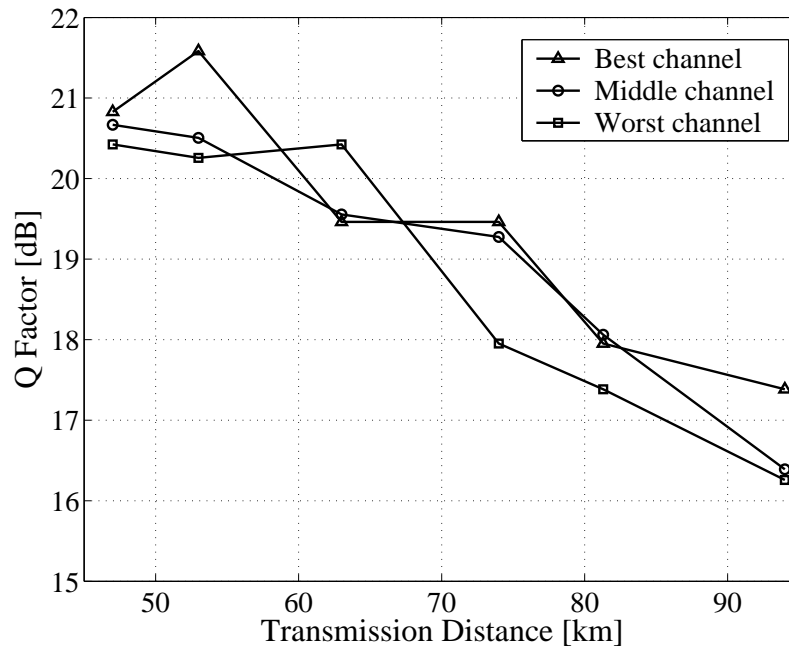


Figure 4.16: DPSK: Q-factors vs distance for the best, middle and worst WDM channels

differences between the 43.7 km, 52.4 km and 62.9 km setups are noticeable. There is only around 1 dB Q-factor degradation in the 62.9 km system compared to the 43.7 km system. This degradation is very small, which is unnoticeable in Fig. 4.15. By comparing the 94.2 km system to 43.7 km system, around 3.7 dB penalty can be observed. In that setup the signal is highly bandwidth limited. However, the performance is still above 15.6 dB.

In Fig. 4.17, the performance parameter is the eye opening penalty (EOP). By looking at the eye diagram of the shortest and the longest wavelength, it can be concluded that slope compensation is satisfactory. In the 62.9 km setup, less than 3 dB EOP is noticed. The eye shape is still preserved. However, an OSNR degradation can already be noticed when comparison inside the same time slot is made against the back-to-back eye diagram. In the 81.3 km case, the system experienced around 2 dB higher EOP than the previously mentioned case. The eye opening is smaller due to the lower OSNR. However the eye shape is still preserved. In the longest transmission case (94.2 km), we can see that the eye diagram quality is seriously degraded. By comparing these eye diagrams and those presented in Appendix D, it is concluded that this degradation is caused by bandwidth limitation. However, the eye opening is still visible.

In comparison to CS-RZ OOK, the MTDC showed better performance in NRZ-DPSK, especially the ability to compensate the huge dispersion of 94.2 km of SSMF (1520 ps/nm). Even though NRZ is less tolerant to CD than CS-RZ, this factor is not significant anymore when the MTDC is used. A better Q-factor in the NRZ DPSK setup is also contributed by higher transmitted OSNR and the differential detection of the balanced receiver.

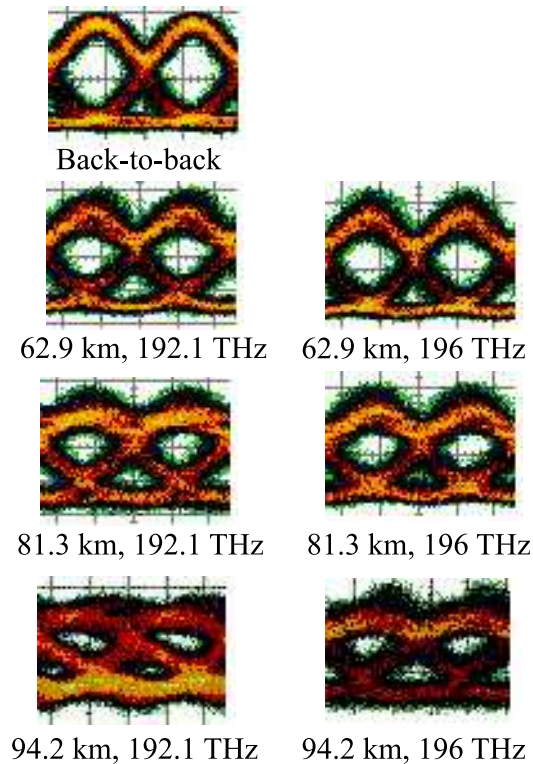


Figure 4.17: DPSK: Eye diagrams for various range of transmission distance

4.3.4 Differential-Quadrature-Phase-Shift-Keying (DQPSK)

In this section, MTDC operation is tested in a DQPSK system, which is a multilevel modulation format. 40 Gbit/s of data carried by two quadratures produces an 80 Gbit/s signal. This experiment pushes the capability of the 10 Gbit/s MTDC to the limit. At the same symbol rate, this format is more vulnerable to CD than DPSK or OOK [13] due to its closer symbol distance. In our WDM setup, the back-to-back Q-factor of DQPSK is not more than 16 dB. This is low compared to OOK and DPSK. Therefore, to achieve the performance of above FEC limit after transmission is already a significant achievement. In this experiment CS-RZ modulation format is used.

4.3.4.1 Experimental Setup

The setup for this experiment was modified from the DPSK system in the previous section. After NRZ modulator (I), a 3-bit delay MZDI (II) was installed, generating the DQPSK signal. This device contributed around 7 dB loss, which caused insufficient power to the subsequent RZ modulator (III). Therefore an EDFA was installed between the MZDI and RZ modulator. As a result, the input signal of the booster has a higher peak power compared to the OOK setup, but a lower OSNR. There was no modification involved at the receiver.

4.3.4.2 Results and discussions

Figure 4.18 shows the Q-factors for all quadrature and wavelength channels at different transmission distances. From one specified distance to another, the Q-factors are not differentiable. Therefore, four graphs are plotted where each graph represents a specified range of transmission distance. The best Q-factor achieved is around 15.5 dB, which is below the error free threshold and worst than for DPSK and OOK. One of the reasons is that a DQPSK system is more vulnerable to linear interchannel crosstalk. At the same time, the requirement on the laser linewidth is more stringent compared to DPSK or OOK [74]. We have tried to reduce the system degradation due to laser linewidth by limiting it to at most 5.6 MHz (Appendix I). This value is expected to contribute less than 1 dB penalty to the system. In addition to the mentioned limitations, DQPSK is also more sensitive to the nonlinear phase noise effect [42, 43] as well as CD variation. By including also the MTDC bandwidth limitation factor, we do not expect error-free transmission, but only performance above the FEC limit. In Fig. 4.18(a), the Q-factors of both I and Q quadrature channels are shown for 41.5 km setup. In general all Q-factors are above FEC limit. Looking into details, we can see that the performance of some WDM channels around 195.5 THz is around 3 dB worst than for the others. We refer to these WDM channels as “bad channels”, and the others as “good channels”. At 62.9 km, the average Q-factors for good channels degrade around 1 dB compared to 41.5 km setup. There is no significant degradation noticed in the bad channels. The worst performance is observed in the 73.7 km setup, where only several channels reach 12 dB. In average, only a Q-factor of 10.7 dB can be achieved. This is 4 dB worst than the average Q-factor of the good channels in the 41.5 km setup.

In order to improve the comprehension of Fig. 4.18, Fig. 4.19 is plotted. This figure presents the receiver sensitivity of the system for various transmission distances. In the experiment, a variable optical attenuator was placed before the preamplifier to change the received optical power. Among the WDM channels, the 193.8 THz channel was chosen as the sample channel. This is because this channel has a middle value of Q-factor for all transmission distances. Furthermore, this is the middle WDM channel where the linear crosstalk effect is significant. In 73.7 km case, by referring to BER of 1×10^{-4} , around 10 dB penalty can be noticed when compared against the back-to-back curve. The Figure shows that at longer distance, the BER improvement against the increment of the received power is low, which is mainly caused by bandwidth limitation of the MTDC. When a signal lost its bandwidth, power increment can not help to improve the BER quality.

Fig. 4.20 shows the eye diagrams at every distance for the lowest, middle and highest optical frequencies. It can be noticed that at 196 THz, the eye is noisier than that of 192.1 THz, even in a back-to-back setup. These eye diagrams help us to understand the reason of bad performance experiences by the channels after 195.5 THz in Fig. 4.18. The eye degradation is also monitored against the transmission distances. A huge EOP can be noticed in the 73.7 km setup, but this eye diagram still produces a performance of around 1 dB above FEC limit. Surprisingly at the same distance, the eye opening of the 196 THz channel is still sufficient to produce an acceptable Q-factor. For all cases the eye shape was preserved, which shows sufficient CD and CD slope compensation. At long transmission distance, the OSNR is reduced, closing the eye opening. Assuming the implementation of FEC, the results presented in this section show us that a 10 Gbit/s MTDC with minimum bandwidth of 33 GHz is able to support an 80 Gbit/s advanced transmission system. We expect that the

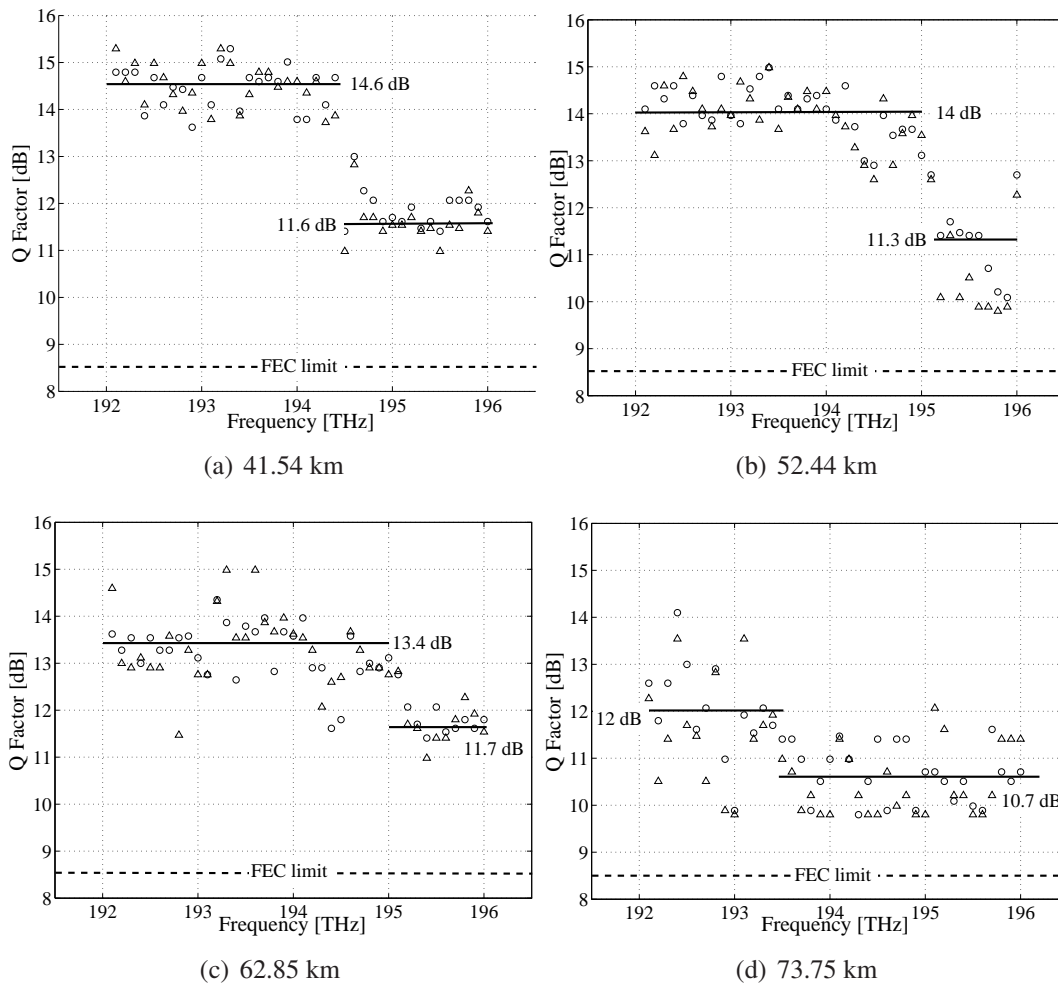


Figure 4.18: DQPSK: Q-factors vs optical frequencies for several transmission distances. Markers \triangle represent I-quadrature, and \circ represent Q-quadratures.

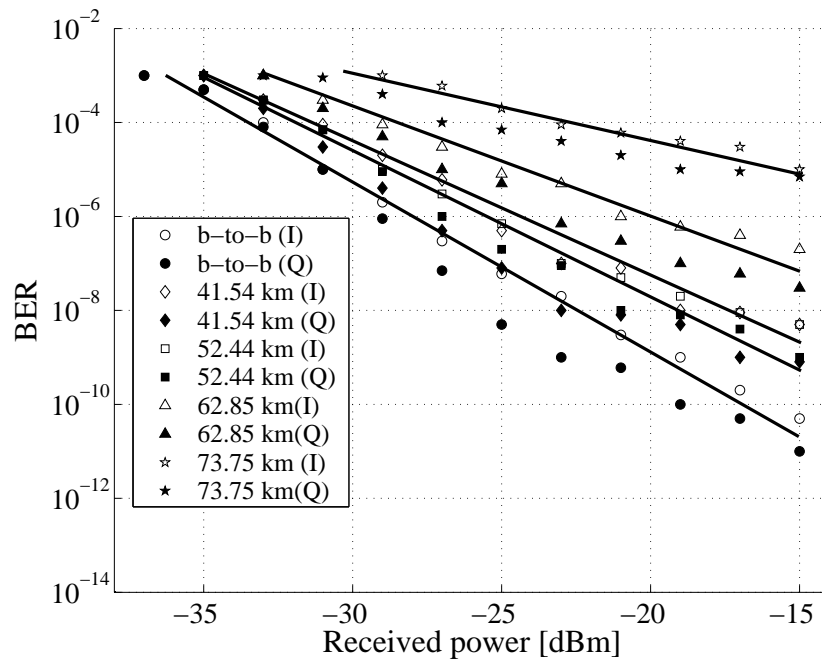


Figure 4.19: DQPSK: Receiver sensitivity at various compensation settings.

overall performance is also affected by high PMD (5 ps) introduced by our MTDC. With a standard MTDC (1 ps PMD), the results of this experiment can be improved.

4.3.5 Automatic CD detection and compensation

40 Gbit/s transmission system is sixteen times more sensitive to CD than its 10 Gbit/s counterpart. Small CD variations is sufficient to introduce errors into the system. Different soil temperatures for different seasons cause CD variations in underground fiber [68, 69]. In WDM reconfigurable optical networks, when the required wavelength at one receiving station changes, or its transmission path is switched, the amount of required CD compensation changes. Therefore, automatic CD detection and compensation is important in order to obtain a set-and-forget optical network.

The MTDC which is used in this experiment has one advantageous characteristic in favour of automatic CD detection and compensation. In order to compensate for all C-band wavelengths, only the CD value of one specified wavelength need to be determined and set as discussed earlier in this chapter. This simplifies the CD detection part because the similar method used for a single wavelength automatic CD compensation, which was already demonstrated in Sandel et. al. [72], can be implemented. In this experiment the available arrival time detection [73] is used for CD detection.

4.3.5.1 Experimental setup

The setup used in this experiment in general is similar to the previous three setups. Only some minor modifications are needed at transmitter and receiver sides in order to realize automatic CD detection and compensation. At the transmitter 5 MHz signal was modulated

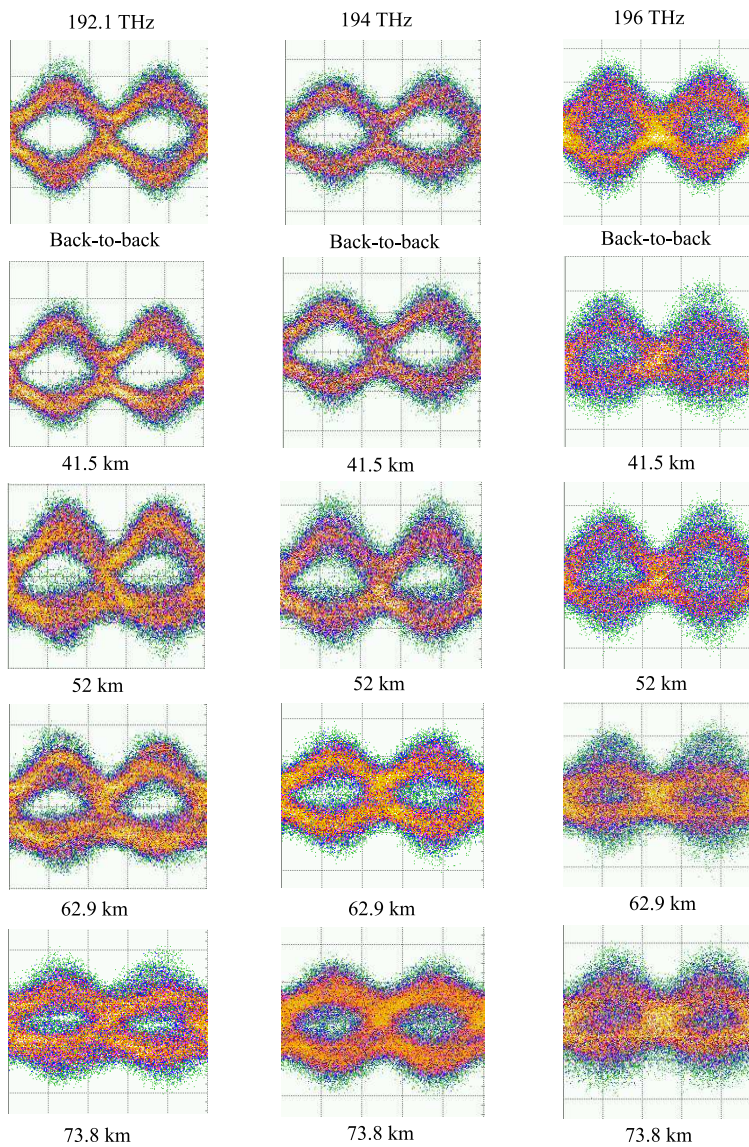


Figure 4.20: DQPSK: Eye diagrams of the first (192.1 THz), middle (194 THz) and last (196 THz) optical frequencies for back-to-back and various transmission distances

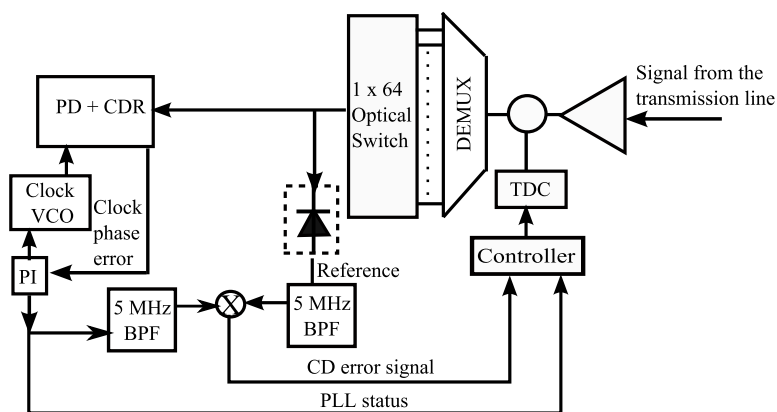


Figure 4.21: Automatic chromatic dispersion compensation setup

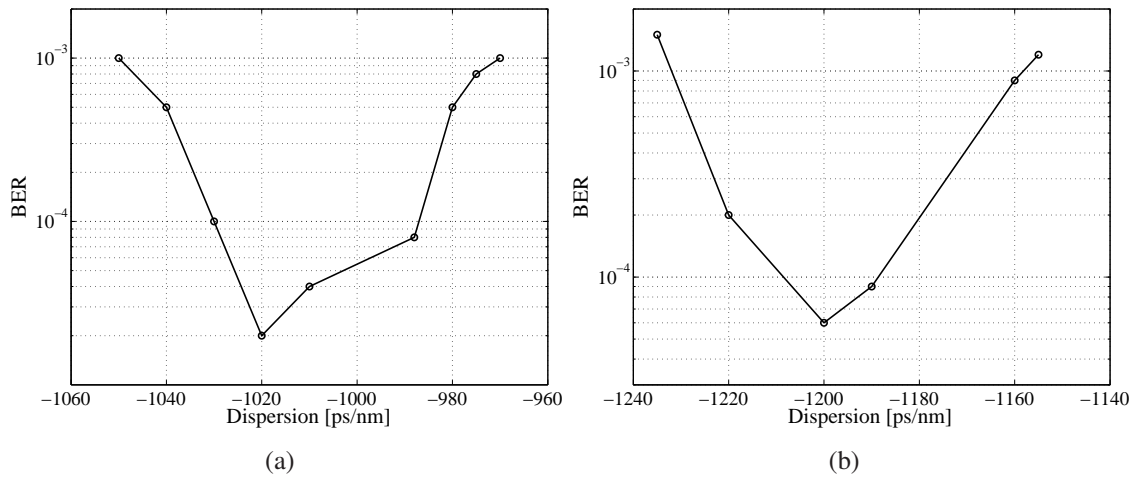


Figure 4.22: BER vs dispersion value for different transmission distances.

onto the 194 THz channel [19]. This signal was used as the reference signal in CD detection. As shown in Fig. 4.21, at the receiver, a small portion of the received signal was tapped and detected by a photodiode. The AM part of the signal was used as the reference signal. At the same time, the signal which was affected by CD, caused arrival time modulation due to the 5 MHz FM signal, and was detected as clock phase error signal. This signal was multiplied with the reference signal, which resulted in a value proportional to the CD value. The detected value was given to the controller that controlled the MTDC. The MTDC set the correct compensation value, and hence the clock phase error was minimized. For residual CD detection and compensation, the PLL normally locked. However, there are also some cases where large CD changes occur. This normally happens when the transmission path changes. When CD changes by more than the system CD tolerance, the PLL will unlock. In this case the controller will automatically assign the MTDC to scan its compensation value for the whole tuning range. This scanning process took around 10 minutes. At a specified dispersion compensation value where the CD is fully compensated, the PLL is locked. This is taken as an initial value for the compensator. This method is also used to set the compensator initially when it is installed for the first time. In this experiment the automatic dispersion control was implemented by using the 194 THz channel. It was tested for all modulation formats (OOK, DPSK and DQPSK). The temperature inside the laboratory was nearly constant. Therefore, it was difficult to observe CD changes due to temperature. In order to test the automatic control, the MTDC setting was manually changed which consequently produced residual uncompensated CD. As a result, the automatic control operation can be monitored.

4.3.5.2 Results and discussions

For all modulation formats, the initial MTDC CD setting was successful and the automatic control worked. For OOK and DPSK, the system worked quasi-error-free after detection and compensation. The clock phase error was effectively minimized and the MTDC was correctly controlled. When the PLL unlocked the TDC scanning also worked and the appropriate CD value was obtained to relock the PLL. The detailed results on OOK and DPSK

are not presented here because they are principally similar to those of the single channel experiment [72]. However, automatic dispersion compensation on DQPSK has never been demonstrated. Therefore the results are chosen for a detailed discussion.

Fig. 4.22 (a) and (b) show the system performance for various MTDC dispersion settings at 62.9 km and 73.7 km. The experiment was started by determining the initial compensation value of the MTDC for a given fiber lengths. For this purpose, the controller assigned the MTDC to continuously change its compensation value through its full compensation range. While the scanning process took place, the status of PLL and the BER quality was closely monitored. This scanning process took around 10 minutes. For 62.9 km and 73.7 km, the PLL locked with the best BER at MTDC compensation values of -1020 ps/nm and -1200 ps/nm, respectively. These two values were used as the initial setting. At these two values, with a proper interferometer control, the BER remained unchanged at the minimum values. Because there were no large temperature changes in the laboratory, the good BER was maintained for relatively long time. To test the MTDC control, residual dispersion was introduced in both positive and negative direction by changing the MTDC compensation setting. The BER degraded as can be seen in both Figures. However the control was able to track the changes and move the MTDC dispersion values to its initial setting. This process took around 10 seconds until the best BER was obtained. For both transmission distances, similar responses were observed. When the MTDC setting was changed by more than the values shown in Fig. 4.22, the PLL unlocked, which made the TDC scanning operated and as a result the correct setting was reestablished. From the Figures, we learned that from the minimum BER until the PLL is unlocked, the DQSPK system allow the CD changes of about ± 40 ps/nm, for both transmission distances. Referring to the curves in Fig. 4.19 (please refer to the previous section), it is shown that a BER degradation of the same order resulted from a power penalty of around 10 dB. For a penalty of around 2 dB the tolerance is around ± 25 ps/nm

4.4 Conclusion

In this Chapter, single span MTDC-supported transmission experiments have been demonstrated. The working principles and some important characteristics of the MTDC have been discussed. In comparison to DCF, the MTDC has a relatively low insertion loss and non-linear effect. The transmission experiments were conducted by using several modulation formats, namely OOK, DPSK and DQPSK at 40 Gbaud symbol rate. SSMF was used as the transmission fiber. In OOK and DPSK systems, good Q-factors were achieved at span lengths of below 60 km. Beyond that distance, the bandwidth limitation characteristics of MTDC became significant, and as a result the system performance degraded. Within the C-band, the MTDC performed satisfactory dispersion slope compensation. Therefore, by setting one dispersion compensation value for a specified wavelength, all wavelengths within the band were compensated. This is an interesting feature that makes the MTDC comparable to the modern DCF in term of slope compensation. An 80 Gbit/s per channel DQPSK WDM transmission experiment, which is supported by MTDC was also conducted. Performance above the FEC limit was achieved over a span distance of up to 73.7 km. Automatic CD detection and compensation on 80 Gbit/s DQPSK signal was also successful. In this experiment, arrival time detection was used for CD detection. The results of this

experiment suggest that the MTDC has a good potential to replace bulky DCF in the network. Transmission systems will benefit from by its low insertion loss and nonlinearity effect penalty. In 40 Gbit/s systems, the 10 Gbit/s MTDC with 33 GHz minimum bandwidth is suitable for short span Metro networks. For long haul application, the MTDC with at least 60 GHz of optical bandwidth is preferable to avoid a bandwidth limitation penalty [20, 46, 47]. However, in a network that is fully supported by NZDSF, the MTDC will show better performance in long span transmission due to the reduced compensation value required. The low compensation setting increases the MTDC's bandwidth and eliminates the passband filtering penalty. Modification to the dispersion slope of current MTDC is necessary in order to support NZDSF.

Chapter 5

Conclusions and Future Work

Chromatic Dispersion introduces pulse broadening and phase variations in PSK system. In this dissertation several important aspects regarding chromatic dispersion management in PSK system are discussed by first introducing the fundamental dispersion concepts, the asynchronous PSK transmission systems, and various dispersion management techniques. Then a low cost single channel dispersion compensator is introduced with the aim to support residual dispersion compensation in 160 Gbit/s advanced transmission systems. In the last part of this dissertation the implementation of a Multichannel Tunable Dispersion Compensator (MTDC) as a transmission line dispersion compensator is presented.

DPSK and DQPSK system were briefly introduced in the beginning of Chapter 2. This was followed by the description of dispersion effects in pseudolinear transmission, and dispersion management requirements for high speed transmission especially with advanced modulation formats. The nonlinear intrachannel effect, which is initiated by pulse overlapping, a phenomenon which is caused by chromatic dispersion, was also highlighted. Dispersion managements which include DCM, TDC and dispersion maps were also covered. It can be concluded that in advanced fiber optic systems, effective dispersion management must also encompass other parameters such as nonlinear phase noise and fiber nonlinearity, rather than the dispersion alone. In the future, it is expected that DCFs with high insertion loss and nonlinearity and fixed dispersion value may be replaced by MTDCs. With lower insertion loss, the EDFAs which are currently installed to compensate DCF loss can be partly eliminated, therefore reducing the effect of NLPN and linear noise, which is important in long-haul transmission system.

Performance assessment of a low cost DCF-based dispersion compensator in a 160 Gbit/s DQPSK PoDM showed that a low cost solution is sufficient to support Tbit/s WDM transmission. In the experiments, the compensator operated as channel-by-channel dispersion compensator, even though it has broadband characteristic. This is because the DCF (raw material) used to develop the CDC did not have 100% dispersion slope compensation of any transmission fiber. Furthermore the transmission line was also built by a mixture of several fiber types. Therefore only dispersion compensation is relevant but not dispersion slope compensation. By using DCF with a 100% slope compensation, a compensator equipped with dispersion slope compensation facility can be developed. Such compensator will be able to compensate the residual dispersion of all WDM channels simultaneously. However it can only operate in a network with a single type of fiber. Consequently, separate compensators are needed to support different networks with different fiber types. This

type of compensator produces a network that is fully supported by DCF. It was proven to be suitable for high bitrates and advanced modulation formats. Supported by this compensator, transmission of around 2 Tbits/s capacity over several long fiber spans (100 km) was successful. Over conventional span distances (60 to 80 km), up to 5 Tbit/s transmission was conducted over a total distance of more than 300 km. The main limitation of this compensator is its high insertion loss and nonlinearity effect. On the other hand its advantages are low manufacturing cost, broadband characteristic and high compensation range.

Experiments to replace DCF by an MTDC have shown promising results. In terms of compensation range, the MTDC is suitable to replace DCF in the network. Depending on the network design, the MTDC could be used either as a non-adaptive dispersion device or an adaptive tunable dispersion device. Normally an adaptive tunable device is only needed at receiver side. However, when the requirement for reconfigurable dispersion map is unavoidable, tunable devices may also be installed as in-line dispersion compensators. In our experiment it was shown that a 10 Gbit/s system MTDC, whose bandwidth is reduced to 33 GHz at maximum compensation, is sufficient to support 40 Gbit/s WDM transmission over the span distance of a Metro network. For a system with transmission spans longer than 60 km, the performance is limited by the narrowing of the MTDC bandwidth. However this bandwidth limitation will not be pronounced when MTDC is used in a network with NZDSF due to the four-fold reduction of the required compensation value. The combination of MTDC and NZDSF could become a good solution to support long span distances in advanced transmission system. In an 80 Gbit/s per WDM channel DQPSK system, performance of above the FEC limit was achieved over up to 73.3 km SSF, where the signal pass through the 33 GHz filter created by MTDC. This is remarkable because the MTDC is designed for 10 Gbit/s operation. Combining MTDC with arrival time detection, automatic chromatic dispersion compensation was demonstrated in OOK, DPSK and DQPSK systems. These experiments showed that the implementation of future highly spectral efficient transmission and dynamic dispersion management is feasible.

As a conclusion, this dissertation has covered some important aspects in implementing dispersion management in future advanced transmission system. We have shown that a low cost solution is sufficient to support advanced systems. However, there are some limitations, which can be solved by using more advanced techniques. This dissertation is hoped to become a useful reference in the future when high capacity WDM systems with advanced modulation formats are ready for implementation.

Appendix A

Optical Fiber Parameters

In this Appendix optical fiber parameters for SSMF, NZDSF and DCF are presented. The parameters are fiber insertion loss, α , dispersion coefficient, D , dispersion slope coefficient, S , and effective area, A_{eff} which are tabulated in Table A.1.

Table A.1: The specifications of several types of optical fiber

	$\alpha \left(\frac{dB}{km} \right)$	$D \left(\frac{ps}{nm.km} \right)$	$S \left(\frac{ps}{nm^2.km} \right)$	$A_{eff} (\mu m^2)$
SSMF	0.20	+17	+0.06	82
NZDSF (TWRS)	0.20	+4	+0.055	80
NZDSF (LEAF)	0.20	+3	+0.1	115
DCF for SSMF	0.50	-100	-0.35	12
Our DCF	0.68	-86	-0.13	12
DMF (positive)	0.19	+20	+0.06	107
DMF (negative)	0.23	-42	-0.13	33

Appendix B

CDC: Number of turns for specified compensation lengths

Table B.1: Number of turns for specified compensation lengths

SSMF length, km	DCF length, km	Dispersion (ps/nm/km)	Number of turns
0.125	0.025	-2.125	68
0.25	0.049	-4.25	136
0.5	0.099	-8.5	271
1.0	0.198	-17.0	542
1.5	0.296	-25.5	813
2.0	0.395	-34.0	1084
2.5	0.494	-42.5	1355
3.0	0.593	-51.0	1626
3.5	0.692	-59.5	1897
5.0	0.988	-65.0	2710
10.0	1.976	-170	5420

Appendix C

Optical Spectrum with filtering effect

In Appendix C, optical spectra of 40 Gbaud DPSK and DQPSK signal are presented. The 40 Gbaud DPSK optical spectrum with and without filtering effect are obtained from Tsuritani et. al. [47] and for DQPSK, the spectra are found in Yoshikane and Morita [46]. It is well known that an optical signal with broader optical spectrum is less tolerant to the effect of fiber impairment such as CD and PMD. Therefore, it is important to compare the optical spectra of DPSK and DQPSK to estimate their relative performance in comparison to each other. In this Appendix, we present the optical spectrum of CS-RZ DPSK, NRZ-DQPSK and also CSRZ-DQPSK. In Fig. C.3(a), it is shown that at the defined 10 dB optical spectral bandwidth, a CS-RZ DPSK signal without optical filtering has around 130 GHz bandwidth. This bandwidth is reduced according the optical bandwidth of the filter. NRZ DQPSK has a smaller spectral bandwidth which is around 80 GHz. As depicted in Fig. C.3, the CS-RZ DQPSK spectral bandwidth is similar to that of CS-RZ DPSK. Even though, the optical spectrum of NRZ DPSK is not presented, based on the comparison between NRZ DQPSK, CS-RZ DQPSK and CS-RZ DPSK, we can expect that the optical spectrum of NRZ DPSK is similar to that of NRZ DQPSK.

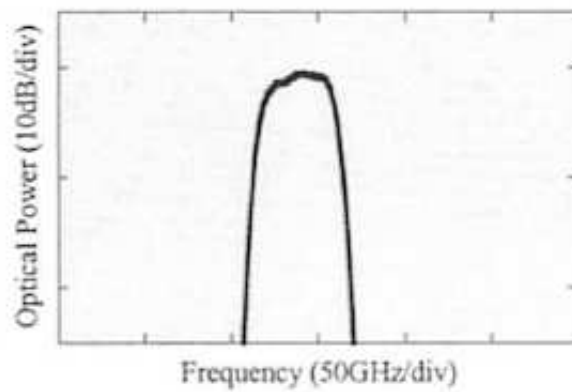
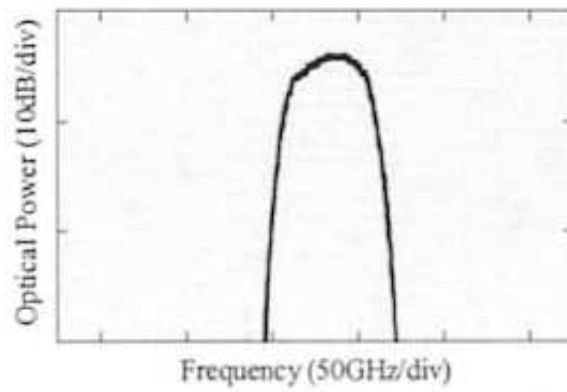
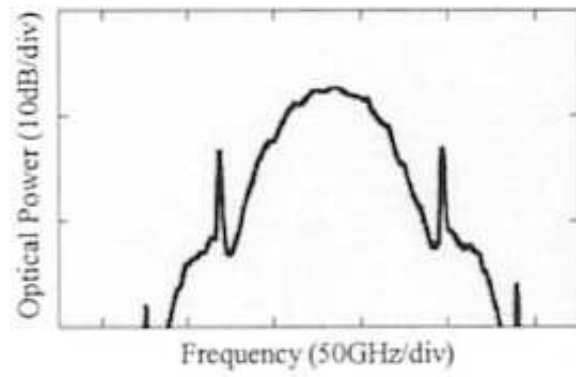


Figure C.1: 40 Gbaud CSRZ DPSK:(a) Without filter, (b) With 65 GHz filter, (c) With 45 GHz filter

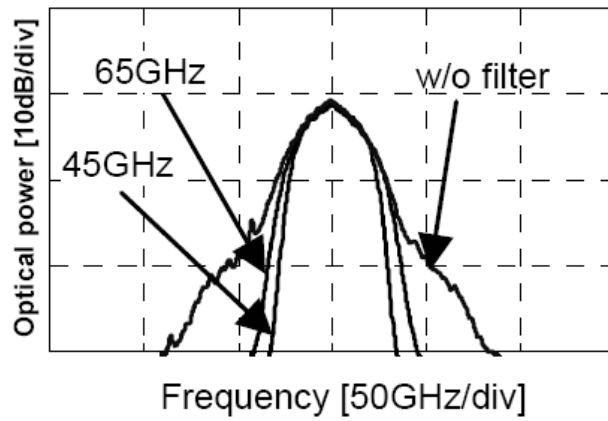


Figure C.2: 40 Gbaud NRZ DQPSK

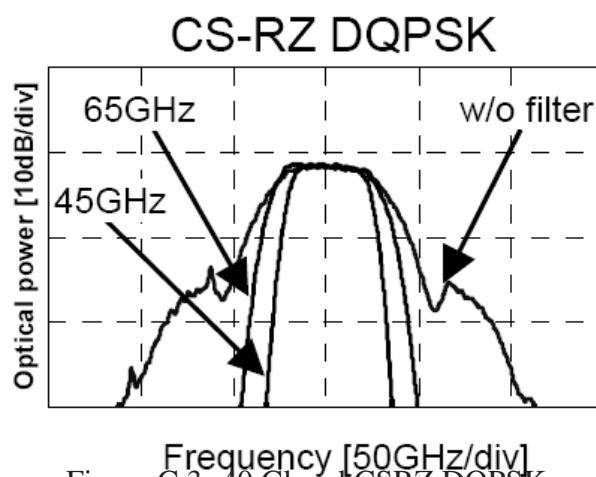


Figure C.3: 40 Gbaud CS-RZ DQPSK

Appendix D

Eye diagrams of filtered 40 Gbaud DPSK and DQPSK signal

In 40 Gbit/s systems, where the optical spectrum is broad, the effect of optical filtering is important. This phenomenon was studied in a 40 Gbaud DQPSK system by Yoshikane et. al.[46] and by Tsuritani et. al. [47] in a 40 Gbaud DPSK system. The main objective of both studies was to investigate the system performance under strong optical filtering condition. Strong optical filtering normally happens in a closely spaced WDM demultiplexing process . Recently, it was also reported that a TDC that is operated at high dispersion setting introduced similar optical filtering effect [19, 71]. In this Appendix the resulting eye diagrams of a strongly filtered signal are presented for both DPSK and DQPSK. Two optical filters with pass-bandwidths of 45 GHz and 65 GHz were used to introduce this effect [46, 47].

D.1 CS-RZ DPSK

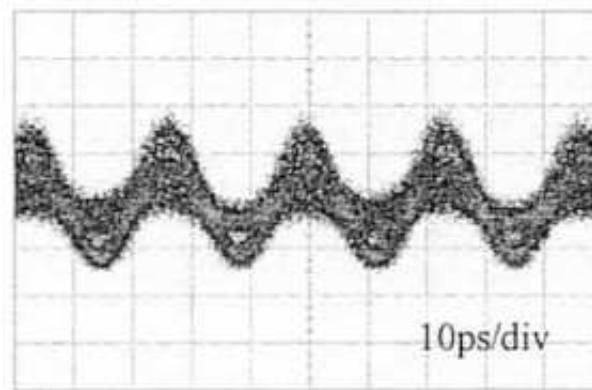
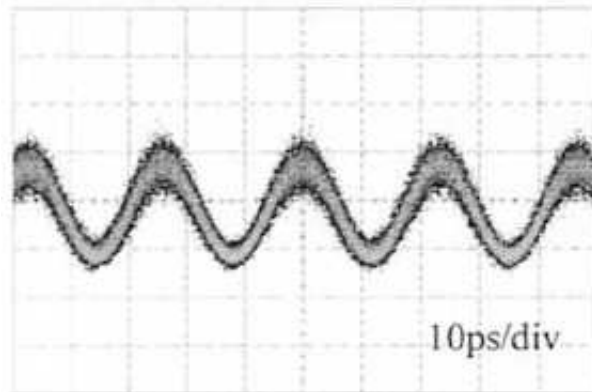
This section presents the eye diagrams of CS-RZ DPSK signal without optical filtering, with 65 GHz optical filtering and 45 GHz optical filtering, which are shown in Fig. D.1. All eye diagrams were recorded before the MZDI. As can be seen, the optical filtering process distorted the eye diagram especially at 45 GHz pass-bandwidth. With the 45 GHz optical filter the RZ waveform was distorted to an NRZ-like waveform. This band limitation was reported to contribute to pattern dependent waveform distortion [47].

D.2 NRZ DQPSK

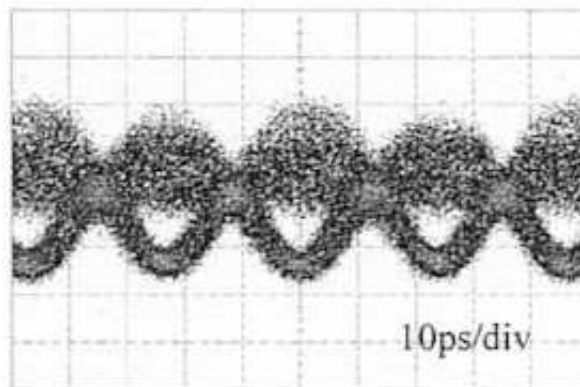
In this Section, the eye diagrams of NRZ DQPSK signal are presented. Similar as in the previous Section, the eye diagrams were recorded before the MZDI. In Fig. D.2, it is shown that this format also suffers to the effect of optical filtering. With the 45 GHz filter the NRZ eye diagram was strongly distorted.

D.3 CS-RZ DQPSK

In this section the eye diagrams before and after the MZDI are presented in Fig. D.3 and Fig. D.4, respectively. After the MZDI, the obtained eye diagrams represent the received

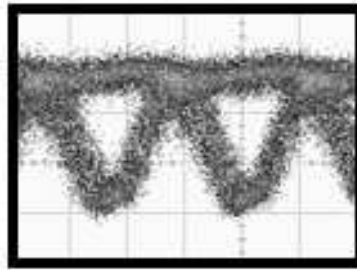


(a)

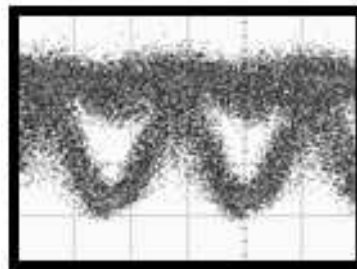


(b)

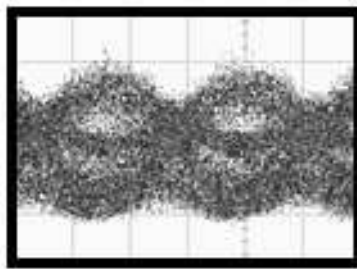
Figure D.1: Optical filtering effect in a CS-RZ DPSK eye diagram : (a) Without filter, (b) With 65 GHz filter, (c) With 45 GHz filter



(a)

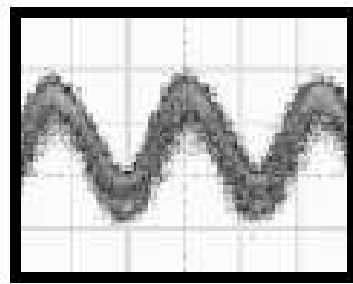


(b)

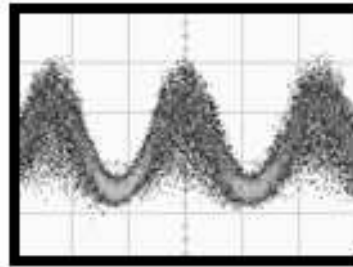


(c)

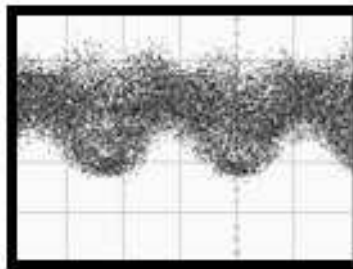
Figure D.2: Optical filtering effect in a NRZ DQPSK eye diagram : (a) Without filter, (b) With 65 GHz filter, (c) With 45 GHz filter



(a)



(b)



(c)

Figure D.3: Optical filtering effect in CS-RZ DQPSK eye diagram before MZDI: (a) Without filter, (b) With 65 GHz filter, (c) With 45 GHz filter

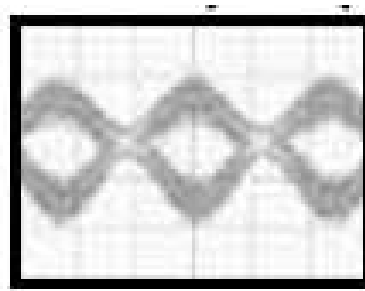
signal of the system.

D.3.1 Before Interferometric demodulation

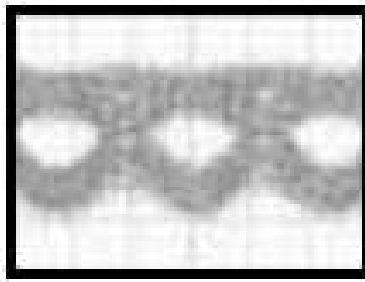
Before the MZDI, a strong eye diagram distortion can be observed in Fig. D.3(c) when 45 GHz optical filtering was used. With the 65 GHz optical filter, only small eye pattern degradation can be noticed.

D.3.2 After Interferometric demodulation

After the MZDI, only two eye diagrams are shown which are the eye diagram without filtering and after 45 GHz filtering. Only a small eye opening penalty can be noticed in Fig. D.4 (b). This highlights that this format survives 45 GHz optical filtering. In term of OSNR



(a)



(b)

Figure D.4: Optical filtering effect in CS-RZ DQPSK eye diagram after MZDI: (a) Without filter, (b) With 45 GHz filter

penalty, CS-RZ DQPSK experienced a 2 dB penalty after 45 GHz optical filtering. It was reported in Yoshikane et. al. [46] that CS-RZ DQPSK outperformed NRZ DQPSK in terms of tolerance to optical filtering.

Appendix E

Double-stage Erbium-doped fiber amplifier

This Appendix discusses the characteristics of double-stage EDFAs which were used in the experiments. For all EDFAs, 980 nm pump is used for the first stage, followed by the second stage that uses 1480 nm pump. In the 980 nm EDFA (first stage), gain filter is used to filter out the EDFA peak around 1530 nm region. As a result, the gain inside this region is expected to be lower than that of other wavelengths. The second stage of the EDFA uses a single internal 1480 nm pump and two external 1480 nm pumps, without gain filter. The highly polarized outputs of both external 1480 nm pumps were combined by using a polarization beam splitter (PBS). The output of this stage has a higher gain at 1530 nm compared to other wavelengths. Therefore, in principle, the combination of both EDFA stages is able to produce a flat gain for the whole C-band. In practice, DCF is installed between the first and the second stage for in-line dispersion compensation. In this Appendix the results of the characterization of two double-stage EDFAs with different 980 nm pump powers (first stage) are compared (the second stage of both EDFAs uses similar 1480 nm pump). To avoid confusion, we name the EDFA with high current 980 nm pump as EDFA-H and the one with low current 980 nm pump as EDFA-L. The experiment was conducted by using a 40 channels WDM signal from 192.1 THz to 196.0 THz.

E.1 First Stage (980 nm)

The first stage EDFA output signal was recorded for various input power. Two EDFAs which are differentiated by the first stage (980 nm) pump current were used. EDFA-H supports high pump current around 554 mA and the second EDFA, namely EDFA-L uses a low pump current which is 138 mA. By changing the input power per channel, the EDFA gains were recorded and plotted in Fig. E.1. Fig. E.1(a) and (b) show the characteristics of the first stage amplifier of EDFA-L and EDFA-H, respectively. A gain slope was observed, which increased with input power. At low input power the gain slope was negative. The results also showed that the EDFA with low pump current experienced a gain slope about two times higher than the high current pumped-EDFA. For the low current EDFA, the maximum total output power was +14 dBm, which corresponds to -2 dBm/channel in a 40-channel 100 GHz-spaced WDM system. For the high pump current EDFA (EDFA-H), the maximum total output power was +18 dBm, or +2 dBm per channel. In the 1530 nm wavelength

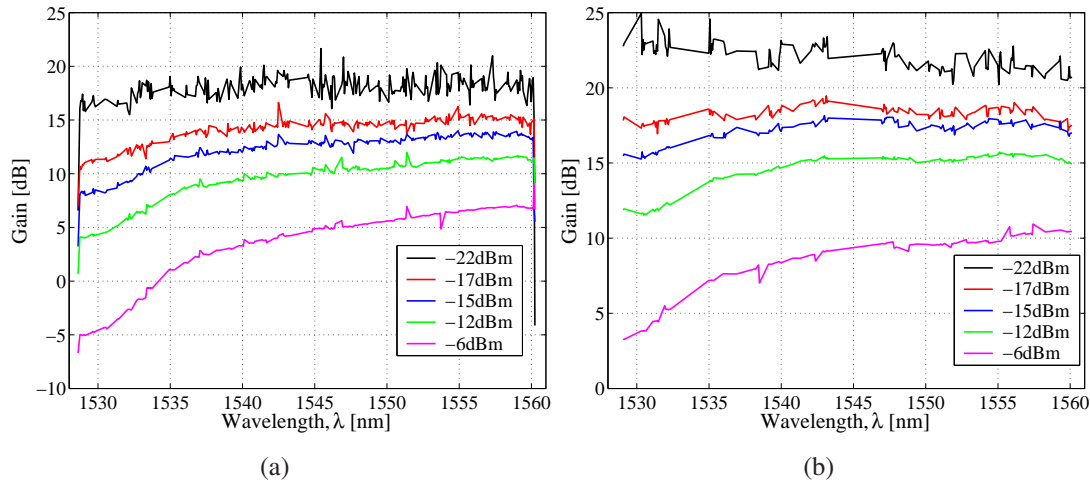


Figure E.1: First stage EDFA characteristics: (a) EDFA-L ,(b)EDFA-H

region the lowest gain was experienced by both EDFAs. This happened due to the installed gain filter. The ripple can also be seen in the output signal when the lowest input power is used. This is because of the low OSNR of the input signal. During measurement, the Optical Spectrum Analyzer (OSA) measurement sensitivity was low. This ripple will be eliminated when higher OSA sensitivity is used, but longer measurement time is needed.

E.2 Second Stage (1480 nm)

The design of the second stage EDFA for both amplifiers is similar (pump laser has similar maximum pump current), and hence showed similar characteristics. The maximum total output power for both EDFA was limited to +22 dBm, so that the fiber optics connectors are protected. The gain slope characteristic was similar to the first stage except for the high gain in 1530 nm wavelength region. In contrast to the first stage, no gain filter is used in this EDFA stage. As a result, the gain characteristics of the second stage becomes a complement to the first stage, thus producing flat gain for the whole C-band.

E.3 Cascaded configuration (980 nm + 1480 nm)

In cascaded configuration, a Variable Optical Attenuator (VOA) was installed between the stages to control the input power to the second stage. In all cases, both EDFA stages were operated at saturated output power. Three input powers were tested in this experiment.

E.3.1 Pin = -22 dBm

For low input power, a negative gain slope was produced at the first stage output. Therefore, a high input to the next stage is required to produce flat gain output signal. The disadvantage of this configuration is the resulting non-uniform OSNR between the two outermost channels which is caused by highly positive gain slope produced in the second stage.

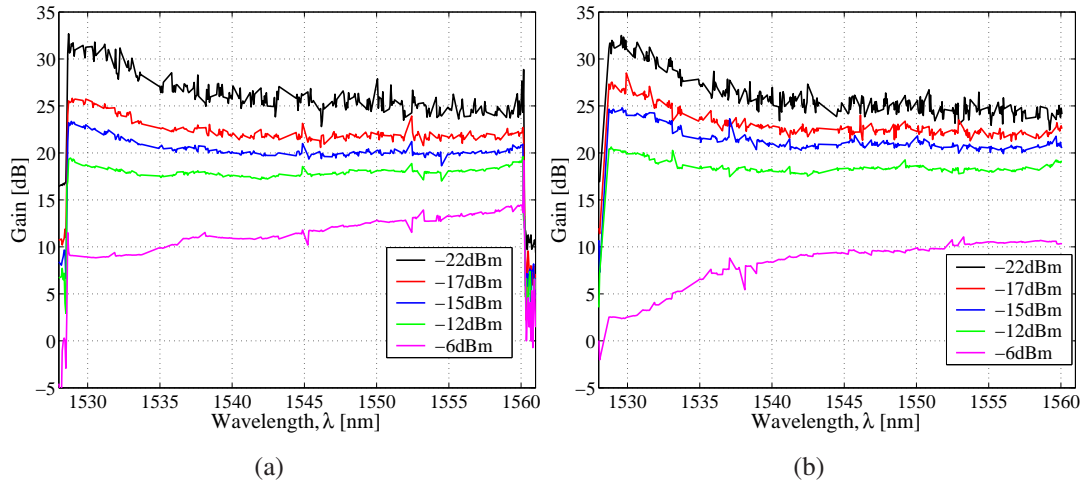


Figure E.2: Second stage EDFA characteristic: (a) EDFA-L ,(b) EDFA-H

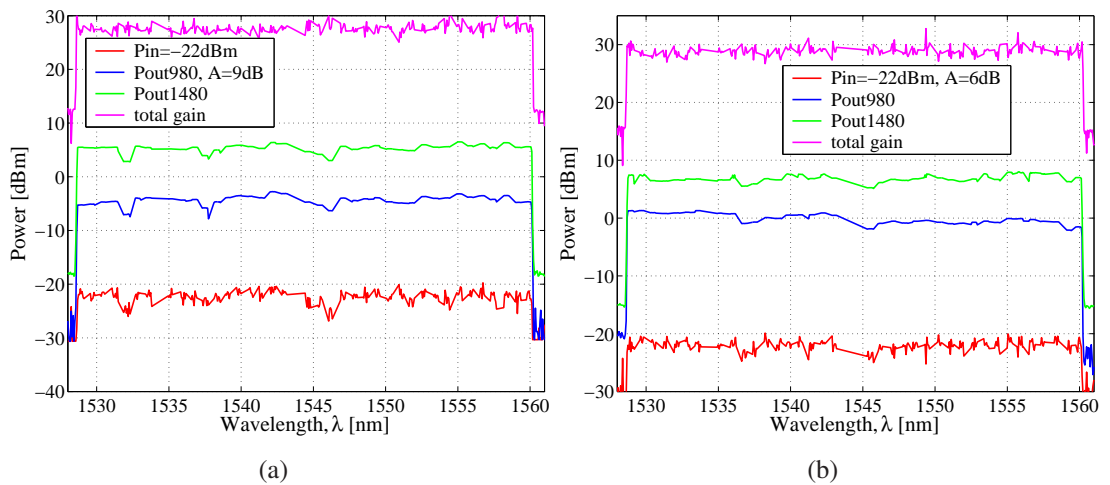


Figure E.3: Gain characteristic at -22 dBm/ch input power: (a) EDFA-L: 980 nm EDFA output is -5 dBm/ch and +11 dBm total ,(b) EDFA-H: 980 nm EDFA output is 0dBm/ch and +16 dBm total

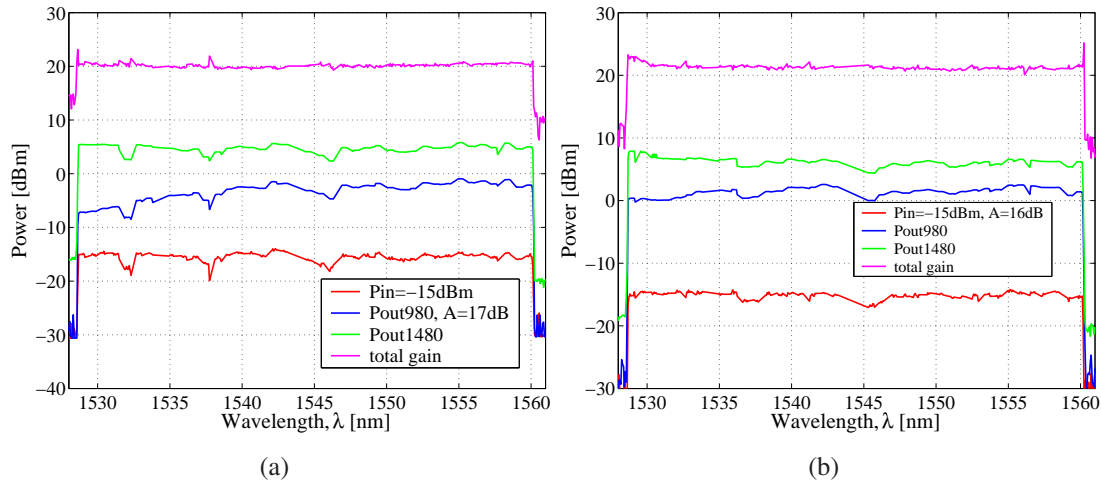


Figure E.4: Gain characteristic at -15 dBm/ch input power: (a) EDFA-L: 980 nm EDFA output is -5 dBm/ch in average, and +11 dBm total, (b) EDFA-H: 980 nm EDFA output is 0 dBm/ch in average, and +16 dBm total

E.3.2 Pin= -15 dBm

For -15 dBm/channel input power, flat gain was produced at the double-stage EDFA output without affecting the OSNR uniformity between the two outermost WDM channels. Except for the output power of the wavelengths that is located within 1530 nm region, which is low for the first stage and high for the second stage, the respective output gain slopes for both EDFA were flat, which produced flat output power for all WDM channels at the output of the second stage. It turned out that the input power per channel for the second stage was similar to that of the first stage for the best gain characteristic. Comparing Fig. E.4(a) and (b), at high input power to the first stage, it is noticed that the EDFA with high current 980 nm pump required less attenuation in the middle of the stages than the low pump current 980 nm EDFA. This is because, at the same input power, the slope steepness produced by the first stage of EDFA-H is lower than that for EDFA-L. This is very convenient because less attenuation is needed in the middle of the stages, therefore the final output will have higher OSNR in comparison to the EDFA-L.

E.3.3 Pin= -6 dBm

For the input power of -6 dBm per channel, high attenuation was needed in the middle of the stages in order to reverse a very high positive slope produced by the first stage. As a result, the final output signal has low OSNR value at the shorter wavelength channels. This is a disadvantage of this configuration. By using EDFA-H, the OSNR is higher due to the higher input power to the second stage. In conclusion the best input power per channel is around -15 dBm per channel, which is similar for both EDFA stages.

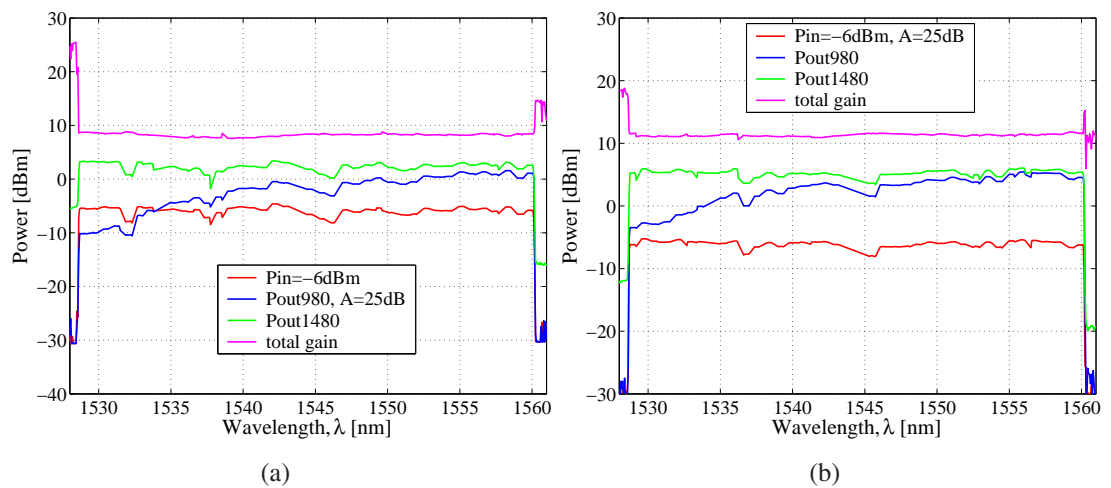


Figure E.5: Gain characteristic at -6 dBm/ch input power: (a) EDFA-L: 980 nm EDFA output is -5 dBm/ch in average, and +11 dBm total, (b) EDFA-H: 980 nm EDFA output is 0 dBm/ch in average, and +16 dBm total

Appendix F

Raman Amplifier

This Appendix demonstrates an example of the Raman amplifier gain characteristic. In contrast to an EDFA, Raman amplification needs transmission fiber as an amplification medium. In this example, 60 km of NZDSF was used as the transmission fiber. The experimental setup is illustrated in Fig. F.1. In this experiment forty 100 GHz spaced WDM channels were used as the input signal. Variable Optical Attenuators (VOA) were used to control the power level at several specified points.

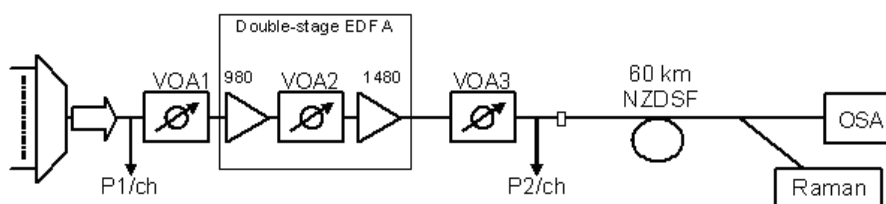


Figure F.1: Experiment setup

In the first experiment, VOA1, the double-stage EDFA and VOA2 were excluded. Raman gain was monitored by changing the input power per channel from -12 dBm to -8 dBm. As shown in Fig. F.2, no obvious slope change was noticed. Therefore it is concluded that the Raman gain is independent of input power in this power range.

The second experiment combined the double-stage EDFA with Raman amplification. The result is shown in Fig. F.3. By referring to the original input signal, a gain slope and a large gain ripple were observed. However by changing the reference point to the EDFA output, less gain ripple was noticed. Therefore the combination of Raman amplification and EDFA increases the gain at the cost of gain slope and gain ripple.

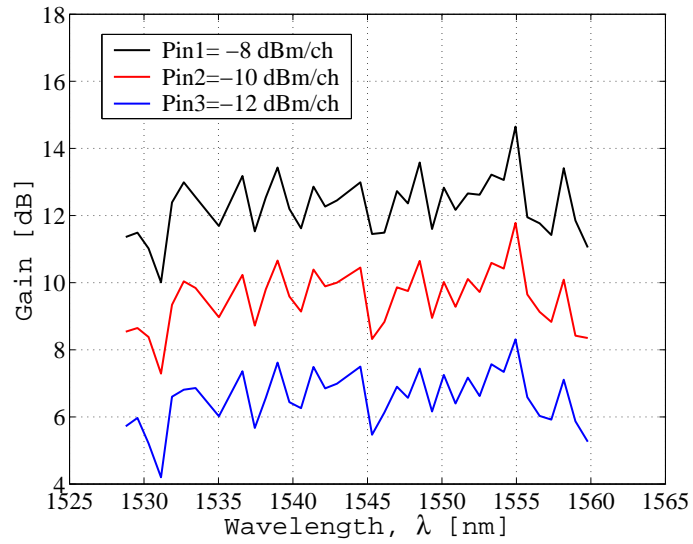


Figure F.2: Raman gain at different input power

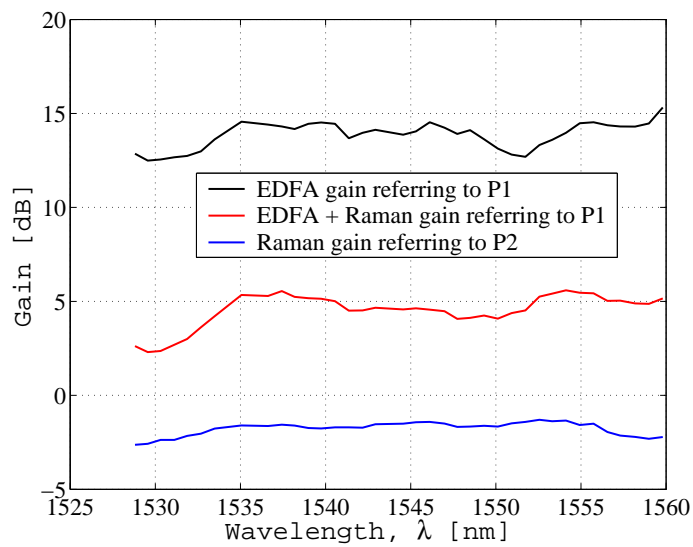


Figure F.3: Combination of Raman and EDFA gain

Appendix G

Phase variance in quasi-linear system

Non-linear Phase Noise (NLPN), specifically SPM induced NLPN, which is contributed by the combined effect of ASE noise and Kerr effect, was considered by Gordon and Mollenauer. The Kerr nonlinearity converts amplitude fluctuation into phase fluctuation. At that time, it was argued that the higher nonlinear tolerance of a Phase Modulated (PM) systems which is due to its constant amplitude, may be reduced by this effect. However, it was shown later on that the NLPN effect reduces in high dispersion transmission links without dispersion compensation.

In order to show the effect of CD to NLPN, in Green et. al. [54], an equation describing the phase variance in the optical fiber in relation to chromatic dispersion was derived. The input signal is given by $\begin{pmatrix} a\phi \\ \delta a \end{pmatrix}_{in}$ with a , ϕ are the signal amplitude and phase respectively. The fiber transfer matrix is

$$M(\alpha, \beta, \gamma; L, \omega)$$

and the output signal after propagation along distance, L is

$$\begin{pmatrix} a\phi \\ \delta a \end{pmatrix}_{out} = M(\alpha, \beta, \gamma; L, \omega) \begin{pmatrix} a\phi \\ \delta a \end{pmatrix}_{in} \quad (\text{G.1})$$

In this derivation, dispersion compensation and fiber loss, α was not considered, therefore, α equals to zero.

$$M(0, \beta, \gamma; L, \omega) = \begin{bmatrix} \cos(\delta L) & (\delta/\beta\omega^2)\sin(\delta L) \\ (-\beta\omega^2/\delta)\sin(\delta L) & \cos(\delta L) \end{bmatrix} \quad (\text{G.2})$$

where $\delta(\omega) = [\beta\omega^2(\beta\omega^2 + 2\gamma a^2)]^{\frac{1}{2}}$; β , γ , L and ω are the CD coefficient, nonlinear coefficient, fiber length and angular frequency respectively. By inserting Eq. G.2 into Eq. G.1, the output phase variance is given by

$$2\rho \langle \phi^2(t) \rangle = 1 + \frac{\Delta L_D}{2L_{NL}} \int_{-\pi\Delta}^{\pi\Delta} \frac{d\omega}{2\pi\omega^2} \left\{ 1 - \frac{\sin [2L\delta(\omega)]}{2L\delta(\omega)} \right\} \quad (\text{G.3})$$

where $\rho = \frac{a^2}{N\Gamma}$ is the signal-to-noise ratio, with N is the number of span and Γ is the total noise.

L_D is the dispersion length,

$$L_D = \frac{1}{\beta\Delta^2} \quad (\text{G.4})$$

Δ is the system bandwidth, and L_{NL} is the nonlinear length

$$L_{NL} = \frac{1}{(2\gamma'a^2)} \quad (\text{G.5})$$

with γ' is the average nonlinearity over a span of fiber.

In Eq. G.3, the second part of right-hand-side of the equation represents the NLPN. It can be notice that NLPN increases with signal amplitude and nonlinear coefficient, and reduce with dispersion and bandwidth increament. In a highly dispersed system, NLPN value approaches zero and the output phase variance only depends on linear noise, $\frac{1}{2\rho}$.

In a simulation without CD compensation, it was shown that the phase variance reduced when CD is increased, showing the phase variance suppression by CD. With CD compensation, it was demonstrated that the phase variance suppression depends on the dispersion map. In the dispersion map with full dispersion compensation after every span, the phase variance suppression is less when compared against the uncompensated case. This means that phase variance suppression does not survive this dispersion map. However, the system performance improved in the system with under-compensated span, and superior performance is produced in a system with lump-compensation at the receiver end. But, in this analysis, for lump-compensation, the effect of DCF nonlinearity was neglected. By including the DCF nonlinearity effect, the lump-compensation system will give very poor performance due to the very long DCF used and very high DCF launch power needed. Therefore, it is concluded that the under- or over-compensated span system is the best solution to ensure phase variance suppression by the system CD to survive CD compensation. From Eq. G.3, it can also be concluded that the NLPN reduces with the increase of system bandwidth, and as a consequence, the phase variance reduces. For example changing from 10 GHz to 40 GHz system leads to sixteen folds reduction of the phase variance. Therefore, in highly dispersed 40 Gbit/s systems, the phase variance is very low which reduces the tight requirement of dispersion map management.

Appendix H

Chromatic Dispersion Tolerance

In most literature, the CD tolerance of DQPSK signals are normally compared to that of DPSK and OOK signals with the same bitrate. In this case, DQPSK systems have nearly twice the CD tolerance in comparison to DPSK or OOK. This is because the signal is transmitted at a two times lower symbol rate, and hence two times larger pulsewidth. In this Appendix, performance comparison is also made between DQPSK and DPSK signal with the same symbol rate. The result for CD tolerance of 40 Gbaud DPSK and 20 Gbaud DQPSK were taken from Charlet et. al. [4], and for the 40 Gbaud DQPSK system, the result was obtained from our own measurement. This comparison is important, in order to estimate how much transmission penalty we need to suffer as a cost for doubling the transmission data rate. From Fig. H.1, we can notice that at the same bitrate, DQPSK is more tolerant to CD than DPSK. But at the same symbol rate it is seen that DQPSK is more sensitive to CD than DPSK. This is because in DQPSK, by referring to the phasor diagram (please refer Section 2.1), it is seen that the symbol separation distance is closer in comparison to DPSK (only $\frac{\pi}{2}$ for DQPSK compared to π for DPSK), which makes this format less tolerant to the phase variation introduced by CD. Theoretically, the CD tolerance of DQPSK is two times worst than that of DPSK or OOK. In Fig. H.1, we can see that at a 1 dB penalty the CD tolerance of DQPSK is about 1.5 times worst than that of DPSK, which is near to the theoretical expectation.

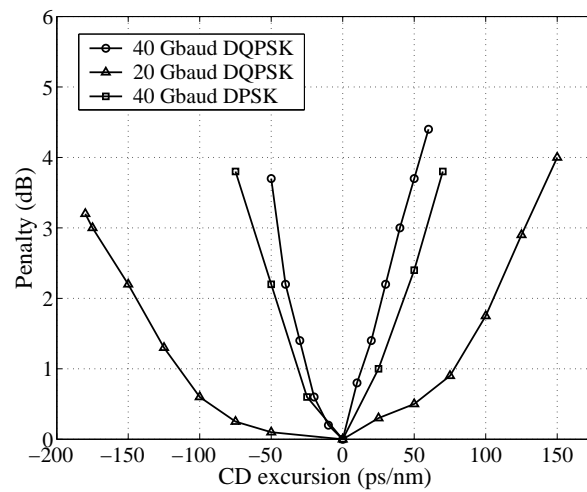


Figure H.1: The comparison of CD tolerance between 40 Gbaud DPSK, 20 Gbaud DQPSK and 40 Gbaud DQPSK

Appendix I

WDM Laser Linewidth

In this Appendix the linewidth of all lasers that were used in the experiments are listed. In PSK systems, especially DQPSK, it was suggested by Savory and Hadjifotiou [74] that the phase noise from the finite linewidth laser will result in perturbation of the the $\pm \frac{\pi}{2}$ phase difference in the MZDI at the receiver. It was also showed by Gene et. al. [14] that the increase in laser linewidth limited the achievable transmission distance in a DQPSK system. Therefore, it is important to have the information on the laser linewidth in order to correctly investigate the performance of DQPSK system. The relation between phase variance ϕ^2 , and laser linewidth is as follows.

$$\phi^2 = 2\pi\tau \Delta f \tag{I.1}$$

where τ is the pulse duration, and Δf is the laser linewidth.

Optical Frequency, THz	Linewidth, MHz	Optical Frequency, THz	Linewidth, MHz
192.1	1.4	194.1	2.7
192.2	5.0	194.2	5.5
192.3	4.0	194.3	3.5
192.4	1.8	194.4	3.0
192.5	1.6	194.5	5.0
192.6	1.7	194.6	1.8
192.7	2.0	194.7	2.0
192.8	2.5	194.8	2.5
192.9	2.1	194.9	2.7
193.0	2.3	195.0	1.0
193.1	1.5	195.1	5.0
193.2	1.6	195.2	1.0
193.3	3.4	195.3	2.0
193.4	5.6	195.4	1.2
193.5	5.2	195.5	2.5
193.6	5.1	195.6	5.2
193.7	1.8	195.7	3.3
193.8	1.4	195.8	5.0
193.9	5.0	195.9	3.7
194.0	3.5	196.0	0.8

Table I.1: List of WDM lasers linewidth

Appendix J

Detailed description of WDM Transmitter

This Appendix presents the complete transmitter setup which we used to produce OOK, DPSK and DQPSK modulation formats, together with PoIDM. The transmitter setup is depicted in Fig. J.1. Forty 100-GHz spaced WDM channels (maximum) with optical frequencies from 192.1 THz (1560.61 nm) to 196 THz (1529.55 nm) are used. The WDM channel count differs from one experiment to another. The laser output signals are combined with equal polarizations, and simultaneously modulated using a dual-drive Mach-Zehnder modulator to generate an NRZ differential-phase-shift-keyed (DPSK) signal. The linewidths of the lasers are in the range of 0.8 to 5.6 MHz. The 40 Gbit/s NRZ data pattern has PRBS of $2^7 - 1$. Longer bit pattern can not be used. This is because at longer bit pattern, the electrical multiplexer generates intersymbol interference which caused errors, even in purely electrical back-to-back operation. By using dual-drive Mach-Zehnder Modulator, either the OOK or the DPSK format can be produced. A DQPSK format is generated by combining two DPSK signals in a subsequent fiber-based Mach-Zehnder Delay Interferometer (MZDI). One of the MZDI's arms has a delay τ of 3 symbol duration (~ 75 ps) to simulate uncorrelated data streams. In order to maintain optical phase orthogonality of the in-phase and quadrature components of the DQPSK signal, an active phase control is employed. A quadrature control loop based on a 10 kHz lock-in detection scheme stabilizes the MZDI's phase by minimizing the RF power. The depth of the 10 kHz phase modulation is ~ 0.01 rad (rms).

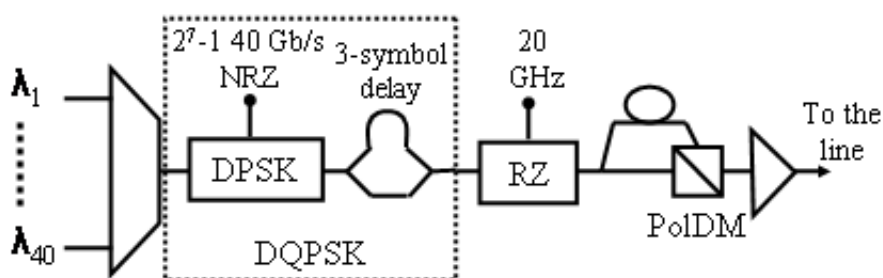


Figure J.1: The setup of WDM transmitter for OOK, DPSK and DQPSK formats with PoIDM

This control efficiently compensates slow environmental phase perturbations of the MZDI. This scheme could also be employed in each WDM channel if two parallel Mach-Zehnder modulators are employed for a completely random DQPSK signal generation. Another dual-drive modulator driven at half the clock rate and biased at the transmission minimum carved ~13 ps long pulses and thereby generated the RZ-DQPSK signal. This signal then splits into two branches and recombined in a Polarization Beam Combiner (PBC) to produce a PolDM signal. In one of the branches, a 112-symbol delay is introduced to decorrelate the data streams carried by two polarizations.

Appendix K

Detailed description of WDM Receiver

In this Appendix, the WDM receiver setup, which is shown in Fig.K.1 is explained in more detail. The received WDM signal is optically preamplified and subsequently demultiplexed in a flat-top optical demultiplexer. The demultiplexed signals are fed into an optical switch with four inputs, which allows selecting any desired WDM channel. The residual CD is compensated by a home made CDC. For OOK, the signal is directly detected by a photodiode for quality assessment. For DPSK and DQPSK, the signal is demodulated by using a one symbol delay MZDI before it is detected by a balanced-receiver. For DPSK, π phase-shift is introduced in one of the MZDI arms. For DQPSK, two values of phase shift are introduced in order to recover both quadratures, which are either $+\frac{\pi}{4}$ or $-\frac{\pi}{4}$. For PolDM system, one polarization is selected by an automatic polarization controller and a polarizer, after CD compensation and before the MZDI. In the transmission system with MTDC, the compensator was located before the DEMUX.

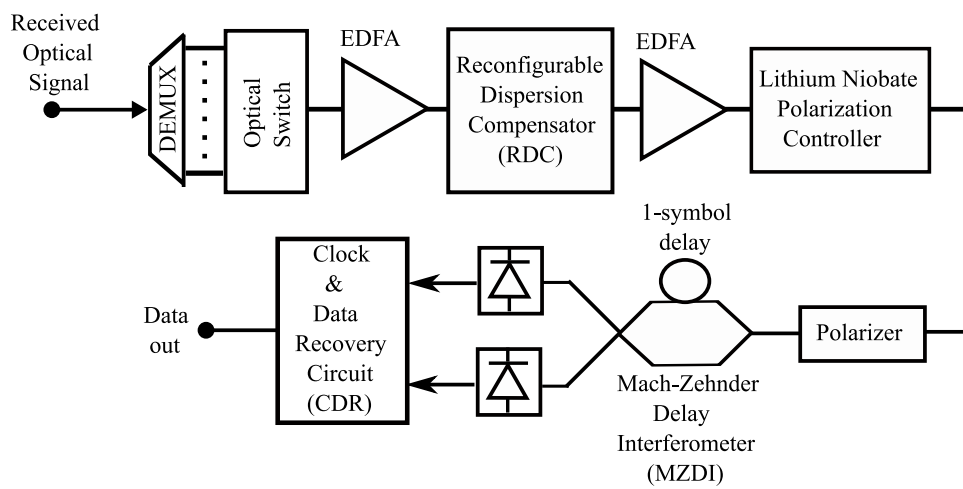


Figure K.1: WDM receiver setup

Appendix L

MTDC: Dual-grating arrangement

Chirped-Fiber Bragg Grating-based Multi-channel Tunable Dispersion Compensators (MTDC) can be designed to compensate both positive and negative dispersion [23]. In order to realize this, two gratings are packaged into one housing as shown in Fig. L.1. The position of the reflection-points of the fast (red) and slow (blue) optical frequency components inside the two gratings is arranged inversely to each other. The dispersion of the two gratings can be independently controlled by temperature gradient, similar to the tuning concepts discussed in Chapter 4. Because of the inverse position of the reflection points, the two gratings produce a dispersion values in opposite sign, and the sum of these two values produces both positive and negative dispersion. For an example, if both gratings produce the same dispersion values, but one of them is in opposite sign, the input signal to the MTDC will experience zero dispersion. If D_{of1} and D_{ol1} are the nominal dispersion (grating dispersion value without temperature changes) of the first and the last channel of the first grating, and D_{of2} and D_{ol2} are the nominal dispersion of the first and the last channel of the second grating, their dispersion values under temperature tuning D_{f1} , D_{l1} , D_{f2} and D_{l2} are linked together according to [23]:

$$\frac{1}{\lambda_f} \left(\frac{1}{D_{f1}} - \frac{1}{D_{of1}} \right) = \frac{1}{\lambda_l} \left(\frac{1}{D_{l1}} - \frac{1}{D_{ol1}} \right) = \frac{1}{\lambda_f} \left(\frac{1}{D_{f2}} - \frac{1}{D_{of2}} \right) = \frac{1}{\lambda_l} \left(\frac{1}{D_{l2}} - \frac{1}{D_{ol2}} \right) \quad (\text{L.1})$$

In comparison to the single-grating MTDC, dual-gratings arrangement offers better uniformity over the tuning range, and can produce up to ± 900 ps/nm dispersion value [23].

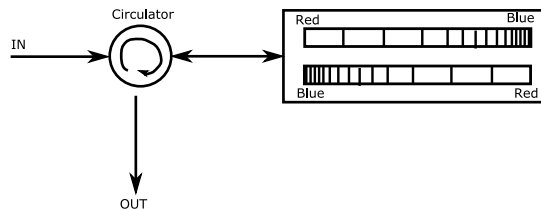


Figure L.1: Schematic of the dual-grating MTDC [23]

Bibliography

- [1] T. H. Wood, G. C. Wilson, R. D. Feldman, and J. A. Stiles, "FiberVista: A Cost-Effective Fiber-to-the-Home (FTTH) System Providing Broad-Band Data Over Cable Modems Along with Analog and Digital Video", *IEEE Photon. Technol. Lett.*, Vol.11 , No.4 , Apr. 1999, pp. 475-477
- [2] G. Charlet, E. Corbel, J. Lazaro, A. Klekamp, R. Dischler, P. Tran, W. Idler, H. Mardoyan, A. Konczykowska, F. Jorge, and S. Bigo, "WDM Transmission at 6 Tbit/s capacity over transatlantic distance, using 42.7Gb/s Differential Phase-Shift Keying without pulse carver", in *Proc. OFC 2002*, paper PDP36
- [3] A. H. Gnauck, P. J. Winzer, S. Chandrasekhar, and C. Dorre, "Spectrally Efficient (0.8 b/s/Hz) 1-Tb/s (25×42.7 Gb/s) RZ-DQPSK Transmission Over 28 100-km SSMF Spans With 7 Optical Add/Drops", in *Proc. ECOC 2004*, paper Th4.4.1
- [4] G. Charlet, P. Tran, H. Mardoyan, M. Lefrancois, T. Fauconnier, F. Jorge, and S. Bigo, "151x43 Gb/s transmission over 4,080 km based on Return-to-Zero Differential Quadrature Phase-Shift Keying", in *Proc. ECOC 2005*, paper Th4.1.3
- [5] R. Freund, L. Molle, F. Raub, C. Caspar, M. Karkri and Ch. Weber, "Triple-(S/C/L)-Band WDM Transmission Using Erbium-Doped Fibre Amplifiers" in *Proc. ECOC 2005*, paper Mo4.2.3
- [6] E. Ciaramella, "Nonlinear Impairments in Extremely Dense WDM Systems", *IEEE Photon. Technol. Lett.*, Vol.14 , No.6 , Jun. 2002, pp. 804-806
- [7] K. Schuh, B. Junginger, H. Rempp, P. Klose, D. Rösener, E. Lach, "85.4 Gbit/s ETDM Transmission over 401 km SSMF Applying UFEC", in *Proc. ECOC 2005*, paper Th4.1.4
- [8] P. J. Winzer, G. Raybon, and M. Duelk, "107-Gb/s optical ETDM transmitter for 100G Ethernet transport", in *Proc. ECOC 2005*, paper Th4.1.1
- [9] C. Xu, X. Liu, and X. Wei, "Differential Phase-Shift Keying for High Spectral Efficiency Optical Transmissions", *IEEE Journ. Of Select. Top. in Quan. Elect.*, Vol. 10, No. 2, Mar/Apr 2004, pp. 281-293
- [10] A. H. Gnauck, and P. J. Winzer, "Optical Phase-Shift-Keyed Transmission", *IEEE Journ. of Lightw. Tech.*, Vol. 23, No. 1, Jan 2005, pp. 115-130
- [11] R. A. Griffin and A. C. Carter, "Optical Differential Quadrature Phase-Shift Key (oDQPSK) for High Capacity Optical Transmission", in *Proc. OFC 2002*, paper WX6

- [12] J. Wang, and J. M. Kahn, "Impact of Chromatic and Polarization-Mode Dispersions on DPSK Systems Using Interferometric Demodulation and Direct Detection", *IEEE Journ. of Lightw. Tech.*, Vol. 22, No. 2, Feb. 2004, pp. 362-371
- [13] D. Sandel, S. Bhandare, A. F. Abas Ismail, F. Wüst, B. Milivojevic, A. Hidayat, R. Noe, M. Guy and M. Lapointe, "2x40 Gb/s RZ-DQPSK transmission over 263 km of fiber with tunable chromatic dispersion compensator", in *Proc. OECC/COIN 2004*, paper 16C2-3
- [14] J. M. Gené, M. Soler, R. I. Killey, and J. Prat, "Investigation of 10-Gb/s Optical DQPSK Systems in Presence of Chromatic Dispersion, Fiber Nonlinearities, and Phase Noise", *IEEE Photon. Technol. Lett.*, Vol.16 , No.3 , Mar. 2004 , pp. 924-926
- [15] N. Yoshikane and I. Morita, "160 % Spectrally-Efficient 5.12 Tb/s (64 x 85.4 Gb/s RZ DQPSK) Transmission without Polarisation Demultiplexing", in *Proc. ECOC 2004*, paper Th4.3.3
- [16] D. Sandel et al., "Standard (NRZ 1x40Gbit/s, 210km) and polarization multiplex (CS-RZ, 2x40Gbit/s, 212km) transmissions with PMD compensation", *IEEE Photon. Technol. Lett.*, Vol 14. , 2002, pp. 1181-1183
- [17] A. F. A. Ismail, D. Sandel, A. Hidayat, B. Milivojevic, S. Bhandare, H. Zhang, R. Noé, "2.56 Tbit/s, 1.6 bit/s/Hz, 40 Gbaud RZ-DQPSK polarization division multiplex transmission over 273 km of fiber", in *Proc. OECC/COIN 2004*, paper PD1-3
- [18] Y. Painchaud, E. Pelletier, and M. Guy, "Dispersion compensation devices: applications for present and future networks", in *Proc. Photonics North 2004*, paper [5579-67] (Invited Paper)
- [19] A. Hidayat, S. Bhandare, D. Sandel, A. F. Abas, H. Zhang, B. Milivojevic, R. Noe, M. Guy, and M. Lapointe, "Adaptive -700... -1350 ps/nm chromatic dispersion compensation in 1.6 Tbit/s (40x40 Gbit/s) DPSK and ASK transmission experiments over 44...81 km of SSMF", in *Proc. ITG-Fachtagung Photonische Netze 2005*, pp. 91-93
- [20] R. L. Lachance, S. Lelièvre, and Y. Painchaud, "50 and 100 GHz multi-channel tunable chromatic dispersion slope compensator", in *Proc. OFC 2002*, paper TuD3
- [21] M. Morin, M. Poulin, A. Mailloux, F. Trépanier and Y. Painchaud, "Full C-band slope-matched dispersion compensation based on a phase sampled Bragg grating" in *Proc. OFC 2004*, paper WK1
- [22] M. Guy, and Y. Painchaud, "Fiber Bragg Gratings: A Versatile Approach to Dispersion Compensation", *Photonics Spectra*, Aug. 2004, pp. 1-7
- [23] Y. Painchaud, M. Lapointe and M. Guy, "Slope-matched tunable dispersion compensation over the full C-band based on fiber Bragg gratings", in *Proc. ECOC 2004*, paper We3.3.4
- [24] J. Mora, A. Díez, M. V. Andrés, P.-Y. Fonjallaz, and M. Popov, "Tunable Dispersion Compensator Based on a Fiber Bragg Grating Written in a Tapered Fiber", *IEEE Photon. Technol. Lett.*, Vol. 16, No. 12, Dec. 2004, pp. 2631-2633

- [25] M. Shirasaki, "Compensation of chromatic dispersion and dispersion slope using a virtually imaged phased array", in Proc.OFC 2001, paper TuS1.
- [26] H. Ooi, K. Nakamura, Y. Akiyama, T. Takahara, T. Terahara, Y. Kawahata, H. Isono, and G. Ishikawa, "40-Gb/s WDM Transmission With Virtually Imaged Phased Array (VIPA) Variable Dispersion Compensators", IEEE Journ. of Lightw. Technol., Vol. 20, No. 12, Dec. 2002, pp. 2196-2203
- [27] D. Yang, C. Lin, W. Chen, and G. Barbarossa, "Fiber Dispersion and Dispersion Slope Compensation in a 40-Channel 10-Gb/s 3200-km Transmission Experiment Using Cascaded Single-Cavity GiresTournois Etalons", IEEE Photon. Technol. Lett., Vol. 16, No. 1, Jan. 2004, pp. 299-301
- [28] X. Shu, K. Sugden, P. Rhead, J. Mitchell, I. Felmeri, G. Lloyd, K. Byron, Z. Huang, I. Khrushchev, and I. Bennion, "Tunable Dispersion Compensator Based on Distributed Gires Tournois Etalons", IEEE Photon. Technol. Lett., Vol. 15, No. 8, Aug. 2003, pp. 1111-1113
- [29] S. Doucet, R. Slavík, and S. LaRochelle, "Tunable Dispersion and Dispersion Slope Compensator Using Novel Gires Tournois Bragg Grating Coupled-Cavities", IEEE Photon. Technol. Lett., Vol. 16, No. 11, Nov. 2004, pp. 2529-2531
- [30] R. Noé, D. Sandel, and V. Mirvoda, "PMD in High-Bitrate Transmission and Means for its Mitigation", IEEE Journ. Of Select. Top. in Quan. Elect., Vol. 10, No. 2, Mar/Apr 2004, pp. 341-355
- [31] H. Sunnerud, M. Karlsson, C. Xie, P.A. Andrekson, "Polarization-mode dispersion in high-speed fiber-optic transmission systems", IEEE Journ. of Lightw. Tech., Vol. 20, No. 12, Dec. 2002, pp. 2204 2219,
- [32] S. Hinz, D. Sandel, F. Wüst, and R. Noé, "PMD tolerance of polarization division multiplex transmission using return-to-zero coding", Optics Express, OSA, July 2001, p. 136
- [33] V. Curri, R. Gaudino, A. Napoli, and P. Poggiolini, "Electronic Equalization for Advanced Modulation Formats in Dispersion-Limited Systems", IEEE Photon. Technol. Lett., Vol. 16, No. 11, Nov. 2004, pp. 2556-2558
- [34] D. McGhan, C. Laperle, A. Savchenko, C. Li, G. Mak, M. O'Sullivan, "5120 km RZ-DPSK transmission over G652 fiber at 10 Gb/s with no optical dispersion compensation", in Proc. OFC 2005, paper PDP27
- [35] M. Zaacks, U. Mahlab, and M. Horowitz, "Low Cost Dispersion Sign Monitor for 40Gb/s Systems", in Proc. OFC 2005, paper OTH8
- [36] K. Ogawa, "STINGRAY: A new paradigm in chromatic dispersion measurement", in Proc. CLEO 2005, San Francisco, White paper
- [37] R. -J. Essiambre, B. Mikkelsen, and G. Raybon, "Intra-channel cross-phase modulation and four-wave mixing in high-speed TDM systems", IEE Electron. Lett., Vol. 35, No. 18, Sep. 1999, pp. 1576-1578

- [38] A. Pizzinat, A. Schiffrini, F. Alberti, F. Matera, A. N. Pinto, Member, and P. Almeida, "40-Gb/s Systems on G.652 Fibers: Comparison Between Periodic and All-at-the-End Dispersion Compensation", *Journ. of Lightw. Tech.*, Vol. 20, No. 9, Sep. 2002, pp. 1637-1679
- [39] H. J. R. Dutton, "Understanding Optical Communications", Prentice Hall, 1998, Sect. 2.4.5.1, pp. 88
- [40] F. Forghieri, R. W. Tkach, A. R. Chraplyvy, and D. Marcuse, "Reduction of Four-Wave Mixing Crosstalk in WDM Systems Using Unequally Spaced Channels", *IEEE Photon. Technol. Lett.*, Vol. 6, No. 6, Jun. 1994, pp. 754-756
- [41] H. Kim, and Alan H. Gnauck, "Experimental Investigation of the Performance Limitation of DPSK Systems Due to Nonlinear Phase Noise", *IEEE Photon. Technol. Lett.*, Vol. 15, No. 2, Feb. 2003, pp. 320-322
- [42] K.-P. Ho, "Phase-modulated optical communication systems", Springer, 2005
- [43] X. Huang, L. Zhang, M. Zhang, and P. Ye, "Impact of Nonlinear Phase Noise on Direct-Detection DQPSK WDM System", *IEEE Photon. Technol. Lett.*, Vol. 17, No. 7, Jul. 2005, pp. 1423-1425
- [44] X. Wei and X. Liu, "Analysis of intrachannel four-wave mixing in differential phase-shift keying transmission with large dispersion", *Opt. Lett.*, Vol. 28, No. 23, Dec. 2003, pp. 2300-2302
- [45] A. H. Gnauck, X. Liu, X. Wei, D. M. Gill, and E. C. Burrows, "Comparison of modulation formats for 42.7-Gb/s single-channel transmission through 1980 km of SSMF", *IEEE Photon. Technol. Lett.*, Vol. 16, No. 3, Mar. 2004, pp. 909-911
- [46] N. Yoshikane and I. Morita, "Performance comparison of 85.4 Gb/s pre-filtered DQPSK signals with and without RZ pulse carving", in *Proc. ECOC 2004*, paper We3.4.6
- [47] T. Tsuritani, K. Ishida, A. Agata, K. Shimomura, I. Morita, T. Tokura, H. Taga, T. Mizuochi, N. Edagawa, and S. Akiba, "70-GHz-spaced 40 x 42.7 Gb/s transpacific transmission over 9400 km using prefiltered CSRZ-DPSK signals, all-Raman repeaters, and symmetrically dispersion-managed fiber span", *IEEE Journ. of Lightw. Tech.*, Vol. 22, No. 1, Jan. 2004, pp. 215-223
- [48] D. Breuer, F. Kuppers, A. Mattheus, E. G. Shapiro, I. Gabitov and S. K. Turitsyn, "Symmetrical dispersion compensation for standard monomode-fiber-based communication systems with large amplifier spacing", *Optics Letters*, Vol. 22, No. 13, Jul. 1997, pp. 982-984
- [49] E. Ciaramella and M. Tamburrini, "Modulation Instability in Long Amplified Links with Strong Dispersion Compensation", *IEEE Photon. Technol. Lett.*, Vol. 11, No. 12, Dec. 1999, pp. 1608-1610

- [50] M. Vasilyev, I. Tomkos, M. Mehendale, J. Rhee, A. Kobayakov, M. Ajgaonkar, Sergio Tsuda, and M. Sharma, "Transparent ultra-long-haul DWDM networks with "broadcast-and-select" OADM/OXC architecture", *IEEE Journ. of Lightw. Tech.*, Vol. 21, No. 11, Nov. 2003, pp. 2661-2672
- [51] R. J. Nuyts, Y. K. Park, and P. Gallion, "Dispersion Equalization of a 10 Gb/s Repeated Transmission System Using Dispersion Compensating Fibers", *IEEE Journ. of Lightw. Tech.*, Vol. 15, No. 1, Jan. 1997, pp. 31-42
- [52] C. Peucheret, I. Munoz, A. Buxens, F. Liu and S.N. Knudsen, "L-band transmission over 1000 km using standard and dispersion-compensating fibres in pre-compensation scheme optimised at 1550nm", *IEE Electron. Lett.*, Vol. 35, No. 20, Sep. 1999, pp. 1759-1761
- [53] S. N. Knudsen, M.O. Pedersen and L. Griiner-Nielsen, "Optimisation of dispersion compensating fibres for cabled long-haul applications", *IEE Electron. Lett.*, Vol. 36, No. 25, Dec. 2000, pp. 2067-2068
- [54] A. G. Green, P. P. Mitra and L. G. L. Wegener, "Effect of chromatic dispersion on nonlinear phase noise", *Optics Letters*, Vol. 28, No. 24, Dec. 2003, pp. 2455-2457
- [55] A. F. Abas, A. Hidayat, D. Sandel, B. Milivojevic, and R. Noe, "100 km fiber span in 292 km, 2.38 Tb/s (16x160 Gb/s) WDM DQPSK polarization division multiplex transmission experiment without Raman amplification", *Elsevier Journ. of Opt. Fiber. Technol.*, June 2006, doi: 10.1016/j.yofte.2006.05.001
- [56] R. I. Killey, H. J. Thiele, V. Mikhailov, and P. Bayvel, "Reduction of intrachannel nonlinear distortion in 40-Gb/s-based WDM transmission over standard fiber", *IEEE Photon. Technol. Lett.*, Vol. 12, No. 12, Dec. 2000, pp. 1624-1626
- [57] C. M. Weinert, R. Ludwig, W. Pieper, H. G. Weber, D. Breuer, K. Petermann, and F. Küppers, "40 Gb/s and 4 x 40 Gb/s TDM/WDM Standard Fiber Transmission", *Journ. of Lightw. Tech.*, Vol. 17, No. 11, Nov. 1999, pp. 2276-2284
- [58] A. Mecozzi, C. B. Clausen, M. Shtaif, Sang-Gyu Park, and A. H. Gnauck, "Cancellation of Timing and Amplitude Jitter in Symmetric Links Using Highly Dispersed Pulses", *IEEE Photon. Technol. Lett.*, Vol. 13, No. 5, May. 2001, pp. 445-447
- [59] J. -C. Antona, M. Lefrancois, S. Bigo, and G. Le Meur, "Investigation of advance dispersion management techniques for ultra long haul transmission", in *Proc. ECOC 2005*, paper Mo3.2.6
- [60] S. Banerjee, A. Agarwal, D. F. Grosz, D. N. Maywar, and A. P. Küng, "Doubly periodic dispersion maps for DWDM transmission at 10 Gb/s and 40 Gb/s", in *Proc. ECOC 2004*, paper We4.P.096
- [61] K. Mukasa, R. Sugizaki, S. Hayami and S. Ise, "Dispersion-Managed Transmission Lines with Reverse-Dispersion Fiber", *Furukawa Rev.*, No.19, Apr. 2000, pp. 5-9

- [62] A. Habisawa, N. Takeda, E. Shibano, H. Taga and K. Goto, "32 x 11.4 Gbit/s Transmission Over 4000 km Using Dispersion Managed 200 km Spans", in Proc. OFC 2005, paper OThC4
- [63] T. Mizuochi, "Next Generation FEC", in Proc. OECC/COIN 2004, paper 16C2-1
- [64] T. H. Szymanski, "Optical Link Optimization Using Embedded Forward Error Correcting Codes", IEEE Journ. Of Select. Top. in Quan. Elect., Vol. 9, No. 2, Mar/Apr 2003, pp. 647-656
- [65] C. Rasmussen, T. Fjelde, J. Bennike, F. Liu, S. Dey, B. Mikkelsen, P. Mamyshev, P. Serbe, P. van der Wagt, Y. Akasaka, D. Harris, D. Gapontsev, V. Ivshin, and P. Reeves-Hall, "DWDM 40G Transmission Over Trans-Pacific Distance (10,000 km) Using CSRZ-DPSK, Enhanced FEC, and All-Raman-Amplified 100-km UltraWave Fiber Spans", Journ. of Lightw. Tech., Vol. 22, No. 1, Jan. 2004, pp. 203-207
- [66] Fujikura, "Optical Fiber Fusion Splicer: FSM-50S", datasheet, http://www.teleoptics.com.pl/gfx/fujikura/pdf/fsm-50s_EN.pdf, 2005
- [67] Teraxion, "ClearSpectrum-TDCM Tunable Dispersion Compensation Module", datasheet, www.teraxion.com, 2005
- [68] A. Walter and G. Schaefer, "Chromatic dispersion variations in ultra-long-haul transmission systems arising from seasonal soil temperature variations", in Proc. OFC 2002, paper WU4
- [69] T. Kato, Y. Koyano, and M. Nishimura, "Temperature dependence of chromatic dispersion in various types of optical fiber", Opt. Lett., Vol. 25, No. 16, Aug. 2000, pp. 1156-1158
- [70] S. Lelievre, H. Chotard, S. LaRochelle, K. -M. Feng, S. Lee, R. Khosvarani, S. A. Havstad, and J. E. Rothenberg, "Multi-channel dispersion compensation using cascaded FBGs for 10 Gb/s transmission", in Proc. NFOEC 2003, paper F8.3
- [71] A. Hidayat, A. F. Abas, D. Sandel, S. Bhandare, H. Zhang, F. Wüst, B. Milivojevic, R. Noé, M. Lapointe, Y. Painchaud, M. Guy, "5.94 Tb/s capacity of a multichannel tunable -700 to -1200 ps/nm dispersion compensator", in Proc. ECOC 2005, paper We1.2.5
- [72] D. Sandel, S. Bhandare, A. F. Abas, B. Milivojevic, R. Noé, M. Guy, and M. Lapointe, "Automatic Tunable Chromatic Dispersion Compensation at 40 Gb/s in ASK and DPSK, NRZ, and CSRZ 263-km Transmission Experiments", IEEE Photon. Technol. Lett., Vol. 16, No. 11, Nov. 2004, pp. 2568-2570
- [73] D. Sandel, V. Mirvoda, F. Wüst, R. Noé and C.-J. Weiske, "Signed online chromatic dispersion detection at 40 Gbit/s based on arrival time detection with 60 attosecond dynamic accuracy", IEE Electron. Lett., Vol. 38, No. 17, Aug. 2002, pp. 984-986
- [74] S. Savory and A. Hadjifotiou, "Laser Linewidth Requirements for Optical DQPSK Systems", IEEE Photon. Technol. Lett., Vol. 16, No. 3, Mar. 2004, pp. 930-932